GENERATION OF ULTRASHORT PULSES FROM CHROMIUM DOPED CUNYITE LASER

by

Michelet Jeanty

A dissertation submitted to the Graduate Faculty in Engineering in partial fulfillment of the requirements for the degree of Doctor of Philosophy

The City University of New York

2011

This manuscript has been read and accepted for the Graduate Faculty in Engineering in satisfaction of the dissertation requirement for the degree of Doctor of Philosophy.

Professor Robert R. Alfano

Date — Chair of Examining Committee

Professor Mumtaz Kassir

Date — Executive Officer

Prof. Roger Dorsinville, Dept. of Electrical Engineering, CUNY

Prof. Ping-Pei Ho, Dept. of Electrical Engineering, CUNY

Prof. Ardie Walser, Dept. of Electrical Engineering, CUNY

Prof. Swapan Gayen, Dept. of Physics, CUNY

Prof. Vladimir Petricevic, Dept. of Physics, CUNY

Supervisory Committee

THE CITY UNIVERSITY OF NEW YORK

Abstract

GENERATION OF ULTRASHORT PULSES FROM CHROMIUM-DOPED CUNYITE LASERS

by

Michelet Jeanty

Adviser: Robert.R.Alfano, Distinguished Professor of Science and Engineering

This thesis focuses on the generation of ultra short pulses from the chromium-doped Cunyite laser. The various principles and operation of Cunyite laser systems capable of generating femtosecond pulses in the near infrared are described. Self-starting mode-locking was successfully engineered and implemented with the assistance of semiconductor absorber mirrors (SESAMs).

The broad tunability of Cr^{4+}: Ca_2GeO_4 laser indicates its potential as a source of ultrafast light generation. The spectral range between 1.3 μm and 1.5μm is both important for optical communications and the eye-safe 1.45μm wavelength range. If the entire laser bandwidth of Cr^{4+}: Ca_2GeO_4 are utilized, pulses as short as sub-20 fs of Cr^{4+}: Ca_2GeO_4 may be attainable.

Cr^{4+}: Ca_2GeO_4 laser (Cunyite) is developed at the Institute for Ultra-fast Spectroscopy and Lasers of City College of New York.The setup is formed by a standard confocal X-shaped cavity composed of the active material in the focus, and a broadband output coupler in combination with several flat mirrors used for dispersion compensation.

So far, a semiconductor saturable absorber mirror (SESAM) is necessary to sustain mode-locking. Early attempts to generate mode-locked pulses led to the generation of full width at half maximum 60 picosecond pulses using an intracavity quantum-well-based semiconductor saturable absorber mirror. The SESAM is made of a thin narrow band gap absorption region, which is sandwiched between a cap layer and a spacer layer placed on the top of a high reflectivity semiconductor saturable absorber mirror. The SESAM is prepared by stacking pairs of quarter-wavelength layers that are composed of semiconductors with alternating high and low refractive indices. It consists of 24.5 periods of 123-nm AlAs low-index-104.9nm GaAs high-index quarter-wave layers for 1.43μm. The pulse width was further reduced to 8.6ps and subsequently to 365fs by using a highly-doped crystal. The tuning range of the mode-locked Cunyite laser was determined to be 134 nm. The CW output wavelength was approximately 1430 nm for all output couplers. The corresponding threshold pump power and the slope efficiency with respect to pump power were 0.5W, 1W, 1.5W and 3.125%, 4.58%, 3.75% respectively. The best laser performance was obtained with the 2.5% output coupler (OC). Using this output coupler, the laser produced 240mW of output power with 5W pump power. Subsequently, pulses with duration of 223 fs pulses were generated by this means. In conjunction with the measured spectra, this indicates that the nonlinear refractive index of this material is indeed sufficient to support Kerr-lens mode-locking.

A four-mirror astigmatically X-cavity was found to be more appropriate for mode-locking. The passive mode-locking was achieved using a semiconductor saturable absorber mirror, so-called SESAM. The laser performances concerning the pulse duration

and the output power are quite different using different SESAMs. To explain the experimental results, the key parameters of the SESAMs must be known.

Time-bandwidth measurements indicated the presence of chirp in the output pulses. Numerical calculation of the phase characteristics of various optical materials indicated that a quartz glass plate was used in the cavity in order to compensate for the chirp.. The results obtained indicate that the noise like mode is not significantly affected by the cavity dispersion. To improve the situation, a careful selection of the optical material is needed if the pulse duration is to be minimized. For Cr^{4+}:Ca_2GeO_4, the optimum choice turned out to be quartz plates, which, by minimizing the "Third-Order-Dispersion" in the cavity will allow the generation of nearly bandwidth-limited pulses of sub-100fs in duration around 1.4μm. In fact, extremely broad double-peaked spectra centered at 1.4μm could be obtained. However, the quartz glass plates have the advantage that the desired negative second-order dispersion can be adjusted continuously.

Self-starting mode-locking was demonstrated directly from the laser oscillator with double chirped mirrors in combination with fused silica glass plates. Numerical calculations of the cubic phase characteristics used indicated that the SF10 prisms compensated for quadratic phase but introduced a large cubic phase term. Numerical evaluation of other optical glasses indicated that a fused silica glass plates introduced a smaller cubic phase but the same quadratic phase term as the SF10.

To my mother, Angelina Jeanty

My three children Nobenson Jean-Francois, Michelle and Nobens Jeanty

Acknowledgments

I would like to thank and gratefully acknowledge my thesis adviser Professor Robert R. Alfano. His vast knowledge of science and willingness to spend his valuable time to teach me were of enormous help in achieving the research goals. As my adviser, Professor Alfano provided the environment and guidance to make me the best research scientist I could be in America. Most importantly, I appreciate the fact that he trusted me with mode-locked operation of the Cunyite laser.

Dr. Tuan was my greatest asset at City College. He was a perfect lab partner providing a continuous stream of insights. He has many talents, some of which were useful in the development of the femtosecond Cunyite laser. As a co-mentor, he has made the most significant contribution in my life at City College.

The generation of femtosecond Cunyite laser pulses would not have been possible without Dr. Kartazaev who helped build the apparatus. He taught me how to use the apparatus and align laser beams for generating pulses. It often took me days of tweaking mirrors before I saw the beam. Cunyite laser needs special care and Dr. Kartazaev provided not only the expertise but also that special care and leadership towards all aspects of generation of ultra short pulses from chromium-doped Cunyite laser. Dr. Ketsutkus was a superb administrator and without his persistent supervision,the

generation of femtosecond and Cunyite laser pulses would not have been completed. It was fun working under his supervision.

I am most grateful to Professor Akins who made this research possible by providing financial support. I am obliged to Professor Ping-Pei Ho, Professor Swapan Kumar Gayen, Professor Roger Dorsinville, Professor Ardie D. Walser, and Professor Vladimir Petricevic for serving on the doctoral committee. I am particularly indebted to Dr. Alexei Bykov for growing and providing the Cunyite crystals in a timely manner. I would like to take this opportunity to thank laser engineer Yuri Budanski and coordinator Joan Brijlall, both working at the Institute for Ultrafast Spectroscopy and Lasers(IUSL), for their friendly support and valuable assistance.

I would not have been able to reach this point without the unconditional support of my family. My mother has always given me all the support I needed. I am thankful to my sister Marie-Ange for her endless love.

Acknowledgment of Financial Support

I gratefully acknowledge the research assistantship provided by the NSF, NIH, ARO, NASA and the CENSES.

Table of Contents

CHAPTER 1: INTRODUCTION

1.1 Tunable Solid-State Lasers 1

1.2 Thesis Statement 7

1.3 Thesis Organization 8

1.4 References.....10

CHAPTER 2: INITIAL CHARACTERIZATIONS OFCr^{4+}: Ca_2GeO_4 (CUNYITE) LASER

2.1 Introduction.....12

2.2 Cr^{4+}: Ca_2GeO_4 (Cunyite): a History.....14

2.3 Cr^{4+}:Ca_2GeO_4 (Cunyite) as a Laser Gain Material 16

2.4 Basic Spectroscopic Properties of Chromium-Doped Cunyite Crystal 17

2.4.1 Absorption Spectrum 17

2.4.2 Emission Spectrum 20

2.4.3 Fluorescence Lifetime.....23

2.4.4 SimplifiedTanabe-Sugano of Cr^{4+}:Ca_2GeO_4vs. Cr^{4+}:Mg_2SiO_4.....24

2.5. Thermal Lensing 25

2.6. The Cr^{4+}:Ca_2GeO_4 (Cunyite) Laser Cavity

2.6.1 Cavity Design.....28

2.7. References.....35

CHAPTER 3: GENERATION AND MEASUREMENT OF SHORT PULSES

3.1 Introduction....38

3.2. Modes in a Laser Resonator....39

3.3. Mode-locking

3.3.1 Basic Concept....43

3.3.2 Active Mode-Locking....46

3.3.3 Passive Mode-Locking....50

3.3.3.1 Kerr-lens Mode- Locking....51

3.3.3.2 Solitonic Mode-Locking....56

3.4 The Time-bandwidth Product....59

3.5 Measurement of Duration of Short Pulses....61

3.5.1 Intensity Autocorrelator....63

3.5.2 Interferometric Autocorrelator....66

3.5.3 Two-photon Absorption Autocorrelation....69

3.6. Gaussian Pulses....75

3.7 References....82

CHAPTER 4: PICOSECOND AND FEMTOSECOND OPERATION OF THE Cr^{4+}: Ca_2GeO_4 (CUNYITE) LASER

4.1 Introduction....85

4.2 Propagation of Gaussian Pulses in a Dispersive Medium 86

4.3 Dispersion Management

4.3.1 Dispersion Measurement on Cunyite Laser Crystals.....100

4.4 Glass Slabs-A simple method 104

4.5 Pulse Compression using DCM's 106

4.6 Broadband SESAM for self-starting Mode-locking 112

4.7. Experimental results

4.7.1 Continuous-wave performance of Cr^{4+}:Ca_2GeO_4 (Cunyite) Laser.....116

4.7.2 Passively Mode-locking performance of Cr^{4+}:Ca_2GeO_4 (Cunyite) Laser 119

4.8 Multiple pulsing regime.....125

4.9 Conclusion 126

4.10 References.....128

CHAPTER 5: SUMMARY AND FUTURE DIRECTIONS

5.1 Summary.....131

5.2 Future Directions

5.2.1 Additional Kerr-Mode-Locked Cr^{4+}:Ca_2GeO_4

(Cunyite) Laser 132

5.2.2. Improved Self-Starting Passively Mode-Locked Cr^{4+}:Ca_2GeO_4

(Cunyite) Laser .with Double Chirped Mirrors in Combination with Fused

Silica Glass Plates.....134

5.3 Femtosecond Cr^{4+}:Ca_2GeO_4 (Cunyite) for applications in Telecommunications and Biophotonics

5.3.1 Introduction 135

5.3.2 Applications of Cr^{4+}:Ca_2GeO_4 (Cunyite) ultrashort pulses in the 1300 nm spectral region.....136

5.4 Conclusions.....139

5.5 References.....142

APPENDIX

Appendix A: Coatings of Four Mirrors Cavity Design……...144

Appendix B: Calculated Group Velocitydispersion ……...146

Appendix C: Cunyite crystal dispersion data……..147

BIBLIOGRAPHY

CHAPTER1 … ……...149

CHAPTER 2… ……...150

CHAPTER 3… ……...153

CHAPTER 4… ……...155

CHAPTER 5… ……...158

LIST OF TABLES

CHAPTER 2:

Table 2.7.1 Physical, thermal, and optical properties of Cr^{4+}:Ca_2GeO_4 (Cunyite) and Nd: YAG lasers…….33

Table 2.7.2 Comparison of basic spectroscopic and laser properties of Cr^{4+}:Ca_2GeO_4 (Cunyite) and Cr^{4+}:Mg_2SiO_4 (forsterite) lasers……..34

CHAPTER 3:

Table 3.4.1: Values of k for various pulse shapes ……60

CHAPTER 4:

Table 4.4.1 List of the zero-GVD of the BK7, fused silica, quartz glasses, as well as their negative GVD values……105

Table 4.7.1 Summarizes CW efficiency curves for the Nd: YAG pumped Cr: Ca_2GeO_4 (Cunyite) laser with the 1%, 2%,5% OCs…….....118

Table 4.7.2: Autocorrelation (τac) and pulse τp calculations assuming Gaussian-fit, Hyperbolic-secant, Diffraction versus different spectra widths at the center wavelength (λ_0=1430nm)…….124

LIST OF FIGURES

CHAPTER 1:

Figure 1.1: Key tunable solid-state lasers where the Cr^{4+} extends the NIR region and their tuning ranges…….5

CHAPTER 2:

Figure 2.1.1: Sample of chromium-doped Cunyite grown at City College ……..13

Figure2.1.2. Striking color appearance of transition metal complexes……..14

Figure 2.2.1 olivine crystal structure of octahedral and tetrahedral sites……..15

Figure 2.4.1(a) Polarized NIR single-crystal absorption spectra of Cr^{4+}: Ca_2 GeO_4 (Cunyite) at 28 K (b) Polarized absorption spectra of Cr^{4+}: Ca_2 GeO_4 (Cunyite) for all three crystal orientations……18

Figure 2.4.2 Unpolarized luminescence spectrum at 15 K of Cr^{4+}:Ca_2GeO_4 (b) High resolution transmission spectrum at 20 K of Cr^{4+}:Ca_2GeO_4 single crystal and high resolution luminescence spectra at various temperatures of the same Cr^{4+}: Ca_2GeO_4 compound…….....21

Figure 2.4.3 Comparison of fluorescence lifetimes among some key infrared tunable lasers grown at the Institute for Ultrafast Spectroscopy and Lasers (IUSL)……...23

Figure 2.4.4 Tanabe-Sugano diagram for (a) Cr^{4+} in tetrahedral coordination….....24

Figure 2.5(a) Schematic of mode mismatched thermal lens detection and tranverse intensity profiles computed from theory for the near field; (b) thermal focusing; (c) thermal defocusing…….....27

Figure 2.6.1(a) A representative schematic of a typical four-mirror, X-folded astigmatically compensated cavity showing the beam mode size (b) shows the variation of the crystal's beam spot size with increasing repetition rate (c) shows the variation of the crystal's beam spot size with increasing long arm's length(d) Beam waist, w(z) as a function of distance, z, plotted for for the Cr^{4+}:Ca_2GeO_4(Cunyite) laser center wavelength λ_0=1400 nm…….....30

CHAPTER 3

Figure 3.2.1: Simple two-mirror laser cavity ……40

Figure 3.2.2: First six longitudinal modes of a plane-parallel cavity……....42

Figure 3.2.3: Allowed longitudinal modes in a laser cavity with gain medium……43

Figure 3.3.1 Intensity profile of (a) 4 locked longitudinal modes, (b) 7 locked longitudinal modes, (c) 15 locked longitudinal modes…….45

Figure 3.3.2: Output of a mode-locked laser in frequency and time domains……...50

Figure 3.3.3.1: (a) Soft aperture Kerr-lens mode-locking,(b) Hard aperture Kerr-lens mode-locking ……54

Figure 3.3.3.1(c): Passive mode-locking mechanism (i) Slow Saturable Absorption (SSA) (ii) Fast saturable absorption (FSA) (iii) Solitonic modelocking. The bluish colored area represents the net gain window……55

Figure 3.4.1: Phase ($\Delta\phi$) and frequency ($\Delta\nu$) shift undergoing self-phase modulation….56

Figure 3.5.1 Experimental layout for an intensity autocorrelator using second harmonic generation. A pulse is split into two, one is variably delayed with respect to the respect, and the two pulses are overlapped in a second harmonic crystal.

The second harmonic pulse energy is measured versus delay; yielding the autocorrelation trace…….65

Figure 3.5.2 Experimental layout for an interferometric autocorrelator using second harmonic generation. A pulse is split into two, one is variably delayed with respect to the respect, and the two pulses are overlapped in a second harmonic crystal. The second harmonic pulse energy is measured versus delay; yielding the autocorrelation trace……..67

Figure 3.5.3 Interferometric autocorrelation of Gaussian pulses with FWHM of 10 fs for different values of the chirp parameter (b) a) b=0, b) b=1, c) b=1.5……69

Figure3.5.4:(a)shows a two-photon absorption scheme,(b) shows a two-photon absorption auto-correlator(c):(i)Representative two-photon autocorrelation trace in intensity (ii) Representative two-photon Interferometric autocorrelation trace ……71

Figure 3.6.1: Gaussianl pulse with linear chirp…….76

CHAPTER 4

Figure 4.2.1: shows three instances in time of the modulated wave. A solid line is drawn through the center of the envelope whilst a dashed line is drawn through a peak in the carrier laser……...91

Figure 4.3.1(a) Experimental setup for recording white-light interferograms for the dispersion measurement of Cr^{4+}:Ca_2GeO_4 (Cunyite) crystal (b) Measured group delay dispersion of the Cunyite crystal with Fourier transform of the white-light interferometric cross correlation (c) Measured group velocity dispersion of the Cunyite crystal with Fourier transform of the white-light interferometric cross correlation (d) Measured group delay of the Cunyite

crystal with Fourier transform of the white-light interferometric cross correlation (e) Measured phase of the Cunyite crystal with Fourier transform of the white-light interferometric cross-correlation……100

Figure 4.4.1(a): Comparison between the compensation by a fused silica plate and by a SF10 prism pair (b): The GDD of a prism pair versus distance (L) between the two prisms…….105

Figure 4.5.1(a) Standard Bragg mirror, (b) Simple chirped mirror, (c) Double chirped mirror, (d): The laser pulse compression in CM (red line) with GD oscillations and compression in CM (green line) with desired GD ,(e): The difference between a broadened pulse with pedestals and a compressed pulse with Gaussian shape,(f): Reflectance calculations of the Layertec chirpec mirror(GVD=-50 fs^2) ,(g): Group velocity dispersion (-50 fs^2) calculations of the Layertec chirpec mirrors; (h): Transmission calculations of the Layertec chirpec mirror(GVD=-100 fs^2), (i): Group velocity dispersion (-100 fs^2) calculations of the Layertec chirpec mirrors…….107

Figure 4.6.1: Basic layer structure of the homegrown semiconductor saturable absorber mirror……..116

Figure 4.7.1: Cr^{4+}:Ca_2GeO_4 (Cunyite) laser performance: CW operation (a) the slope efficiency for a 1% output coupler (b) the tuning range with 1% output coupler ……...118

Figure 4.7.2: Schematic diagram of the experimental arrangement for the self-starting passively mode-locked operation of the Cr: Cunyite laser:(λ/2) half-wave plate for 1064 nm; L, focusing lens; M_8 ,output coupling mirror, , $M_1 – M_3$:

5-cm- radius dichroic, curved folding mirrors; M_4 - M_7 : chirped dielectric laser mirror; M_9 highly reflective SESAM mirror (a): Autocorrelation trace of the 8.6-ps pulses recorded. The pulse width was measured to be 5ps by assuming a $sech^2$ pulse profile (b) Autocorrelation trace of the 550fs pulses recorded. The pulse width was measured to be 365fs by assuming a $sech^2$ pulse profile. b) Spectrum of the mode-locked pulses. The spectral width of the pulses was measured to be 5.2nm.The pulsewidth-bandwidth product is $\Delta\tau_p\Delta\upsilon=0.28$ (c) Autocorrelation trace of the 370fs pulses recorded. The pulse width was measured to be 233fs by assuming a $sech^2$ pulse profile……120

Figure 4.8.1: Qualitative plot of the initial chirp variation: (a) normal dispersion, weak nonlinearity;(b) normal dispersion, strong nonlinearity; (c) anomalous dispersion, weak nonlinearity; (d) anomalous dispersion, strong nonlinearity…….126

CHAPTER 5

Figure 5.2.1: Schematic laser setup of a mirror-dispersion-controlled KLM Cr^{4+}:Ca_2GeO_4 (Cunyite) laser. The pump beam is focused by a 38.5mmlens onto a 3.8-mm thick highly doped Cr^{4+}:Ca_2GeO_4 (Cunyite) crystal. M1, M2, single-stack quarter-wave dichroic mirrors highly transmitting at the pump wavelengths with radii of curvature of 5cm; M3-M7chirped dispersive mirrors; OC, 1% broadband output coupler; CP: wedged compensating glass plate. b) GDD of the chirped dispersive mirrors……133

Figure 5.2.2: Design of improved self-starting passively modelocked Cr^{4+}:Ca_2GeO_4 (Cunyite) laser with double chirped mirrors (DCMs) in combination with fused silicaglass plates…….134

Figure 5.3.1: The attenuation and dispersion for a typical optical fiber at 1550 nm…..135

Figure 5.3.2: Infrared light is absorbed primarily by water, while visible and ultraviolet lights are primarily absorbed by hemoglobin and melanin, respectively. As the wavelength decreases toward the violet and ultraviolet, light scatter or absorption from covalent bonds in protein limits penetration depth in this range…… ……136

CHAPTER 1

INTRODUCTION

1.1. Tunable Solid-State Lasers

The discovery of the solid-state ruby [1] laser by Theodore Maiman in May 16, 1960 opened the door to the now-flourishing field of laser research. Trivalent chromium laser operation was first demonstrated with the ruby (Cr^{3+}:Al_2O_3). Research on transition metal–doped tunable lasers exploded in 1980 after Walling et al. demonstrated tunable lasers operating in the 700 to 820 nm range at room temperature in trivalent chromium doped Cr^{3+}:$BeAl_2O_4$ [2].The chromium-doped sapphire crystal that forms the gain medium for the ruby laser provided a model for the discovery of the broadly tunable solid-state laser in alexandrite in1979. The discovery of the emerald laser by Morris and Cline [3,4] in the early 1980s led to a flurry of research focused on finding new laser crystals and new ions that would lase in commonly-used host crystals. Several other materials have seen some commercial interest as possible lamp pumped materials.In particular Cr^{3+}:$LiCaAlF_6$ and Cr^{3+}:$LiSrAlF_6$ [5,6,7] have seen some interest as possible tunable commercial laser sources .A number of chromium-doped materials including Cr^{4+}:Mg_2SiO_4, Cr^{4+}:YAG, Cr:Nd:GSGG, Co:MgF_2, Cr:$ZnWO_4$, Cr^{4+}:Ca_2GeO_4, Cr^{3+}:$LiInSiO_4$, and Cr^{3+}:$LiInGeO_4$ are also showing strong interest.

Other chromium-doped vibronic materials have broader tuning range in the near infrared and have received considerable research interest as possible as diode-pumped tunable sources. These include Cr^{4+}:Ca_2GeO_4 with a tuning range between those of Cr^{4+}:Mg_2SiO_4 and Cr^{4+}: YAG lasers at 1300 to 1600nm. Cr^{4+}:Ca_2GeO_4 lasers operating at

1400nm hence provide enhanced eye safety and are commonly referred to as eye safe lasers. Lasing action in Cr^{4+}: Ca_2GeO_4 (Cunyite) was first reported by Petričevic et.al in early 1996, hereafter Cr^{4+}:Mg_2SiO_4 (forsterite). This fascinating laser system has tremendous potential for applications in NIR imaging, telecommunications and semiconductor inspection.

Applications requiring lasers that operate at a specific wavelength prompted much interest in the development of new gain media. This has led to the emergence of many solid-state materials that produce laser light in different parts of the electromagnetic spectrum from the ultraviolet to the mid-infrared. Examples of the most recent developments and applications of new solid-state gain media include cerium-doped lasers in the ultraviolet, ytterbium lasers, rare-earth ion –doped lasers in the eye-safe region, and tunable Cr^2: ZnSe in the mid-infrared.

For practical applications, the following desirable properties make these sources very attractive: high thermal conductivity, high optical damage threshold, compactness and operational reliability. At the present time, the most widely used lasers are the following types, Ti: sapphire, Alexandrite, Cr^{3+}: LisaF, Cr^{3+}: LiCAF, Cr^{4+}: forsterite and Cr^{4+}: YAG, which provide laser radiation in the 0.7-1.6μm range. Lasers in the mid-infrared region such as Forsterite at 1250nm generated ultrashort pulses with less than 60 fs duration are promising tools for biomedicine and communication applications. Cr^{4+}: Ca_2GeO_4 (Cunyite) is an important solid-state laser which produces broad laser radiation in the near-infrared around 1400 nm. Most importantly, the broad emission band extending from 1300 to1500 nm can potentially be used to generate femtosecond pulses as short as 11 fs. Cunyite lasers are applicable to many research areas including

semiconductors spectroscopy, imaging, material processing, microscopy, biophotonics and telecommunications. To date, different methods of laser operation have been demonstrated with Cr^{4+}: Ca_2GeO_4 lasers. These include gain-switching, continuous-wave tunability [8],and mode-locked operation with milliwatt continuous-wave (CW) output powers. In mode-locking experiments, acousto-optic modulation was first employed to generate 80 ps at 1400 nm. The current drawbacks of existing solid state lasers include: (1) a limited tuning range, (2) difficulty in obtaining crystals of high optical quality, and (3) relatively low emission cross section as compared with dye lasers.

During the past 20 years, tunable solid-state lasers have emerged as a viable alternative to dye lasers. The dye lasers suffer many disadvantages such as toxicity and poor long-term reliability making them unsuitable for hospital, airborne, mobile and space borne use. Tunable solid-state lasers do not possess these and offer many advantages over dye lasers. One of the main advantages includes usage within a confined environment. Some of the other advantages are the following:

1. Tunable solid-state lasers cover a very wide spectrum up to 410 nm (Ti^{3+}: sapphire). This makes them prime candidates as tunable sources of radiation and for the generation of ultra short pulses.
2. The laser medium is a non-toxic material. This makes tunable solid state lasers useful tools in places where the toxicity and containment pose problems, such as hospital operating rooms, airborne operations, and space stations.
3. Solid state lasers are very reliable systems with long life and require minimum maintenance.
4. Solid state can be very compact since they can be pumped by diode lasers.

5. Solid state lasers are relatively easy to use. This makes them useful for people with no background in laser engineering.
6. Solid state lasers are very cost- effective sources of radiation

Although there are several tunable solid-state lasers such as Ruby, Alexandrite, Emerald,and Ti^{3+}:sapphire that cover the spectral range from 700-1100 nm, there are basically only a few of them that look particularly promising. The most developed commercially available tunable solid-state laser is the titanium-doped sapphire laser (Ti^{3+}:Al_2O_3) with the tuning range covering 660-1100 nm. Another rapidly developing laser system is the chromium-doped LiSAF laser (Cr^{3+}: $LiSrAlF_6$) with the tuning range extending from 780 to 1060 nm. The advantages of this laser (Cr^{3+}: $LiSrAlF_6$) over the Ti^{3+}: sapphire laser are the possibility of diode pumping, longer emission lifetime, and consequently better energy storage capabilities.

Unfortunately, neither of the above lasers covers the near infrared range beyond 1100 nm. This void has been successfully filled by introducing a new laser ion, Cr^{4+}. It opens up possibilities of solid state continuous-wave and ultra short pulse operation with a potential tuning range extending from 1.3 μm to beyond 1.5μm. Cr^{4+} doped lasers have several advantages including flexible pumping schemes, impressive output powers, wide tunability, and room temperature operation. The broad absorption bands in the (0.6-1.2) μm regionallows their pumping from a variety of sources Nd: YAG (1064 nm), diode (800 nm or 980 nm), Yb: fiber (1061 nm),Ti^{3+}:sapphire (800 nm). These applications are the driving force for the need of a robust, compact, solid state, tunable laser sources operating at room temperature in NIR range. In this context, transition metal ions have

always been of great interest from the beginning of laser developments because of their broad emission.

Wide tunability in the near infrared range between 1348 nm and 1460 nm and lack of any significant excited absorption make the chromium-doped Cunyite laser a promising tunable solid state laser.

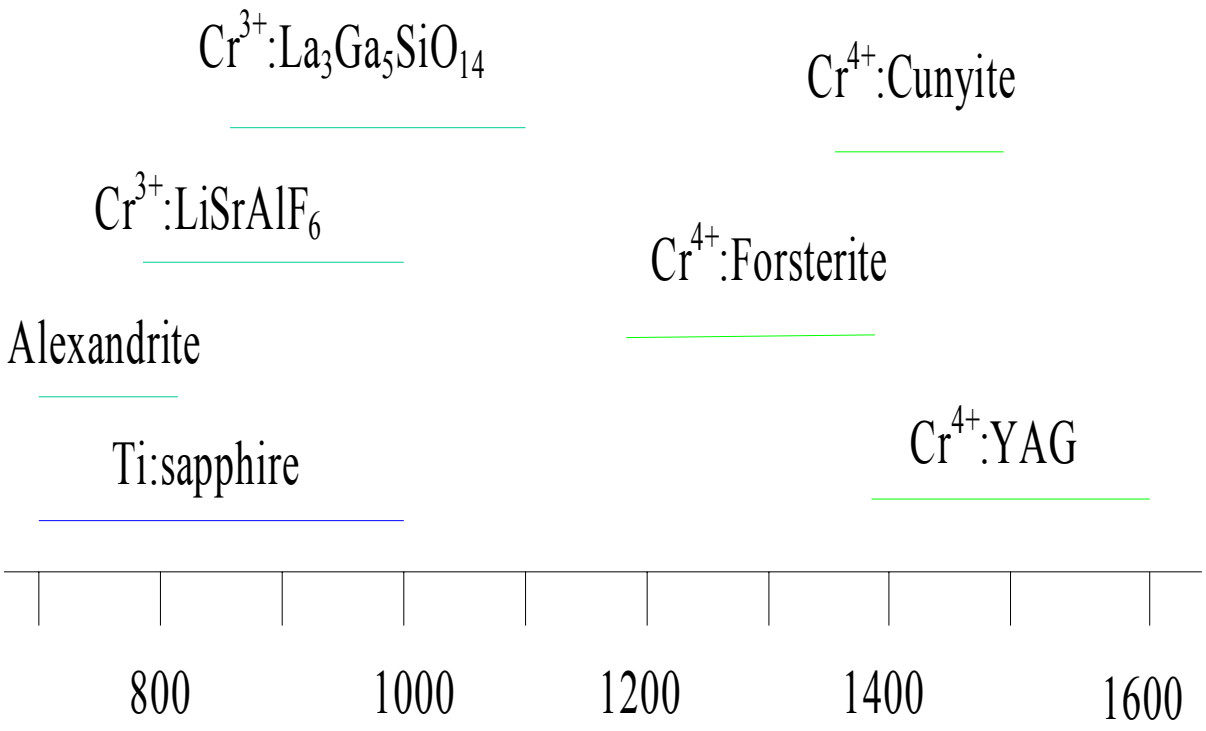

Figure1.1. Key tunable solid state lasers where the Cr^{4+}extends the NIR region and their tuning ranges.

Over the past few years, the number of solid state lasers has dramatically increased due to different requirements from industry and science. These requirements include necessity of coherent and monochromatic light in different wavelengths and with

different characteristics. Nowadays, hundreds of laser crystals have demonstrated laser operation and this number is continuously increasing. These new laser systems can achieve superior performance and reduce complexity as compared to the traditional dye laser technology. The techniques used for ultra short pulse generation are of particular interest because they exemplify several general concepts that can be applied to femtosecond and sub-10-fs laser engineering. In the near future, these concepts enhance the possibility of developing low cost, compact, ultra short pulse laser technology.

These encouraging results in chromium-doped materials led to a rebirth in tunable solid-state laser research [8,9,10,11]. In spite of its many advantages, Ti: sapphire does suffer from a few disadvantages. In particular, its short upper lifetime (3.2μs) make it quite difficult to pump with a lamp. Although lamp-pumped Ti^{3+}: sapphire lasers have been built; most commercial Ti^{3+}: sapphire are pumped with argon-ion or double Nd-YAG lasers.

Several other materials have seen some commercial interest as possible lamp pumped laser materials. In particular, $LiCalF_6Cr^{3+}$ and $LiSrAlF_6:Cr^{3+}$ have seen some interest as possible tunable commercial laser sources. A number of other chromium-doped materials including Cr: YAG, Cr: forsterite and Cr: Cunyite are showing interest [23].They enable the implementation of broadly tunable continuous wave's sources of the generation of short temporal optical pulses in the 1 micron to 1.6 micron spectral range. This emission spectrum is useful as it covers the telecommunication range.

1.2. Thesis Statement

The research primarily focused on the generation of ultra short pulses from the chromium-doped Cr^{4+}: Ca_2GeO_4 (Cunyite) laser. The main objective was the generation of ultra short pulses using self-starting passively mode-locking and ultimately the generation of 200 femtossecond pulses in the near infrared. Self-starting passively mode-locking was successfully engineered and tested. As a result of the continuous research efforts, the chromium-doped Cunyite laser has been established as a reliable source of stable, tunable, femtosecond pulses in the near infrared.

The main accomplishments of this thesis are the following:

1. Design and engineering of a four- mirror X-fold astigmatically compensated
2. Cr^{4+}:Ca_2GeO_4 (Cunyite) laser and the first demonstration of self –starting mode – locking of the Cr^{4+}:Ca_2GeO_4 (Cunyite) laser with SESAM. These experiments resulted in the generation of 8.5ps using passively mode locking [12].
3. Design and engineering of a self-starting mode-locked Cr^{4+}:Ca_2GeO_4 (Cunyite) laser with improved overall cavity dispersion compensation and the generation of 365 fs pulses from a passively mode-locked Cr^{4+}:Ca_2GeO_4 (Cunyite) laser.
4. Design and engineering of a self-starting [13] mode-locked Cr^{4+}:Ca_2GeO_4 (Cunyite) laser with improved overall cavity dispersion compensation and the generation of 224 fs pulses from a passively mode-locked Cr^{4+}:Ca_2GeO_4 (Cunyite) laser.

1.3. Thesis Organization

This thesis is organized into five chapters. Chapter 1 serves as the general introduction.

Chapter 2 serves as an introduction to Cr^{4+}:Ca_2GeO_4 (Cunyite) crystal. Cr^{4+}:Ca_2GeO_4 (Cunyite) is an intriguing laser crystal. The ion responsible for lasing action was identified as tetravalent chromium in tetrahedral coordination. Absorption and emission experiments are presented where the crystal quality was evaluated and also provided the grounds for comparison between different laser crystals used during the mode-locking experiments.

Laser cavities used for model king are usually complex multi-element optical systems where there is a need for careful design in order to eliminate perturbations due to unwanted reflections, astigmatism and heating effects. Chapter 2 continues with the analysis and design criteria for a four-mirror X-fold astigmatically compensated cavities used in self-starting passively mode-locking of the Cr^{4+} :Ca_2GeO_4(Cunyite) laser.To get a more quantitative picture of the effectiveness of our cavity configurations, a more detailed characterization of the thermal effects taking place in the active medium is needed.

Mode locking is achieved using only self-starting Kerr-lens technique. Chapter 3 reviews the basic concepts of mode-locking and the different pulse measurement methods. Chapter 4 continues with the experimental results obtained by using the four-mirror cavity in the self-starting passively mode locking process. Tunability over the 1348-1482-nm spectral range was demonstrated. Slope efficiency experiments resulted in 2.5% slope efficiency. The presence of chirp in the output pulses of the self-starting passively mode-

locked Cr^{4+}:Ca_2GeO_4 (Cunyite) laser indicated that special attention should be given to phase distortions compensation in the laser cavity.

The final chapter of the thesis summarizes the achievements of research and future research to advance femtosecond operation of the Cr^{4+}:Ca_2GeO_4 (Cunyite) is recommended. Some of the subjects presented are intracavity pure Kerr-lens mode-locking improved self-starting passively mode-locking.

1.4. References

1. T. Maiman,"Stimulated Optical Radiation in Ruby", *Nature*, 187, 493-494 (1960).

2. R.C.Morris and C.F. Cline "Chromium-doped Beryllium Aluminate Lasers,"U.S .Patent# 3,997,853.Dec14,1976.

3. M.L.Shand, J.C.Walling, "A tunable emerald laser"*IEEE J. Quant. Elec*, 18, 1829-1830 (1982).

4. Shand.M.L; Lai.S.T,"CW laser pumped emerald laser" *IEEE J. Quant. Elec* (ISSN 0018-9197), 20 p.105-108,(1984).

5. S.A.Payne, L.L.Chase, L.K.Smith, W.L.Kway, and H.W.Newkirk "Laser performance of $LiSrAlF_6:Cr^{3+}$,*J. Appl. Phys.*,1851-1856 (1989).

6. S.A.Payne, L.L.Chase, and G.D.Wilke"Optical spectroscopy of the new laser materials, $LiSrAlF_6:Cr^{3+}$ and $LiCaAlF_6:Cr^{3+}$",*J.Luminesc Phys.*, vol 44,167-176 (1989).

7. Payne et al.,"$LiCaAIF_6:Cr^{3+}$: A Promising New Solid-State Laser Material," *J. Quant. Elect,*24(11), 2243-2252,1988.

8. Norman P. Barnes, "Transition-Metal Solid State Lasers," in *Tunable Lasers Handbook.*ed F. J. Duarte (San Diego: Academic Press, 1995).

9. C. H. Vilain, J. P. Foing and P. Schanne: *Dig. Conf. Advanced Solid-State Lasers*, *Opt. Soc. Am.* 99, 1995.

10. W. R. Rapoport and M. L. Shand: Solid State Commun, Elsevier, 84, 1992.

11. Shkadarevich, A. P., "Recent Advances in Tunable Solid State Lasers," *Opt. Soc. Amer.,* 5, 60-65, 198

12. A.J.DeMaria, W.H.Glenn Jr., M.J. Brienza, and M.E. Mack, " Picosecond laser pulses *", Proc. IEEE,* Vol. 57, pp. 2 (1969).

13. S.Chen, and J. Wang, "Self- starting issues of passive self-focusing mode-locking "*Optics Letters*, Vol. 16, 689, 1991.

14. T. Myint's thesis"Optical spectroscopic properties of active ion doped transparent glasses", January 25, 2010.

15. A. Seas'thesis"Generation of ultrashort pulses from the chromium-doped forsterite laser" (1984).

CHAPTER 2

INITIAL CHARACTERIZATIONS OF Cr^{4+}:Ca_2GeO_4 (CUNYITE) LASER

2.1. Introduction

Cunyite was discovered by IUSL and named after the City University of New York. It belongs to a crystal class called olivines that make up a large proportion of the earth's mantle. The name refers to the greenish color of the family members. The Cunyite crystal has the symbol Ca_2GeO_4. It was this crystal that played the role of the host lattice for the chromium ions to create the gain material for the experiments.

A broadband Cr: Cunyite laser is a very important light at both 1.3μm and 1.5μm for fiber characterization, time-resolved spectroscopy, and biomedical imaging. The tuning range of Cr^{4+}: Ca_2GeO_4 (Cunyite) lasers covers the important spectral range from 1348 nm to 1482 nm, which provides a minimal dispersion in optical fibers. The Cr^{4+}: Ca_2GeO_4 (Cunyite) laser eventually explores its applications for semiconductor characterisation, eye-safe ranging, medical, industrial and scientific research.

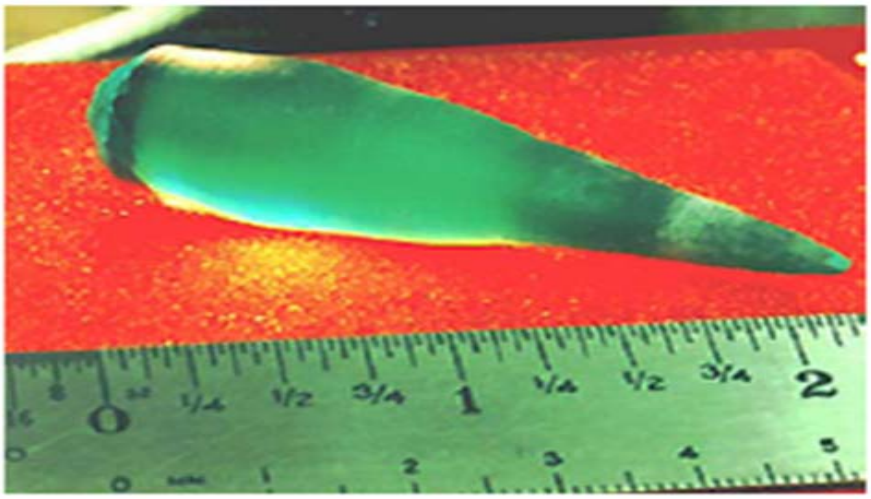

Fig2.1.1. Picture of a chromium-doped Cunyite crystal grown at City College of New York.

Chromium is a transition metal that can be used as a dopant in a host lattice to produce a practical gain medium. There are several possible gain materials that chromium plays a role in including Cr^{4+}: YAG, Cr^{4+}: forsterite, Cr^{3+}: LiSaf, Cr^{2}: ZnSe, Cr^{4+}: Cunyite, Cr^{3+}: sapphire. To be considered as suitable laser gain media, certain criteria such as chemical and mechanical stability, good heat conductivity, and a long upper state lifetime play an important role. The lasing action and the relationship between the energy levels of the lasing ion depend on the host medium. Host materials can include garnets, fluorides, germanates, silicate glasses and sapphire.

Figure 2.1.2.a. Color appearance of transition metal complexes

Since the first demonstration of laser operation with Cr^4:Ca_2GeO_4 (Cunyite) crystals [1] by (Petricevic et al. 1996), various approaches were developed to get shorter pulses with wider spectrum. Picosecond pulses were obtained by self-starting passively modelocking [2]. Three hundred sixty five femtosecond pulses at 100MHz repetition rate, the shortest pulse reported to date, were obtained by self-starting modelocking [3] with dispersion compensation by Double Chirped Mirrors (DCMs).

2.2. Cr^{4+}:Ca_2GeO_4 (Cunyite): a history

The discovery and subsequent development of Cr^{4+}:Ca_2GeO_4 (Cunyite) laser fills the void in the spectral region between 1300 and 1600 nm. Interest in the development of new lasers activated by Cr^{4+} ions followed the demonstration of Cr^{4+}:Ca_2GeO_4. Pulsed [4,] and continuous-wave [5,6] laser action was obtained over the 1335-1492 nm range

for laser pumping . The maximum slope efficiency of 5% was obtained for a 2.5% output coupler. Mode-locked operation of chromium-doped Cunyite laser was achieved using mainly self-starting passively mode-locking to generate 60-ps, 8.6ps respectively. Passive mode-locking Cr^{4+}:Ca_2GeO_4 (Cunyite) laser with intracavity group-velocity-dispersion compensation produces pulses as short as 365fs.

Lasing action in the Cr^{4+}: Cunyite gain material was first reported in 1997. Mode-locked operation of Cr^{4+}: Cunyite in the picoseconds domain (60ps pulses) was first achieved in 2000 using a SESAM. To achieve shorter pulses, passive techniques were used. Cr^{4+}:Ca_2GeO_4 crystals exhibit very large emission bandwidths and thus can generate sub-20-fs pulses, but their poor thermal properties and low emission cross-sections constitute a big disadvantage due to induced low gain and very strong thermal effects.

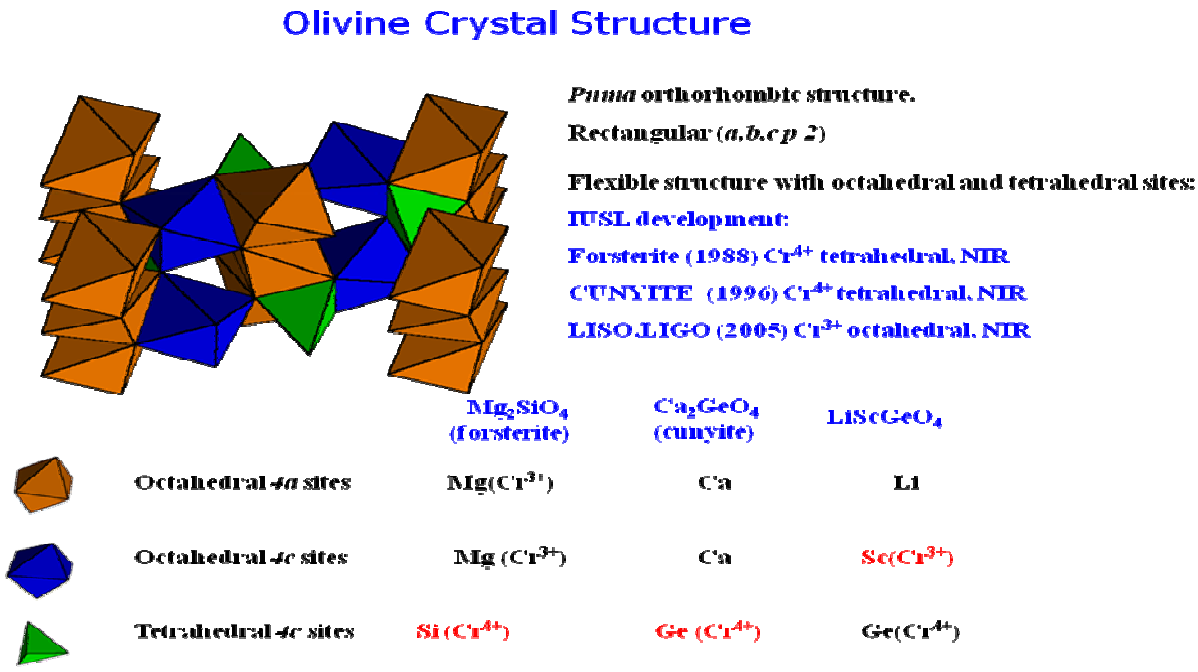

Fig2.2.1 shows the olivine crystal structure of octahedral and tetrahedral sites.

2.3. $Cr^{4+}:Ca_2GeO_4$ (Cunyite) as a laser gain material

Conventional oxide rare earth laser hosts are unsuitable for mid-infrared lasers due to their high rates of multi-photon quenching, so materials with low phonon energies are required. Tetravalent Germanate oxides such as Ca_2GeO_4 crystals offer low phonon energies but their highly hygroscopic nature makes them difficult to grow. The starting and stabilization of mode-locking operation in $Cr^{4+}:Ca_2GeO_4$ (Cunyite) laser are quite difficult compared to other solid-state lasers. Firstly, low thermal conductivity of $Cr^{4+}:Ca_2GeO_4$ (Cunyite) crystal induces strong thermal loading, which hinders stable mode-locking operation. Secondly, the low gain of Cr: Cunyite crystal makes it hard to get a lasing operation and the laser is sensitive to intra-cavity losses. In addition, low absorption coefficient requires longer laser crystals, and this induces large second-third-order dispersion which should be compensated over the whole wavelength region. Improvements in crystal growth and fabrication will lead to sub-20fs pulses.

2.4. Spectroscopic and laser properties of Cr-doped Ca_2GeO_4 (Cunyite) materials

In accordance with spectroscopic characteristics of Ca-based olivines, there no evidence of the presence of trivalent (Cr^{3+}) in Ca_2GeO_4 crystal materials.A feature of these doped Ca_2GeO_4 crystal is a relatively high concentration of tetravalent chromium(Cr^{4+}) due, at least in part, to favorable structure characteristics of Ca_2GeO_4 .It is believed that there are no suitable octahedral positions for trivalent chromium in the Ca_2GeO_4 structure because of the large ionic radius of Ca^{2+} in octahedral positions , as well as the ionic radius of Ge^{4+} in tetrahedral coordination is close to the ionic radius of Cr^{4+} at the same site occupation.

The unique spectroscopic property of Cr^{4+} :Ca_2GeO_4(Cunyite) is that in this crystal the lasing center is the tetravalent chromium Cr^{4+} that substitutes for tetrahedrally coordinated Ge_4. Chromium-doped Cunyite has shown that the Cr^{4+} ion in a suitable crystal can make an attractive laser source for the NIR spectral range. These novel tunable solid state lasers are expected to operate in the technologically important NIR region between 1-2μm.

Single crystals of Cr^{4+}:Ca_2GeO_4 (Cunyite) were grown successfully using the top-seeded solution growth technique from a high concentration solution in an RF(radio frequency)-heated Czochralsky crystal growth system at the City College of New York (CCNY) built by Thermal Technology Inc. A unit cell of Cunyite has four formula units in an orthorhombic structure of the space group Pbnm. The unit cell dimensions are a = 0.5240 nm, b = 1.1400 nm, and c = 0.6790 nm [7]. Because Cr^{4+} and Ge^{4+} have the same valence and similar ionic radii (0.041nm versus 0.039 nm), incorporation of the Cr^{4+} into the germanium tetrahedral site of Ca_2GeO_4 is likely. At the same time, octahedral Ca^{2+} is a much larger ion (0.1nm) than eitherCr^{3+} (0.0615nm) or Cr^{2+} (0.073 nm).

2.4.1. **Absorption Spectrum**

The absorption spectrum in the NIR region at 28 K shows strong polarization dependence. Forsterite and Cunyite are isomorphous and the polarized absorption spectra show a strong similarity. The lines 8340 cm^{-1} for E||b, at 8610 and 9980 cm^{-1} for E||c were assigned to the zero-phonon lines of three separate electronic transitions (1),(2),and(3) respectively. All other absorptions were assigned to vibrational sidebands of these zero-phonon lines. The three transitions (1),(2) and (3) are also observed in the

E||*a* spectrum, but with much smaller intensity. The absorption bands observed in the spectra are attributed exclusively to the transition of the Cr^{4+}-ion. The absorption spectra of the Czochralski-grown crystals used in the laser experiments show features identical to those of the flux-grown crystals, with an approximately fivefold increase of the absorption coefficient (α=2cm^{-1} for lightly doped material at 1064nm and α=10 cm^{-1} for highly doped crystals at 1064nm). The figure of merit of the highly doped Cr^{4+}: Ca_2GeO_4 (Cunyite) crystals for 1064nm pumping is estimated at >100, a factor of-5-increase over that of the flux-grown crystals.

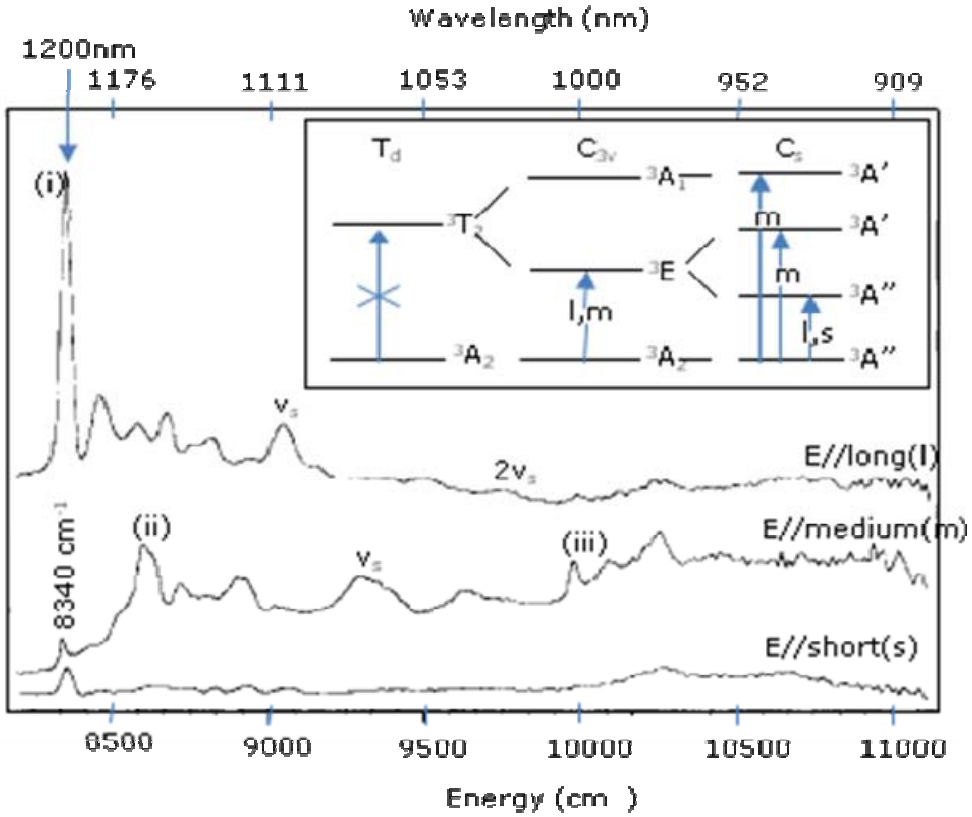

Figure 2.4.1(a) Polarized NIR single-crystal absorption spectra of Cr^{4+}: Ca_2GeO_4 at 28 K with *E* parallel to the crystallographic a, b, and c axes. The inset shows the energy levels and the polarization behavior of the electric dipole allowed transition associated with the

$^3T_2$ excited states of Cr^{4+}:Ca_2GeO_4 as the symmetry is lowered from T_4 through C_{3v} to C_s. Figure reproduced from Ref. [8].

The absorption spectrum is characterized by broad absorption bands spanning from the near ultraviolet to the NIR spectral regions and depend strongly on the polarization of the incident radiation with respect to the crystallographic axes of the host. In particular, the peak position of the strongest band in the red-green spectral region shifts considerably with the polarization. However, the luminescence transition shows a spectra blue-shift of 820 cm-^{1} between Cunyite and forsterite which is ascribed to the stronger field strength a Cr^{4+}: ion experiences when it substitutes for Si^{4+}rather than for Ge^{4+}. The average shift of the three $^3T_2$ components is 1150 cm-^{1}. The absorption and luminescence spectra were found to be very similar to those of Cr^{4+} doped forsterite, the only difference being a red shift of all spin allowed transitions of some 1300 cm^{-1}due to the smaller ligand field strength. The luminescence spectra are assigned to a transition from an excited triplet state, whichis definitely not mixed with ^1E contributions in Ca_2GeO_4.

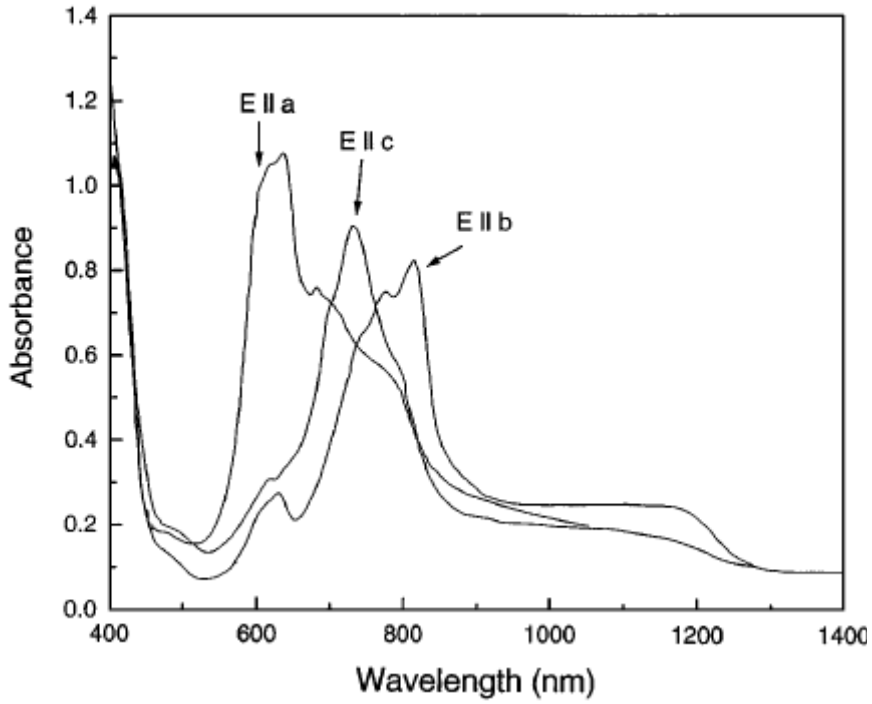

Figure 2.4.1(b) Polarized absorption spectra of Cr^{4+}:Ca_2GeO_4 for three different crystal orientations. Figure reproduced from Ref. [9,12].

2.4.2. Emission Spectrum

The fluorescence spectra were measured by exciting the Cr^{4+}: Ca_2GeO_4 crystals by a chopped 670-nm excitation from the Nd: YAG laser. The single band with a maximum at 1290 nm in the room-temperature emission spectrum of Cr^{4+}: Ca_2GeO_4 was attributed to Cr^{4+} indicating that in the crystal structure of Ca_2GeO_4 only the Cr^{4+} substitution take place. The emission is strongly polarized along the b axis of the crystal. The low-temperature emission spectrum of Cr^{4+}:Ca_2GeO_4 is characterized by a sharp zero-phonon line at 1200nm followed by a vibrational sideband similar to the low-temperature spectrum of Cr^{4+}:Mg_2SiO_4.The emission intensity of Cr^{4+}:Ca_2GeO_4 is at least five times greater than the Cr-ion in forsterite and an order of magnitude higher than that of Cr^{4+}: YAG for the same 670-nm pump power.

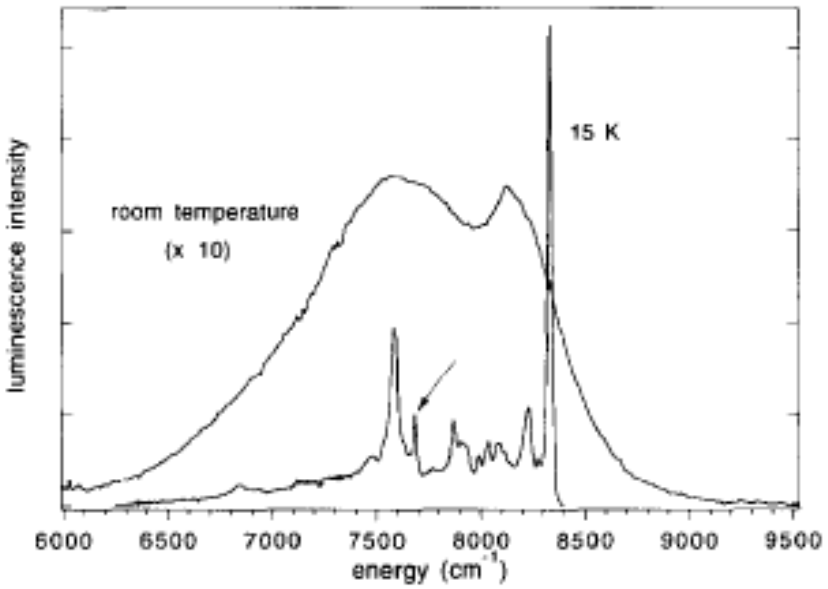

Figure 2.4.2(a) The unpolarized luminescence spectrum at 15 K of Cr^{4+}:Ca_2GeO4. Figure reproduced from Ref. [8].

Figure2.4.2.a. shows the unpolarized luminescence spectrum of Cr^{4+}:Ca2GeO4 at 15 K. The spectrum shows a sharp line at 8330 cm^{-1} and broader vibrational sidebands at lower energies. The integrated intensity of the sharp line relative to the total luminescence intensity amounts to 0.16. We also measure the polarized luminescence spectra for *E*||a and *E*||b. The spectral position and the band shape of the luminescence are identical for the un-polarized and the two polarized spectra. The intensity of the spectrum of *E*||b is about five times that of *E*||a, indicating that the luminescence transition is predominantly *E*||b polarized .The luminescence line at 7685 cm-^{1} (marked with an arrow in Fig2.4.2a) however showed no polarization behavior being equally intense in the *E*||a and *E*||b spectrum. High resolution luminescence spectra between 10 K and 33 K reveal a triplet splitting of the sharp luminescence line (see Fig.2.4.2b).The high resolution luminescence spectra in Fig.2.4.2.b was fitted to the sum of three Gaussians. Their

relative integrated intensities were found to agree approximately with the Boltzmann distribution, assuming equal oscillator strengths for the three transitions. These three luminescence lines coincide with the three components of the lowest lying origin (1) observed in the NIR transmission spectrum (see Fig.24.2.a). When the temperature is increased to room temperature the luminescence spectrum broadens to a band with a peculiar band shape on the high energy side (Fig2.4.2b).

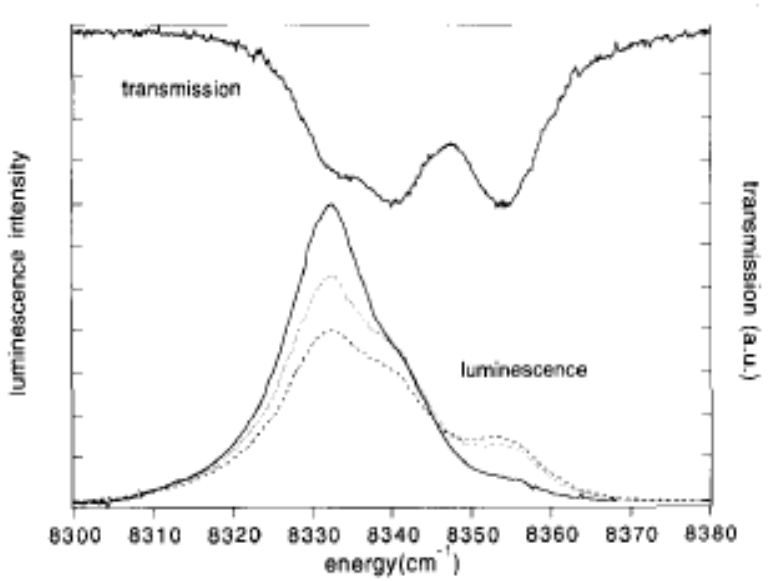

Figure 2.4.2(b) represents high resolution transmission spectrum of Cr^{4+}:Ca_2GeO_4 of single crystal at 20 K and high resolution luminescence spectra at various temperatures of the same compound. Luminescence intensity and transmission are both in arbitrary units 10 K; 20 K; 33K. Figure reproduced from Ref. [8].

2.4.3 Fluorescence lifetime of Cr^{4+}: Ca_2GeO_4 for 1064 nm excitation

The fluorescence lifetime of Cr^{4+} in Ca_2GeO_4 for 1064-nm excitation is ~5μs at room temperature for highly doped crystals grown by the pulling technique and 15μs for the flux-grown crystals. The latter lifetime is six times greater than that of Cr^{4+}: Mg_2SiO_4

(forsterite) (2.5μs) and four times greater than that of Cr^{4+}: YAG (4.1μs). At 8 k the fluorescence lifetime is 25μs.

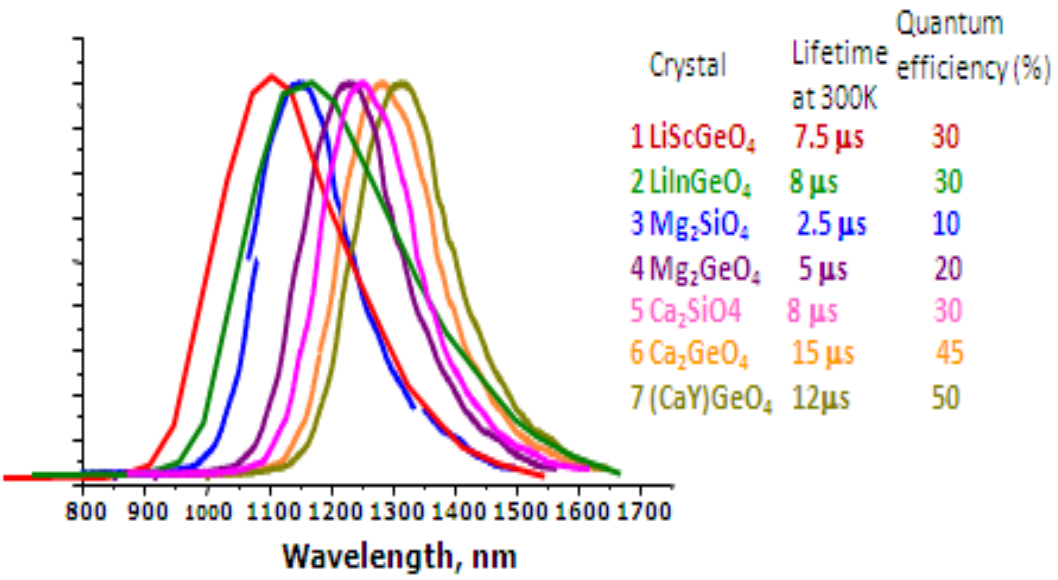

Figure 2.4.3 Comparison of fluorescence lifetimes among some key infrared tunable lasers. Figure reproduced from Ref. [10].

$$\tau(rad) = C \frac{\lambda^2}{n\left[\frac{1}{3}\left(n^2+1\right)\right]^2 f_{ij}^b}$$

In the equation above,C is a constant (1.5x 10^4 s m^{-2}), λ is the wavelength of the transition(1.2x 10^{-2} m), n is the index of refraction 1.73 and f^b_{ij} is the oscillator strength (6.6x 10^{-5} m). Inserting these values, we obtain τ(rad) = 68μs,which is to be compared to the measured (luminescence)decay time 25 μs.

2.4.4 Simplified Tanabe-Sugano diagram

The analysis of the absorption and fluorescence spectra of chromium-doped Cunyite provided conclusive evidence that the lasing ion for chromium-doped Cunyite is

100% Cr^{4+}**.** The absorption in the near infrared spectral region between 800 and 1200nm is due to transition between the ground state and the first excited state $^3T_2$ of the Cr^{4+} ion.

Three absorption bands are observed 630nm,740nm and 810nm due to the three spin allowed transitions between $^3A_2$ ground state and the $^3T_2(^3F)$,$^3T_1(^3F)$,and $^3T_1(^3P)$ excitedstates,respectively. Both transitions are already electric-dipole allowed in T_d symmetry.The transition to the lowest excited state, that is $^3T_2(^3F)$,is between 900 nm and 1200 nm [13,14].

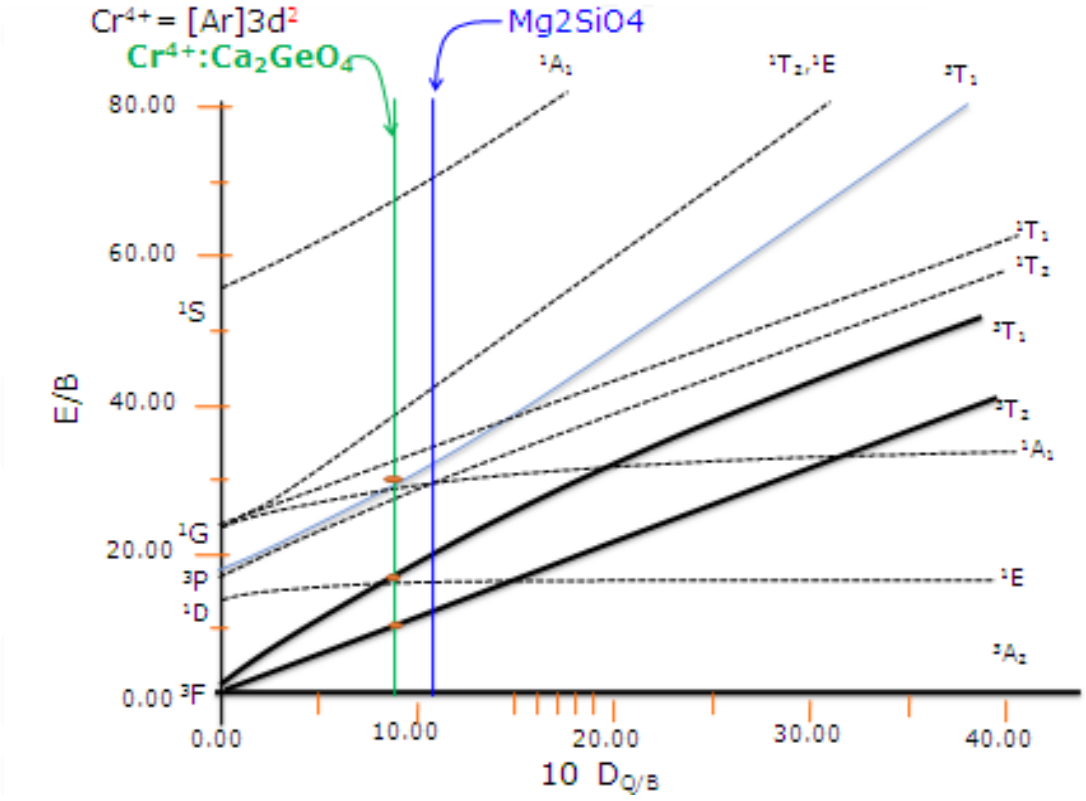

Figure 2.4.4(a) Simplified Tanabe-Sugano diagram of Cr^{4+}:Ca_2GeO_4.

2.5. Thermal Lensing and Loading

Cr^{4+}: Cunyite is an attractive laser material for biomedical and spectroscopic applications since it provides broad tunability from 1300 to 1600nm, operates at room temperature.Both 800-nm and 1-μm laser diodes, fiber, Ti: sapphire, and $1\,\mu$m neodymium lasers can be used for efficient pumping because of the large near-infrared shift of the absorption bands.To this end, its broad fluorescence spectra allow for generation of ultrashort pulses which have been obtained by self-starting passively modelocking techniques. With its favorable laser and spectroscopic properties, this laser material has many potential applications. A better understanding of the thermal loading and thermal conductivity of this laser crystal is necessary to optimize the laser design, particularly for high-power operation.

In solid-state gain media with relatively low heat conductivities, the inherent quantum defect associated with the optical amplification process gives rise to thermal effects induced by the heat load from the absorbed pump. The resulting degradation in power performance can occur in a number of ways. For example, solid-state lasers such as Cr^{4+}: Cunyite, Cr^{4+}: YAG, Cr^{4+}: forsterite experience deterioration in output power with increasing crystal temperature because of the enhancement of non-radiative processes that decrease the upper-state lifetime and cause a reduction in population inversion. Because such thermal effects [15,16] pose serious problems in power scaling and resonator stability, it is of paramount importance to determine accurately the amount of heat generation in the gain media in order to design the most optimum resonator configurations.

The Cr^{4+}:Ca_2GeO_4 (Cunyite) crystal suffers the most from lifetime thermal loading among solid-state crystals. Lifetime thermal loading mainly comes from the

degradation of upper-state lifetime by increasing the temperature and the poor heat conductivity of the crystal. Thermal loading reduces the population inversion and consequently increases threshold power for lasing. Further, it can induce thermal lensing effects in the laser crystal which can change the beam profile and power transmission in the laser cavity. Thus, it is helpful to examine the thermal characteristics of the Cr^{4+}:Ca_2GeO_4 (Cunyite) to determine the proper crystal length and absorption coefficient for best mode-locking operation.

Compared with the more widespread Ti: sapphire ultrafast technology, Cr^{4+}: Cunyite suffers several drawbacks such as poor thermal characteristics, low figure of merit, and fluorescence quenching.

The calculated figure of merit for highly doped Cr: Cunyite crystal is greater than 100. In the same way, figures of merit (FOMs) for other Cr-doped laser crystals can be obtained. The FOMs of Cr^{4+}: YAG, Cr^{3+}: LiCAF, Cr^{2+}: ZnSe are 29,740 and150, respectively. It is obvious that Cr: Cunyite has the most severe thermal loading.

The thermal loading inside the laser crystal can cause two main problems for mode-locking [17]. One problem is the thermal lensing which is caused by a change in refractive index of the crystal due to the change in temperature distribution. The other is the loss increase by thermal absorption in the cavity. Since the resonator condition is critical for critical mode-locking, these thermal effects have a strong influence on lasers.

Given a gain medium, heat conductivity (k), and heating fraction (η_h) are not changeable. The only controllable parameter is the pump absorption coefficient, α_{po}. It is obvious that too low or too high α_{po} causes problems because too low absorption cannot support lasing while too high absorption will give more severe thermal loading to the

crystal. Thus, it is important to find an optimal α_{po} which can absorb sufficient pump power for lasing and of which thermal loading does not damage stable operation.

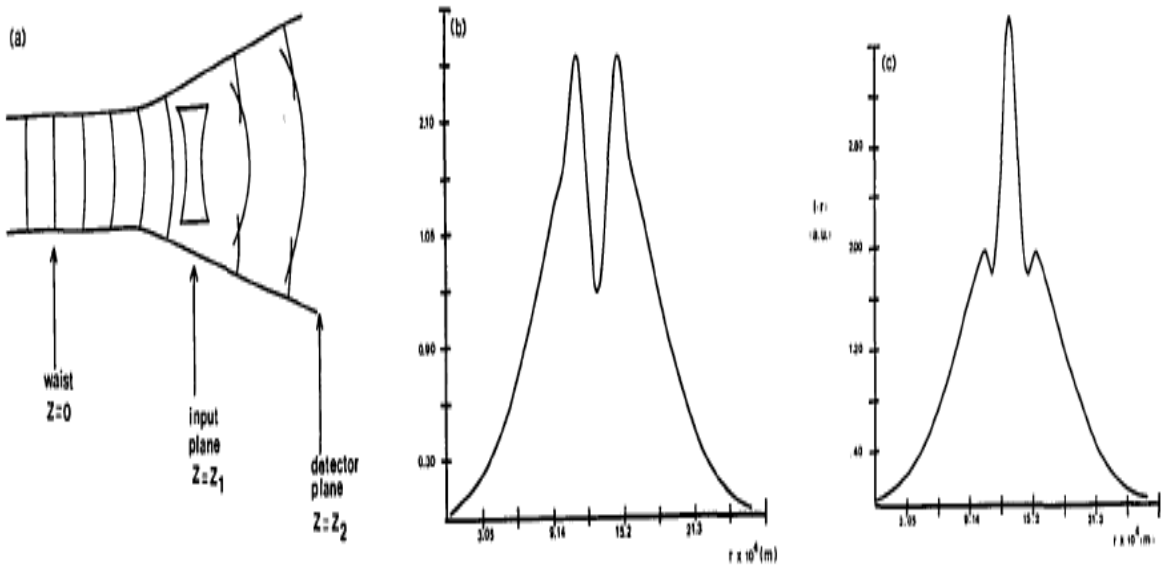

Figure 2.5(a) Schematic of mode mismatched thermal lens detection and tranverse intensity profiles computed from theory for the near field; (b) thermal defocusing; (c) thermal focusing. Figure reproduced from Ref. [18].

Laser-induced thermal lensing occurs as the result of heat dissipation in materials following light absorption by a Gaussian beam. Local heating near the beam axis produces a radially dependent temperature variation which changes the crystal's index of refraction by a factor of $\partial n/\partial t$, the temperature coefficient of the refractive index. This thermally induced refractive index profile is approximately parabolic near the beam axis.

2.6. The Cr^{4+}:Ca_2GeO_4 (Cunyite) laser cavity design

2.6.1. Cavity Design

A major part of the short pulse laser development is the cavity design .In designing a laser cavity there are many many aspects that must be considered prior to its construction. These include the stability of the cavity, the pump source, the mirrors that are to be used and the gain medium itself. The Cr^{4+}:Ca_2GeO_4(Cunyite) crystal is suitable for generating picosecond and femtosecond pulses around the 1430nm spectral region .This section will discuss the design of the continuous-wave(CW) operation around this crystal cavity and the details it entails.

A major consideration in building a Cr^{4+}: Cunyite laser is the low gain nature of the crystal. This dictates that there must be extremely good mode matching of the pump and laser beams.Due to the short upper lifetime of Cr^{4+}: Cunyite (~15 μm), a high intensity pump beam is required to provide and sustain a sufficient population inversion for lasing. To achieve this intensity a tightly focused pump beam size is essential .This can be achieved with appropriate focusing of a near-diffraction limited pump beam (M^2~1). There are a number of possible laser cavities that can be constructed but a four-mirror cavity was adopted as the most suitable option. The cavity determines the beam diameters and intensities at different locations. The resonator design is based on a four-mirror astigmatically compensated X-fold cavity, which allows a small spot size and consequently a high intensity in the laser medium and on the saturable absorber, as required for the mode-locking regime. Basic properties regarding the laser stability and the mode spot sizes in the cavity are derived using the matrix formalism. The large stability regions of this laser cavity design allowed for the simple insertion of intracavity

elements such as chirped mirrors or saturable absorbers. In this approach, the resonator modes are treated as Gaussian beams and the optical elements are described by using their ray-transfer matrices. The explicit forms of the matrices corresponding to the optical elements of the laser resonator, as well the stability criterion and the formula for the mode radius can be found in. It must be noted that some elements like a curved mirror or a plane plate arranged at Brewster angle are described by different matrices for the tangential and sagittal planes. Therefore the calculations must be carried out for both planes. A schematic of a typical four-mirror is shown in Fig. 2.6.1. The active medium is arranged between the two folding mirrors M1 and M2. The saturable absorber mirror is placed at the end of the cavity. The laser beam is focused on the saturable absorber mirror by the curved mirror M3. The asymmetric nature of the four-mirror cavity allows the spot size upon the saturable absorber and inside the crystal to be chosen.

The advantage of using an asymmetric laser cavity is that a tight focus exists at mirror M3. This enables saturable absorber devices placed at M3 to become optically bleached, allowing modelocking to be initiated. The spot size can be slightly altered on the saturable absorber by translating the device, changing the distance between M1 and M2, allowing for a range of incident fluences.The Brewster-cut cunyite crystal introduces astigmatism which is compensated by carefully chosen the angles of the two folding mirrors M1 and M2 that are placed at either side of the crystal. These also keep the intracavity beam focused inside the crystal for mode matching.

In designing the Cunyite laser, there are three main requirements that we take into account.

1) A good overlap between the pump beam and the laser mode in the active medium. The calculations show that the minimum mode size between the folding mirrors is proportional to their radius of curvature. To achieve a mode radius of 40 μm as the pump scheme was designed, 50-mm curved mirrors were found to be suitable.

2) A spot size on the saturable absorber mirror that results in an energy fluence should be larger than the saturable fluence of the device.

3) A very low divergence of the laser beam in the arm with the output coupler.

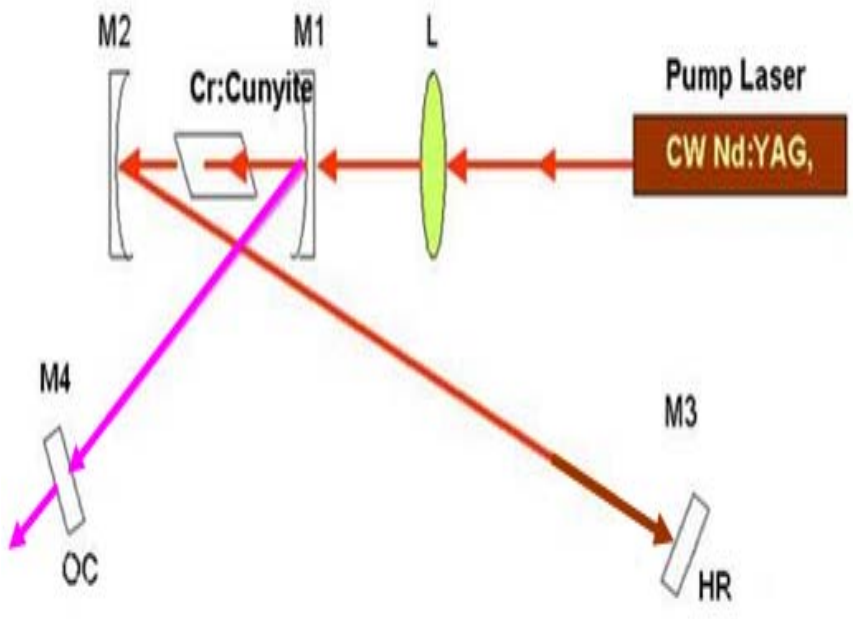

Figure: 2.6.1(a) Representative schematic of a typical four-mirror, astigmatically compensated cavity showing the beam mode size.

The experimental arrangement is shown in figurre 2.6.1. The Brewster -cut Cunyite crystal is placed in a four -mirror X-fold astigmatically compensated cavity. **M1:** Dichroic, curved mirror,1/2-inch with R>99.9% @ 1420 nm and T>90% @ 1064nm, RO C=50mm, **M2** , curved mirror , 1/2-inch with R> 99.9% @ 1064/1420nm, both high

reflecting. ROC=50 mm, **M3**, 1-inch flat mirror, R>99.9% @ 1064/1420 nm, high reflecting at both wavelengths, **M4-OC**: 1-inch flat mirror, R> 99.9% @1064nm and T =5% @ 1420nm.

Throughout this project the laser cavities described were designed using the ABCD matrix multiplication to calculate the mirror and crystal positions and orientations. The associated stability and mode size information for each cavity allow us to determine an appropriate spot size within the crystal and upon the saturable absorber device at M3. In our investigations, the spot size in the crystal was ~24 μm and the one at the output mirror 710μm for a 50-mm ROC cavity at 1.43 μm.

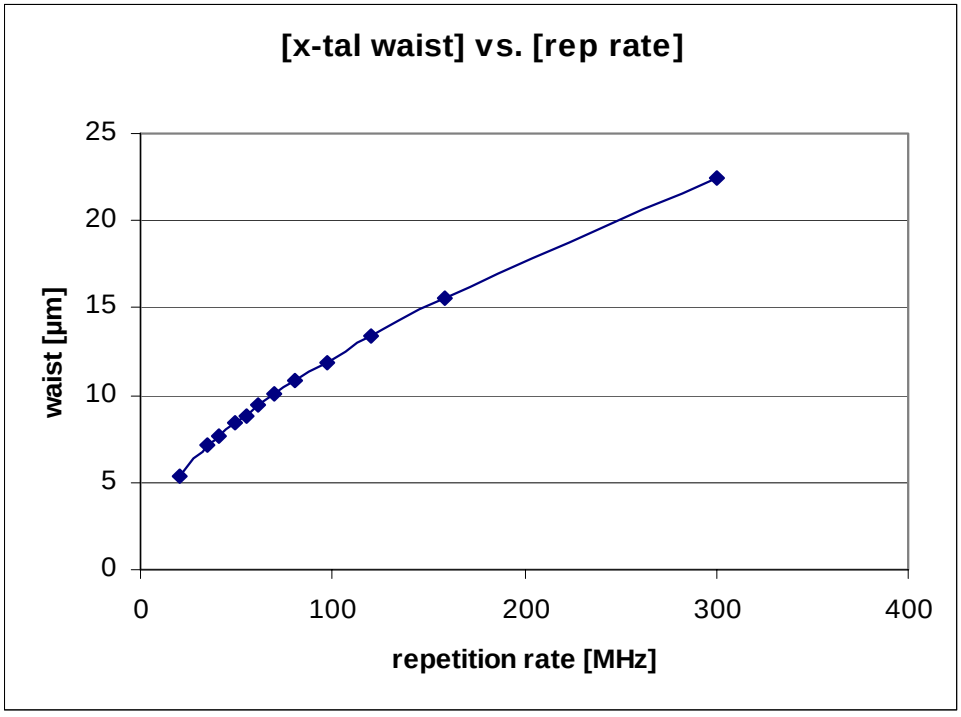

Fig. 2.6.1(b) .The variation of the crystal's beam spot size with increasing repetition rate.

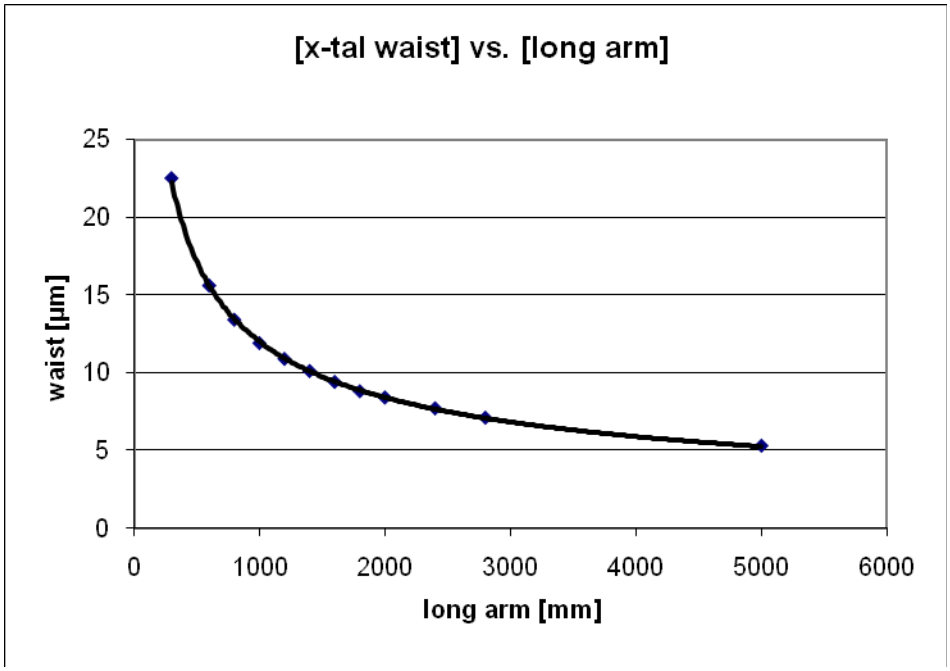

Fig2.6.1.(c) The variation of the crystal's beam spot size with increasing long arm's length.

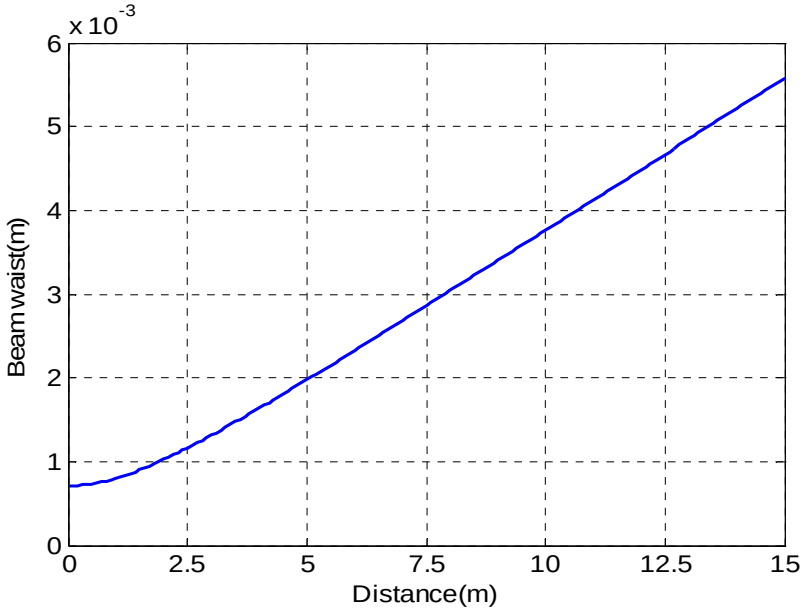

Figure 2.6.1.d: Cunyite laser Beam, λ_0=1400nm where the beam's spot size w_0 is located at the output mirror. It has the value of w_0=710µm. The beam waist w(z) as a function of distance (z) is plotted for the Cunyite laser.

Chromium-doped Cunyite has emerged as an important tunable solid-state laser in the near infrared. The quality of the laser crystal has been greatly improved making it a very reliable source in the near infrared. The most important physical, thermal, and optical properties of chromium-doped Cunyite as compared to Nd: YAG are summarized in Table 2.7.1. Following is table 2.7.2 which summarizes the spectroscopic and laser properties of Cr^{4+}:Ca_2GeO_4 versus Cr^{4+}:Mg_2SiO_4.

Table.2.7.1. Physical, Thermal and Optical properties of Cr^{4+}:Ca_2GeO_4 (Cunyite) and Nd: YAG lasers.

Property	**Nd:Yag**	**Cr^{4+}:Ca_2GeO_4(Cunyite)**
Chemical Formula	Nd^{3+}:$Y_3Al_2O_{12}$	Cr^{4+}:Ca_2GeO_4
Lasing Ion	Nd^{3+} in D_2	Tetrahedral Cr^{4+}
Emission Band	1064 nm	1300-1600 nm
Spontaneous Lifetime	230μs	5μs
Radiative Lifetime	550μs	15μs(300K)
Tuning Range	1064 nm	1350 nm-1500 nm
Surface Damage	> 3GW	>0.4 GW
Slope Efficiency	63%	21%(Pulsed),38% (CW)
Limiting Slope Efficiency	50%	55%(CW)
Stimulated Emission Cross Section	6.5x $10^{-19}cm^2$	8x $10^{-19}cm^2$
Moh's Hardness	8.5	4.5

Table 2.7.2.Physical, Thermal, and Optical Properties of Cr^{4+}:Mg_2SiO_4 and Cr^{4+}:Ca_2GeO_4

Chemical Formula	Cr^{4+}:Mg_2SiO_4	Cr^{4+}:Ca_2GeO_4
Melting Point	1890 °*C*	1900 °*C*
Mohs Hardness	7	4.5
Density	3.22 g/cm^3	3.8 g/ cm^3
Thermal Conductivity	8 W/m/K (300ºK)	0.03 W/m/K (300ºK)
Stimulated Emission Cross Section	$2x10^{-19}$ cm^2	$8x10^{-19}$ cm^2
RelaxationTime of Terminal Lasing Level	<10ps	<10ps
Spontaneous Fluorescence	2.7μs	15μs
Refractive index	1.637	1.7

Conclusion

In this chapter the characteristics of the Cr^{4+}:Ca_2GeO_4 (Cunyite) crystal as a suitable gain medium have been described. Its potential to be pumped by 800-nm and 1-μm laser diodes, fiber,Ti^{3+}:sapphire, and 1μm neodymium lasers have been highlighted.The reasoning behind the use of a four-element cavity was put forward. The different drawbacks such as poor thermal characteristics, low figure of merit, and fluorescence quenching that Cr^{4+}: Cunyite suffers were taken into consideration.

2.7. References

1. V. Petricevic, A. B. Bykov, J. M. Evans, and R. R. Alfano, "Room-temperature near-infrared tunable laser operation of (Cr^{4+}:Ca_2GeO_4) laser *Opt. Lett.*21,1750 1752(1996).

2. B. Xu, J. M. Evans, V. Petricevic, S. P. Guo, O. Maksinov, M. C. Tamargo, and R. R. Alfano, "Continuous-wave and passively mode-locked operation of a cunyite (Cr^{4+}:Ca_2GeO_4) laser*," Appl. Opt.* 39, 4975-4978 (2000).

3. Michelet Jeanty, V. Kartazaev, M. Sharonov, A.Bykov,and R.R.Alfano,"Ultrafast laser pulses from the chromium-doped cunyite laser" Accepted at *Opt. Comm* in November 19, 2010.

4. Petricevic .V, Bykov.A.B, Evans.J.M, Seas.A, Alfano.R.R.,"RoomTemperature CW and Pulsed Near-Infrared Tunable Laser Operation of Cr4+: Ca_2 GeO_4",*CLEO 97,OSA Technical Digest Series*,11 (1997) 425.

5. J. M. Evans, V. Petričević, A. B. Bykov, A. Delgado, and R. R. Alfano, "Direct diode-pumped continuous-wave near-infrared tunable laser operation of Cr^{4+}:$^{+}$:Ca_2GeO_4 and Cr^{4+}:Mg_2SiO_4," *Opt. Express*, 22, 1171-1173(1997).

6.M.Yu .Sharonov,S. Owen, A.B. Bykov, W. B.Wang , R. R. Alfano, "Optical properties of Cunyite(Cr^{4+}:Ca_2GeO_4)crystals co-doped with Er^{3+} ions" *Optics Comm*, Volume 209,Issues 1-3, 1 August 2002, Page 209-216.

7. R.W.G.Wyckoff. Crystal structures Vol. 4,2ndEd.(Interscience, New York 1968).

8. M.F.Hazenkamp,U.Oetliker,H.U.Güdel,U.Kesper and D.Reinen,"Absorption and luminescence spectroscopy of Cr^{4+}-doped Ca_2GeO_4.A potential near infrared laser

material", *Chemical Physics Letters*, Volume 233, Issue 4, 17 February 1995, Pages 466-470.

9. J. M. Evans, V. Petricevic, A.B. Bykov, and R. R.Alfano, "Continuous-wave all-solid-state laser operation of Cr^{4+}: forsterite and Cr^{4+}: Ca_2GeO_4 ," in *Diode Pumped Solid State Lasers: Applications and Issues,* Vol. 17 of 1998 OSA Trends in Optics and Photonics Series, M. W. Dowley, ed, (Optical Society of America, 1998), pp. 101.
10. T. Myint'sthesis"Optical spectroscopic properties of active ion doped transparent glasses", January 25, 2010.
11. Hazenkamp et al.,"Optical Spectroscopy of Cr^{4+}-doped Ca_2GeO_4 and Mg_2SiO_4," *Phys. Rev.*,53(5):2367-2377 (1996).
12. M.Yu .Sharonov,S. Owen, A.B. Bykov, W. B.Wang , R. R. Alfano, "Flux and characterization of Cr^{4+}: Ca_2GeO_4 crystals as a new near infrared tunable laser material", *Journal of Crystal Growth*,volume 211, Issues 1-4, 1 April 2000, Pages 295-301.
13. Güdel. H.U, Hazenkamp M. F, Huber.G.Kück.S"Excited state absorption measurements and laser potential of Cr^{4+}-doped Ca_2GeO_4", *Applied Physics B,* vol. 64 6 p.647-650.
14. T. Ishii,K.Ogasawara,I. Tanaka, U.Kesper and H.Adachi,"Absorption First-Principle Calculation of peak energies and intensities in optical absorption spectrun of Cr^{4+}-doped Ca_2GeO_4", In advanced solid-state lasers, *OSA Technical Digest Series* (Optical Society of America,2000).

15. A. Sennaroglu, A. Askar, and F. M. Atay, “Quantitative study of laser beam propagation in a thermally loaded absorber” *J. Opt. Soc. Am.* B 14, 356-363 (1997).

16. A. Sennaroglu, “Analysis and optimization of lifetime thermal loading in continuous wave Cr^{4+}-doped solid-state lasers”, *J. Opt. Soc. Am. B* 18 1578-1586 (2001).

17. A. Agnesi, E. Piccini, G.C. Reali, “Influence of thermal effects in Kerr-lens mode-locked femtosecond Cr^{4+}: forsterite lasers*”, Opt. Comm.* 135, 77-82 (1997).

18. J. F. Power, "Pulsed mode thermal lens effect detection in the near field via thermally induced probe beam spatial phase modulation: a theory," Appl. Opt. 29, 52-63 (1990).

19. R. Paschotta, “Beam quality deterioration of lasers caused by intracavity beam distortions*”, Opt. Express* 14 (13), 6069(2006).

20. N. Hodgson and H. Weber,“Laser Resonators and Beam Propagation”, Springer Series in Optical Sciences, Springer, Berlin (2005).

21. V. Magni,“Multielement stable resonators containing a variable lens”, *J. Opt. Soc. Am. A* 4 (10),1962 (1987).

CHAPTER 3: GENERATION AND MEASUREMENT OF SHORT PULSES

3.1 Introduction

Ultra-short light pulses are a rather unique and useful form of light, with widths ranging from a few picoseconds [ps] down to attoseconds [as]. Ultra-short laser pulses are a versatile tool in technological applications. They open up new area of research in ultrafast phenomena. The value of ultra-short pulse lasers lies in their time and frequency domain properties. In the time domain, the pulse train produced by a mode-locked laser consists of a broad spectrum of equidistant modes with a defined phase relationship. The short pulse duration is applied advantageously in picosecond and femtosecond spectroscopy. Ultra-short pulses also hold great promise for all-optical signal transmission and information processing, from ultra-high-bit rate solitonic fiber transmission systems to ultrafast all-optical computing.

Many laser-processing operations require much shorter pulses than conventional Q-switched pulses. Such pulses can be generated by the mode-locking technique. An understanding of this technique begins with an understanding of the structure of the oscillating modes in the laser resonator.

This chapter presents a brief review of mode-locking and the methods for measurement of ultra-short pulses. Section 3.2 briefly reviews the concept of modes in a laser resonator. The next section 3.3 analyzes the basics of mode-locking and the different methods employed in the generation of ultra-short pulses from Cr^{4+}:Ca_2GeO_4laser. Section 4 reviews the method of measuring short pulses.

3.2. Modes in a Laser Resonator

The light emitted by most lasers contains several discreet optical frequencies, separated from each other by frequency differences that can be associated with different modes of the optical resonator. It is common practice to distinguish two types of resonator modes: transverse and longitudinal [1,2,3]. Longitudinal modes differ from one another not only in their oscillation frequency but in their field distribution in a plane perpendicular to the plane of propagation. Longitudinal modes correspond to different resonances along the length of the laser cavity which occur at different frequencies or wavelengths within the gain bandwidth of the laser. Transverse modes, however, manifest themselves in the cross-sectional profile of the beam. They are considerably more difficult to analyze mathematically than are longitudinal modes, and resonators are usually designed with the intention of ensuring that higher order transverse modes do not occur.

To describe the electromagnetic field variations inside optical resonators, three indices are used to indicate the TEM modes- TEM_{mnq}, where q is the longitudinal mode order number and m and n are the transverse mode order number. Physically, the subscripts m, n, qspecify the number of times the electric (magnetic) field crosses the x, y, z axes respectively. TEM stands for transverse electromagnetic waves and the first two indices identify a particular TEM mode, where q describes the longitudinal modes. Therefore the index q which specifies the number of nodes along the axis will be high. The TEM_{10q} shows that the intensity goes through a minimum (falls to zero) once in the X direction and goes through no minimum in the Y direction. The TEM_{21q} indicates that there are two minima in the X direction and one in the Y direction. To determine the

location and amplitude of the peaks and nodes of the oscillation modes, it is necessary to employ higher-order equations [4,5] which involve Hermite polynomials. If rectangular symmetry is assumed, then the cross-sectional distribution E(x,y) of the transverse modes is given by the expression.

$$\mathbf{E}(x,y)= E_{m,n}\left[H_m\left(\frac{\sqrt{2}x}{\omega}\right)H_n\left(\frac{\sqrt{2}y}{\omega}\right)\right]e^{-\frac{x^2+y^2}{\omega^2}} \qquad 3.2.1$$

Where x and y are the transverse coordinates, m and n are the transverse modes, $E_{m,n}$ is a constant amplitude factor whose value depends on the field strength of the mode, and ω is the radius of the fundamental mode (m=0,n=0) at $\frac{1}{e}$ maximum amplitude.

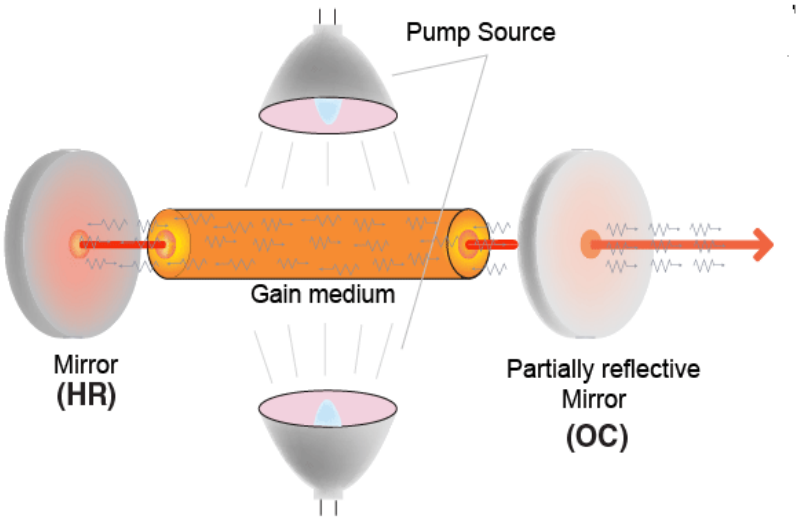

Figure 3.2.1 Simple two-mirror laser cavity.Figure reproduced from Shore Laser (Ref 27)

Thus, the fundamental mode of resonators is Gaussian with a1/e maximum amplitude. Figure 3.2.1 shows the x-variation of the field distribution and intensity distribution of order numbers; $H_m(\sqrt{2}\ x/w_0)$ and $H_n(\sqrt{2}\ y/w_0)$represent Hermite polynomials and w_0 is the characteristic mode width which depends on the wavelength of operation and the

resonator dimensions such as the mirrors' radii of curvature and the distance between them.

The fundamental transverse mode corresponds to m=0, n=0 for which we get some longitudinal modes.A simplified model for the longitudinal modes in a real laser is illustrated in Fig.3.2.2. The resonant frequency for a given longitudinal mode in a two-mirror laser resonator is determined by the expression.

$$v_{mnq}=\frac{c}{2L}\left[\left[(q+1)\frac{m+n+1}{\pi}\cos^{-1}\sqrt{\left(1-\frac{L}{R_1}\right)\left(1-\frac{L}{R_2}\right)}\right]\right] \qquad 3.2.2$$

q+1= number of half wavelengths of light across the resonator axis, m and n are the transverse mode order numbers, and R_1 and R_2 are the mirror radii of the laser resonator.

For a given transverse mode (given m and n) longitudinal modes with mode number differing by one are spaced in frequency by $\frac{c}{2L}$. If we assume that the laser operates in a single transverse mode, then

$$\upsilon_q \equiv q\frac{c}{2nL} \quad \text{or} \quad \omega_q \equiv q\frac{\pi c}{nL} \qquad 3.2.3$$

The difference in frequency between adjacent longitudinal modes can be estimated

$$\Delta\omega' \equiv \omega_{q+1} - \omega_q \equiv \frac{\pi c}{nL} \qquad 3.2.4$$

In a real laser the number of modes which can oscillate is limited by the bandwidth $\Delta\omega$ over which the laser gain exceeds the losses. The total number of oscillating longitudinal modes, m, can be estimated by $\frac{\Delta\omega}{\Delta\omega'}$

$$M=\frac{\Delta\omega}{\Delta\omega'}=\frac{\Delta\omega Ln}{\pi c} \qquad 3.2.5$$

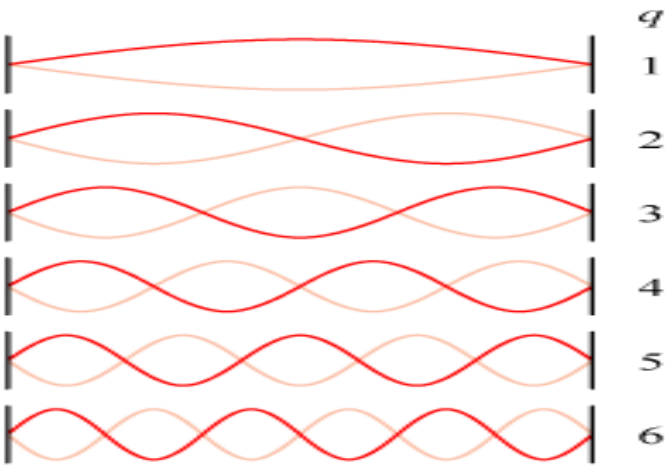

Figure 3.2.2 The first six longitudinal modes of a plane-parallel cavity.

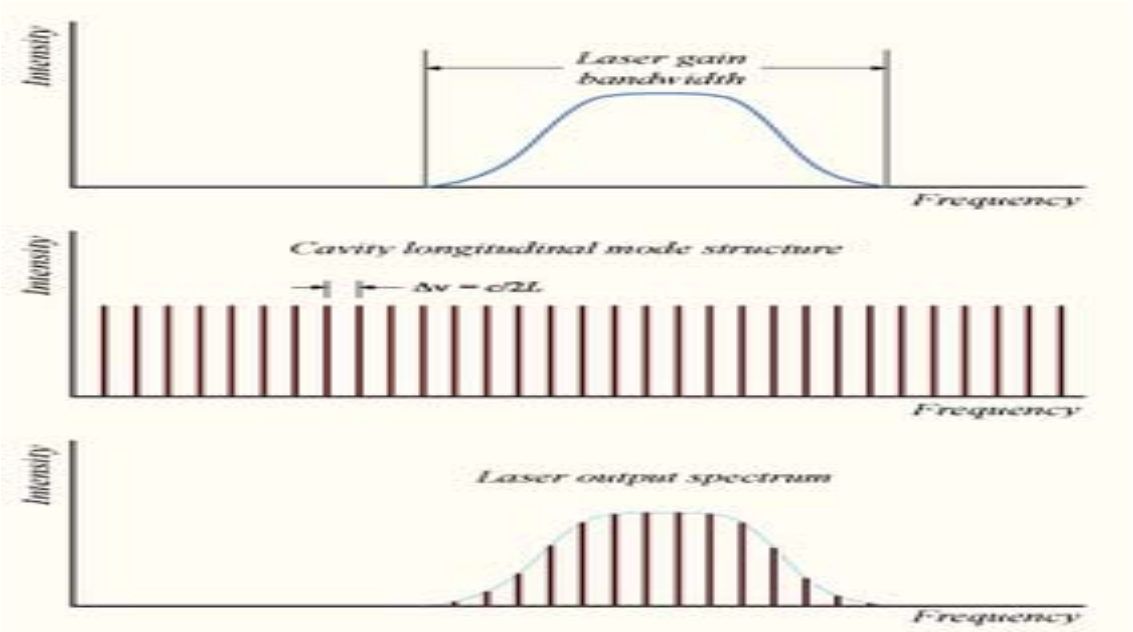

Figure 3.2.3 Allowed longitudinal modes in a laser cavity with gain medium.

3.3. Mode-locking

3.3.1 Basic Concept

Mode-locking is a common technique in optics by which a laser can be made to produce pulses of extremely short duration. Mode-locking [6] occurs when the modulation frequency corresponds to the cavity round-trip time. Both pulsed and continuous lasers can be mode-locked. In either case, mode-locking produces a train of pulses separated by the cavity round-trip time. Ultra-short light pulses are, in most cases, generated by mode-locked lasers. In some cases, a mode-locked laser is operated with several pulses circulating in the cavity. This mode of operation, called "harmonic mode-locking,"can be attractive for the generation of pulse trains with higher repetition rates.
At a given point inside the laser, the electromagnetic field can be expressed as the sum of the fields of all the various longitudinal modes. Thus, the field can be written as

$$E(t) \equiv \sum_{n} e^{-i[(\omega_0 + n\omega)t + \phi_n]} \qquad (3.3.1)$$

φ_n = phase of the n_{th} longitudinal mode, E_n= amplitude of the n_{th} longitudinal mode, and ω_0 = reference frequency.

$$T = \frac{2L}{c} \equiv \frac{2\pi}{\omega} \qquad (3.3.2)$$

One property of eq (3.3.1) is that E (t) is periodic in $T = \frac{2L}{c} \equiv \frac{2\pi}{\omega}$, which is the round-trip transit time inside the resonator. Note that the periodic property of E (t) depends on the fact that the phase $\varphi_n$are fixed. This is the so-called "mode-locked" technique proposed and demonstrated in the early history of the laser.

Assume that the phases φ_n are made equal to zero and that all of the oscillating modes have equal amplitudes ($E_{n=0}$).

$$E(t) = \sum_{-\frac{(N-1)}{2}}^{(\frac{N-1}{2})} e^{i(\omega_0 + n\omega)} \qquad (3.3.3)$$

$$E(t) = e^{i\omega_0 t} \frac{\sin(\frac{N\omega t}{2})}{\sin(\frac{\omega t}{2})} \qquad (3.3.4)$$

$$I(t) = \frac{\sin^2(\frac{N\omega t}{2})}{\sin^2 \frac{\omega t}{2}} \qquad (3.3.5)$$

Some of the characteristics of the mode-locked laser output are the following;

1. The individual pulse width, defined as the time from the peak to the first zero is

$$\tau_0 \equiv \frac{T}{N}. \qquad (3.3.6)$$

2. The number of oscillating modes can be estimated by $N \equiv \frac{\Delta\omega}{\omega}$. As well, $T \equiv \frac{2\pi}{\omega}$. Hence, we obtain

$$\tau_0 \equiv \frac{2\pi}{\Delta\omega} \equiv \frac{1}{\Delta\upsilon}. \qquad (3.3.7)$$

The length of the mode-locked pulses is approximately the inverse of the gain line-width.

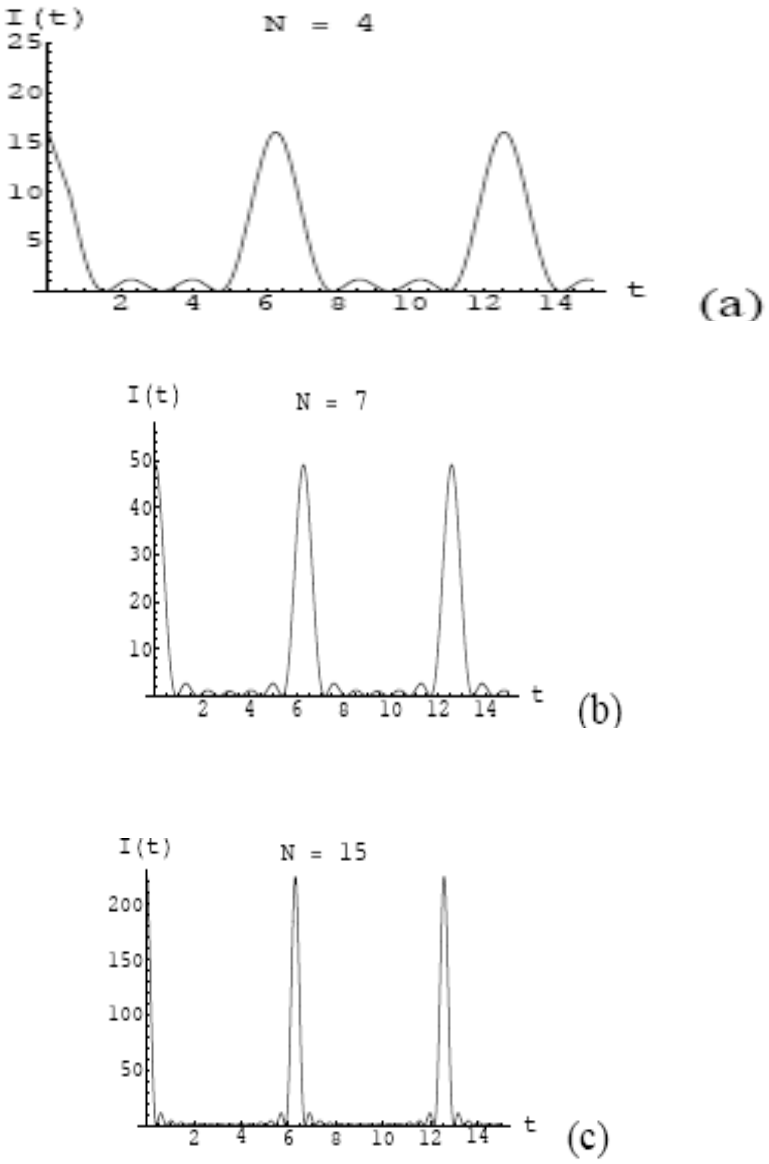

Figure 3.3.1 Intensity profile of a) 4 locked longitudinal modes, b) 7 locked longitudinal modes, c) 15 locked longitudinal modes.

Mode-locking means the phases of the different axial modes are aligned with one another. When the modes are locked, the laser produces pulses. To give rise to such an alignment, interaction between the modes is required. Interaction can be present either as

a result of driving (modulation) or by nonlinearity. These indeed are the two classes of techniques that are used for mode-locking: active and passive, respectively.

Some of the commonly used methods for mode-locking are: active mode-locking, synchronous-pumped mode-locking, Kerr-lens mode-locking, and self-starting passively mode-locking. In the following project, we discuss some details of active and passive mode-locking. A major enabling technology is the development of semiconductor saturable absorber mirrors (SESAMs) as intracavity laser elements to passively initiate and maintain the pulse generation process with a higher degree of stability than apply in Kerr-lens mode locking. The emphasis is on self-starting mode-locking, because such techniques clearly dominate in ultrafast optics.

3.3.2. Active modelocking

An actively mode-locked laser contains some kind of externally controlled modulator, in some cases acoustic-optical and sometimes electro-optical. The basic idea is to place an element in the cavity whose loss is externally modulated. Because the mode-locking frequency,in some cases acoustic-optical and sometimes electro-optical frequency, is set by an externally tuned source. This type of mode-locking is typically termed active [7, 8].

Active mode-locking has been studied by many scientists, but analytical expressions describing the transient effects that occur during the process of mode-locking are not possible due to the multimode nature of the problem. One of the most widely used theories has been presented by Kuizenga and Siegman, who considered the steady state theory of active mode-locking. In the analysis, Kuizenga and Siegman assumed that the resulting mode locked pulse has a Gaussian profile.

An optical pulse with a carrier frequency, ω_0, a complex Gaussian function and a linear chirp b is written in the form

$$E(t) = \frac{E_0}{2} e^{-at^2} e^{i\left(bt^2 + \omega_0 t\right)} \qquad (3.3.9)$$

ω_0 is the center frequency of the optical pulse, b is the linear frequency shift (chirp) during the pulse, and "a" is the term describing the envelope.

The instantaneous intensity I(t) of the Gaussian pulse can be written as

$$I(t) = E(t)\, E^*(t) = I_0 e^{-2at^2} \qquad (3.3.10)$$

$$\text{At FWHM, } I(t_1) = \frac{I_0}{2} \qquad (3.3.11)$$

$$\text{At } t = t_1, \text{ one obtains } \frac{1}{2} = e^{-2at^2} \qquad (3.3.12)$$

Taking natural logarithm of both sides

$$\ln 1 - \ln 2 = -at_1^{\,2} \qquad (3.3.13)$$

$t_1 = \frac{\Delta t_p}{2}$ and Δt_p are defined as FWHM of the pulse (3.3.14)

$$\text{Then } \ln 2 = 2a \frac{\left(\Delta t_p\right)^2}{4} \qquad (3.3.15)$$

$$\text{Hence } \Delta t_p \equiv \sqrt{\frac{2\ln 2}{a}} \qquad (3.3.16)$$

$$\text{The FWHM pulse duration is } \sqrt{\frac{2\ln 2}{a}} \qquad (3.3.17)$$

The complex amplitude of the optical pulse with linear frequency chirp is

$$E(t) = E_0 e\left(-at^2\right) e^{i\left(\omega_0 t + bt^{t2}\right)} \qquad (3.3.18)$$

Combining the linear and the quadratic terms in time of eq (3.3.18) becomes

$$\text{E (t)} = E_0 e^{-(a-ib)t^2} e^{i\omega_0 t} \qquad (3.3.19)$$

$$\text{Define } \gamma \equiv \alpha - i\beta \qquad (3.3.20)$$

The field amplitude becomes, $\text{E (t)} = E_0 e^{-\gamma t^2} e^{i\omega_0 t}$ (3.3.21)

To find the amplitude of the pulse in the frequency domain, one takes the Fourier transform of eq (3.3.21).

$$E(\omega) \equiv \int_{-\infty}^{\infty} \left(E_0 e^{-\gamma t^2} e^{i\omega_0 t} \right) e^{-i\omega t} \qquad (3.3.22)$$

The following integral may be useful $\int_{-\infty}^{\infty} e^{-(\alpha x^2 + \beta x)} dx \equiv \sqrt{\frac{\pi}{\alpha}} e^{\frac{\beta^2}{4\alpha}}$ (3.3.23)

$$\text{Where } \omega_0 - \omega \equiv a, \gamma \equiv b \qquad (3.3.24)$$

$$E(\omega) \equiv \sqrt{\frac{\pi}{\gamma}} e^{\frac{(\omega_0 - \omega)^2}{4\gamma}} \qquad (3.3.25)$$

Recall that $\gamma \equiv a - ib$ or $\frac{1}{\gamma} \equiv \frac{1}{a - ib} \equiv \frac{a + bi}{a^2 + b^2}$ (3.3.26)

$$\text{Again, } \frac{1}{4\gamma} \equiv \frac{a + ib}{4\left(a^2 + b^2\right)} \qquad (3.3.27)$$

Substituting this in equation (3.3.25), the frequency spectrum E(ω) associated with the pulse E (t) can be evaluated by taking the Fourier transform

$$E(\omega) \equiv E_0 \sqrt{\frac{\pi}{\gamma}} \left[a + \frac{ib}{a^2} + b^2 \right] e^{-\frac{(\omega - \omega_0)^2}{4}} \qquad (3.3.28)$$

Leaving only the real part in the exponential form, the intensity in the frequency domain

$$\text{becomes } I(\omega) \equiv I_0 \frac{a}{2\left(a^2 + b^2\right)} e^{-(\omega - \omega_0)^2} \qquad (3.3.29)$$

At the half power point $\omega_1 \equiv \frac{\Delta\omega}{2}$ (3.3.30)

$$I(\omega_1) \equiv \frac{I_0}{2}\frac{a}{a^2+b^2}e^{-(\omega-\omega_0)^2} \qquad (3.3.31)$$

$$\frac{1}{2} \equiv \frac{a}{2(a^2+b^2)}e^{-\frac{(\Delta\omega)^2}{4}} \qquad (3.3.32)$$

$$\ln 2 \equiv \frac{(\Delta\omega)^2}{4}\frac{a}{2(a^2+b^2)} \qquad (3.3.33)$$

The function for $E(\omega)$ is also a Gaussian function. The spectral width $(\Delta\omega_p)$ defined as the frequency between half power points is given by (Fig.3.3.3).

$$\frac{\Delta\omega}{2} \equiv \sqrt{\frac{a^2+b^2}{2a\ln 2}} \qquad (3.3.34)$$

If $\Delta\omega \equiv 2\pi\Delta\nu$, then $\pi\Delta\nu \equiv \frac{\Delta\omega}{2}$ (3.3.35)

$$\Delta\nu \equiv \frac{1}{\pi}\sqrt{\frac{a^2+b^2}{2a\ln 2}} \qquad (3.3.36)$$

Recall that $\Delta t_p \equiv \sqrt{\frac{2\ln 2}{a}}$ (3.3.37)

$$\Delta\nu\Delta t_p \equiv \frac{1}{\pi}\sqrt{\frac{2\ln 2}{a}}\sqrt{\frac{a^2+b^2}{a}2\ln 2} \qquad (3.3.38)$$

$$\Delta\nu\Delta t_p \equiv \frac{2\ln 2}{\pi}\left(\sqrt{\frac{a^2}{b^2}+1}\right) \equiv 0.44\left(\frac{b^2}{2a^2}+1\right) \qquad (3.3.39)$$

$$\Delta\upsilon\Delta t_p = 0.44 \qquad (3.3.40)$$

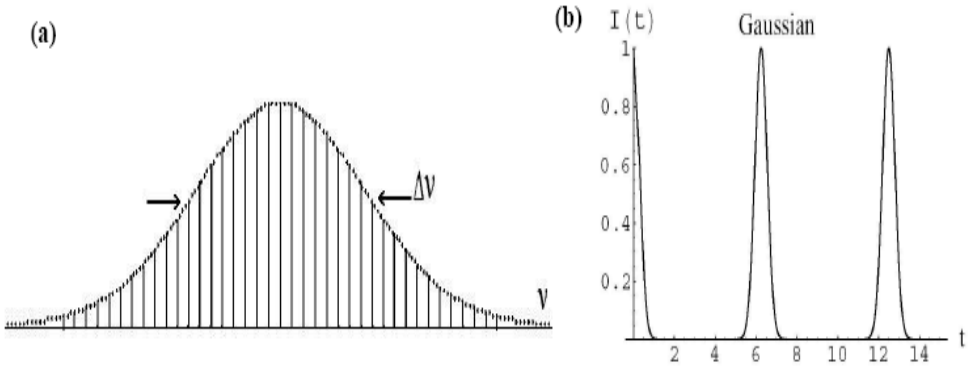

Figure 3.3.2.An output of a mode-locked laser in frequency and time domains.

3.3.3 Passive mode-locking

Passive mode-locking is the most widely used method of generating ultra-short pulses. This type of mode-locking is called "passive" since the phases of the longitudinal modes in the cavity are locked without the need of an external modulator. Rather, they use the light in the cavity to cause a change in some intracavity element, which will then itself produce a change in the cavity light. Passive mode-locking is achieved when a thin cell with a saturable absorber is placed within the cavity in contact with a totally reflecting mirror. Saturable absorbers are commonly liquid organic dyes, but they can also be made from doped crystals and semiconductors.

A saturable absorber is a medium whose absorption coefficient decreases as the intensity of light passing through it increases; thus it transmits intense pulses with relatively little absorption and absorbs weaks ones. When a saturable absorber is used to mode lock a laser, the laser is simultaneously Q-switched. For example, a saturable dye can mimic the fast shutters used for active mode locking provided that the pulse has a sufficiently large irradiance to allow it to saturate the absorber each time it passes through. The recovery time must be shorter than the roundtrip time; otherwise multiple

pulses could form. Initially, the laser medium undergoes spontaneous emission, which gives rise to random temporal fluctuations of the energy density. Some of these fluctuations may be amplified by the laser medium and grow in irradiance to such an extent that the peak part of the fluctuations is transmitted by the saturable absorber with little attenuation. Adjusting the concentration of the dye within the cavity may cause an initial fluctuation to grow into a narrow pulse traveling within the cavity, producing a periodic train of mode-locked pulses.

There are several methods of mode-locking. Two will be described: Kerr-lens mode-locking (KLM) and mode-locking where semiconductor saturable absorbers are employed to create intensity-dependent loss mechanisms. Both of these are classified as passive mode-locking techniques and rely on phase locking through amplitude modulation.

3.3.3.1 Kerr-lens mode-locking

Prior to 1991, a variety of mode-locking techniques had been applied to Ti: sapphire. These techniques included synchronous pumping, acousto-optic modulation, injection seeding, and additive pulse mode-locking. The only common feature was that the techniques were difficult. However in 1991, Spence et al. demonstrated a new mode-locking in Ti: sapphire. This technique described the first demonstration of Kerr-lens mode-locking [9,10,11] and demonstrated that the critical nonlinearity was produced solely by the Ti: sapphire crystal itself.

Since the first demonstration of a self-mode-locked Ti:sapphire laser in 1991 by Spence et al, the demonstration of ultra-short pulse generation, high power and large tunability from solid-state lasers is stimulating a new range of applications in

spectroscopy, telecommunications and biophotonics. The key to this development has been the demonstration of Kerr- Lens Mode-locking (KLM) in many of the commonly used solid-state systems. The passive mode-locked ultrashort pulse Ti: sapphire laser on which most current designs are based was developed by Spence, Kean, and Sibbet in late 1990.

Kerr-lens mode-locking (Spence et al.1991 of Ti: sapphire lasers produced the shortest laser pulses - pulses of less than 6fs duration directly from the laser cavity without any additional external cavity pulse compression. The mode-locking occurs due to the Kerr effect induced in the laser rod by the beam itself, hence, the alternative name, Kerr-lens mode-locking. Slightly shorter sub-5fs pulses have been demonstrated with external pulse compression and continuum generation together with parametric optical amplification. Above all, sub-5fs pulse generation techniques rely on the same three main components: Kerr effect, higher order dispersion control, and ultra-broadband amplification. KLM, however, has serious limitations because the mode-locking process is generally not self-starting and critical cavity alignment close to the cavity stability limit is required to obtain stable pulse generation. The shortest pulses generated to date all rely on chirped mirrors for dispersion compensation. A major limitation in the chirped mirror design arises due to the interference between light reflected at different penetration depths inside the mirror structure. This results in residual oscillations in the group delay dispersion (GDD) which ultimately limits pulse shortening.

Many researchers have analyzed self-mode-locking and the effects of the nonlinear index of refraction. They suggested that one of the key parameters in a self-mode-locked laser is the relative position of the gain medium with respect to the folding

mirrors (d_1, d_2). Other parameters that affect self-mode-locking is the aperture size, the gain medium thickness and nonlinear index of refraction, and the beam power.

The formation of the Kerr-lens causes the beam to undergo "self-focusing" when it passes through the medium. Since the degree of self-focusing [12, 13] is intensity-dependent, there exists the possibility of introducing an intensity dependent loss mechanism in the cavity. Mode-locking can then occur.

The major advantage of KLM is its inherently broadband nature. The process of self-phase modulation (SPM) [14,15,16] causes the spectral components to broaden, allowing access to oscillating bandwidths, and, as a result**,** shorter pulses to be formed. Indeed the shortest pulses, to date, have been generated from the KLM. However KLM is not usually self-starting and requires an initial noise perturbation. Also the laser requires critical cavity alignment and is susceptible to environmental perturbations. When dealing with low gain materials such as Cr^{4+}:Ca_2GeO_4 (Cunyite), the intra-cavity power instabilities can make starting and stabilization rather difficult. . For these reasons, and others, pure Kerr-lens mode-locking will likely be the direction of future projects.

Since "self-focusing" results in a spatial change of the beam, one method is to introduce an aperture or slit into the cavity. The size of the aperture is chosen so that a sufficiently self-focusing beam can pass through the aperture without attenuation, due to the smaller beam size, whilst a less focused beam will undergo attenuation due to diffraction losses. Refractive index experienced by the beam is greater in the center than at the edge.

Use of a physical aperture called a “hard aperture” can create an intensity-dependent loss mechanism that favors higher intensities. This mechanism acts like a fast saturable absorber.

The optical Kerr-lens effect will cause an intense pulse in the cavity to undergo self-focusing. The cavity is designed in such a way that continuous-wave operation is discouraged**.** This can only be achieved by means of hard aperture KLM where an intracavity slit is introduced to attenuate the continuous-wave (CW) beam or by soft aperture KLM where the pump beam geometry is chosen to favor mode-locked operation. The self-focusing effect of the mode-locked pulses brings the intracavity beam into a more favorable environment for lasing, either focusing through the aperture or increasing the mode matching between the pump and the intracavity beams. This acts as the intensity dependent gain mechanism to provide the modulation needed for mode-locking.

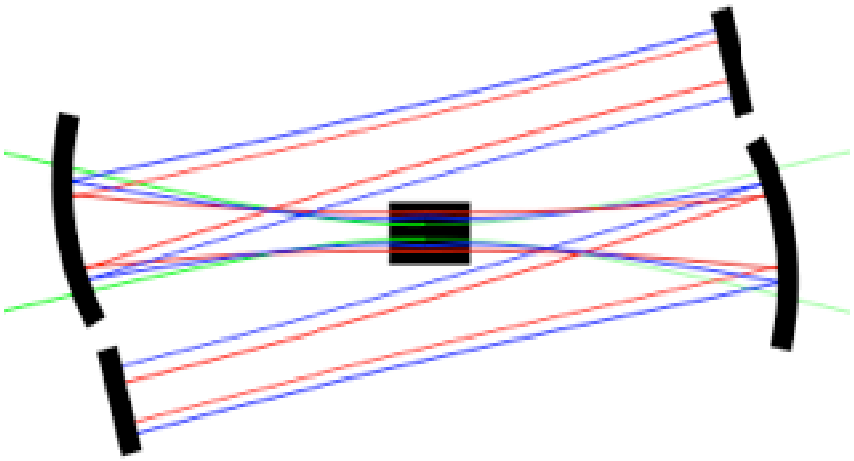

Figure .3.3.3.1(a) Soft aperture (KLM): Green =Pump, Blue = Pulse, Red= CW

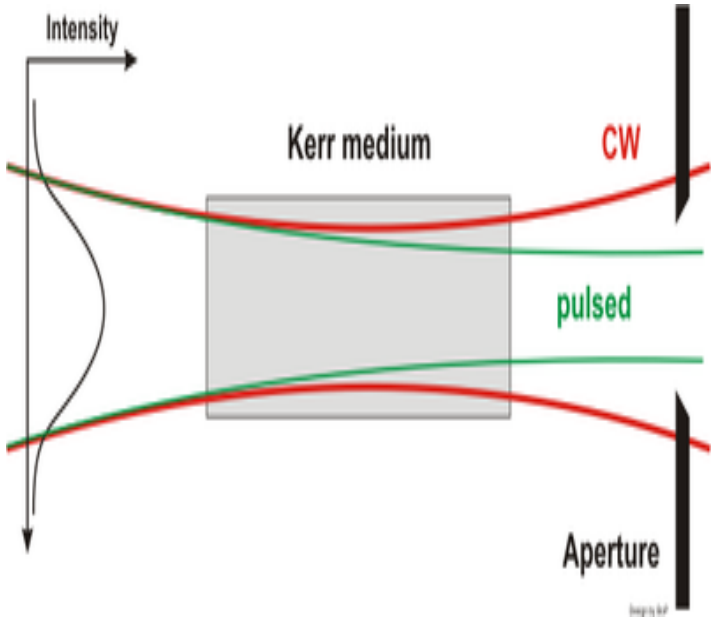

Figure 3.3.3 (b) Hard aperture Kerr-lens mode-locking

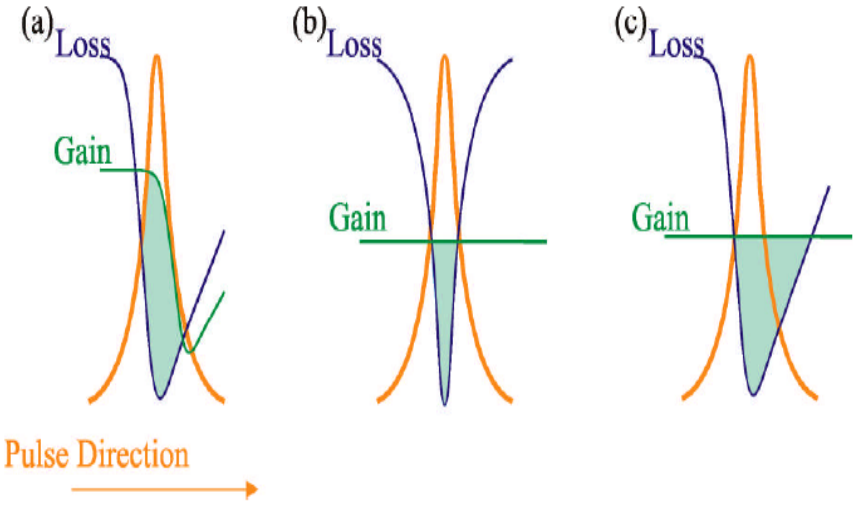

Figure 3.3.3.1(c) Passive mode-locking mechanism (i) Slow Saturable Absorption (SSA) (ii) Fast saturable absorption (FSA) (iii) Solitonic mode-locking. The blue colored area represents the net gain window.

3.3.3.2 Solitonic modelocking

The third technique is known as solitonic mode-locking. For solitonic mode-locking [17,18] the pulse shaping mechanism that leads to the mode-locked operation relies on the formation and propagation of soliton-like pulses. This is achieved by the careful balancing of the group velocity dispersion in the system with self-phase modulation. The mode-locked pulse train builds up from background noise spikes. An additional loss mechanism, at the cavity roundtrip frequency,is required to initialize the mode-locking and to stabilize the soliton. This loss mechanism can be active or passive but will typically take the form of a saturable absorber.

In solitonic mode-locking (figure 3.3.3.2.iii), the pulse is completely shaped by soliton formation, i.e. the interplay between the negative group velocity dispersion (GVD) and self-phase modulation (SPM). The absorber dynamics only stabilizes the soliton against the growth of "continuum"as the lost energy is called in soliton perturbation theory**.** This energy is initially contained in a low-intensity background pulse with a bandwidth much smaller than the bandwidth of the soliton. Therefore this pulse exhibits a higher gain and after a sufficient buildup time can reach the lasing threshold, destabilizing the soliton. The insertion of a saturable absorber in the cavity increases the losses experienced by the low-intensity pulse and will diminish in time. In the final stage of pulse formation, it is the soliton-like pulse shaping that locks the modes together. With this method, one can generate pulses which are considerably shorter than the recovery time of the absorber.

The pulse shaping is done solely by balancing group velocity dispersion (GVD) with self-phase modulation (SPM) at steady-state, with no additional requirements on the

cavity stability regime. Balancing is achieved through soliton formation. An additional loss mechanism such as a saturable absorber or an acousto-optic mode-locker is necessary to start the mode-locking process and to stabilize the soliton. The soliton loses energy for stable mode-locking. The main limitation for stable mode-locking is due to mode-locked Q-switching. In the steady state, both a soliton pulse and a low-intensity continuum background pulse exist inside the cavity. Without a saturable absorber the continuum experiences a higher gain than the soliton, because it only sees the gain at the line center, whereas the soliton experiences an effectively lower average gain because of its larger bandwidth. Thus, the continuum would grow and eventually de-stabilize the soliton. By introducing the saturable absorber we add high loss for the continuum but only negligible loss for the intense soliton pulse.

The need to compensate normal GVD in the laser, along with the balance of nonlinearity in soliton-like pulse shaping, underlies the presence of anomalous GVD in femtosecond lasers. With large anomalous GVD, soliton-like pulse shaping produces short pulses with little chirp. Some amplitude modulation is required to stabilize the pulse against the periodic perturbations of the laser resonator.

Figure 3.3.3.1(c) illustrates the three possible mechanisms that can give rise to femtosecond pulses. The short net gain window for mode-locking provided by slow saturable absorber (SSA) and fast saturable absorber (FSA) is not necessary in this case, as the soliton formation itself is the dominant mechanism for pulse shaping. This means that solitonic mode-locking can have a much longer gain window as shown in (Figure 3.3.3.2.iii). This allows saturable absorbers with much longer recovery times to be used, with recovery times of up to ten times the pulse duration being acceptable.

If we consider a saturable absorber with a recovery time that is long compared to the duration of the pulse, then we have a slow saturable absorber (SSA) mechanism. This causes the front of the pulse to be suppressed while the tail of the pulse will pass through without attenuation. Since the recovery time is slow, this method relies on a fast recovery of the gain saturation between pulses to create a "shutter" effect. The combination of a long recovery time of the absorber and the gain saturation provide a short net gain window for mode-locking, (Figure 3.3.3.2.a). For solid-state lasers the upper state lifetime is generally much longer than the pulse repetition frequency, so there is insufficient gain saturation for this process to take place. For mode-locking in solid-state lasers, other techniques such as fast saturable absorber mode-locking (FSA) and solitonic mode-locking [19] were contemplated.

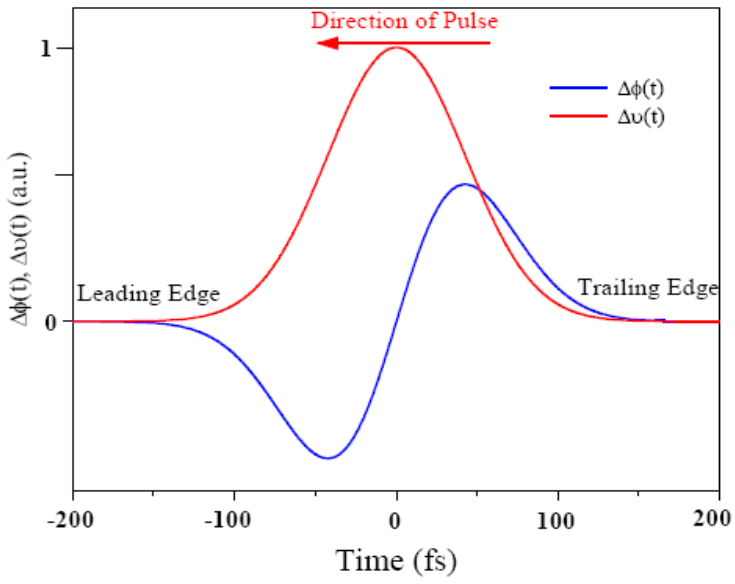

Figure 3.3.3.2 Phase $(\Delta\phi)$ and frequency $\Delta\nu$ shift undergoing self-phase modulation.

3.4. Time-bandwidth product or product of temporal and spectral widths of a pulse

To form the shortest pulse possible, the net dispersion of the cavity must be zero. When this condition is fulfilled, the spectral width of the pulse is given by the Fourier transform of its time-domain profile. This mathematically translates into $\Delta t.\Delta\nu \geq 1$, where $\Delta\nu$ is the pulse spectral bandwidth, Δt is the pulse duration and the precise value on the right-hand side depends on the definition of Δ. The minimum time-bandwidth product depends on the pulse shape. For a Gaussian pulse in time, the spectrum is Gaussian in frequency and when Δ is taken from the full width half- maximum (FWHM), the formula becomes $\Delta t.\Delta\nu \geq 0.441$.

The pulse is said to be bandwidth-limited (i.e. transform-limited) when the time-bandwidth product is at its minimum. For a $sech^2$ shaped pulse, the time-bandwidth product is $\Delta t.\Delta\nu \geq 0.315$. Bandwidth-limited pulses have the minimum possible time–bandwidth product, whereas chirped pulses have larger values. The condition of being at the transform limit is essentially equivalent to the condition of a frequency-independent spectral phase (which leads to the maximum possible peak power), and basically implies that the time–bandwidth product is at its minimum and that there is no chirp. Many mode-locked lasers can generate nearly bandwidth-limited pulses, particularly when they are based on soliton mode locking.

Optical bandwidth values may be specified in terms of frequency or wavelength. Due to the inverse relationship of frequency and wavelength, the conversion factor between gigahertz and nanometers depends on the center wavelength or frequency. For

converting a (small) wavelength interval into a frequency interval, we can use the equation.

$$\Delta\upsilon=c/\lambda^2\Delta\lambda \parallel E(t)\parallel^2 \qquad (3.9.1)$$

In addition, we characterize our lasers in the time-domain (with sampling oscilloscopes and autocorrelators) and in the frequency domain with optical spectrum analyzers. This two-domain approach allows us to better characterize our lasers performance and to ensure they operate at the peak of their capabilities.

The pulse duration is the full width at half maximum of the intensity profile of the pulse $\|E(t)\|^2$. The spectral width is the full-width at half maximum of the intensity of the pulse$\|E(\omega)\|^2$. If $\Delta\nu$ stands for the spectral width and $\Delta\tau$ stands for the pulse duration,$\Delta\nu\Delta\tau \geq 1/2$ relates them to each other.

A pulse is said to be Fourier-limited when $\Delta\nu\Delta t= k$, where k depends only on the pulse shape. In this case the phase temporal variation is linear and the pulse has the shortest possible duration. For a Fourier-limited Gaussian pulse $\Delta\nu\Delta t= 0.441$.Table 3.4.1.gives values of k for a few symmetrical pulse shapes.

Shape	**$E(t)/E_0$**	**K**
Gaussian	$e^{-\alpha t\hat{}2}$	0.441
Hyperbolic Secant	sech(t)	0.135
Lorentzian	$1/(1+\alpha^2t^2)$	0.142
Exponential	$e^{-\alpha t}$	0.14

Table.3.4.1 Values of k for various pulse shapes.

3.5. Measurement of Duration of Ultra-short Pulses

Femtosecond optical pulses provide a unique means for studying ultrafast processes associated with the interaction of light with matter. Implementation of these studies has required the development of new measurement techniques capable of femtosecond time resolution. In this thesis, we describe the various methods that are now available for characterizing femtosecond**.** Cr^{4+}:Ca_2GeO_4 laser pulses. Our emphasis here is not only on the relative advantages and limitations of the techniques themselves but also on the results of particular experiments. An understanding of these techniques is necessary for proper evaluation of any femtosecond experiment. At the same time, a better understanding of ultrafast processes leads to better measurement technique.

The advent of femtosecond lasers brought a new problem of measurement. Most electronic devices cannot measure transients much faster than about a nanosecond. The direct combination of a photodiode and an oscilloscope are no longer adequate to temporally resolve the ultra-short pulses generated. Although there are specialized electronic devices such as streak cameras that may be able to resolve 100fs transients in real-time, in most cases it makes more sense to look for alternative detection techniques. A variety of optical phenomena have been used to measure short pulses, including two-photon absorption, two-photon fluorescence**,** and second-harmonic or third-harmonic generation. Since it is not expected that direct electronic techniques are capable of measuring time durations down to 10^{-13}s, new measuring techniques [20] had to be found for the measurement of the time duration of sub-10-fs laser pulses. The techniques that are most frequently used are based on auto- or cross-correlation of two beams of femtosecond pulses. However, recently it has been shown that an LED based

measurement system can provide a much simpler and much more compact method of auto-correlating pulses. For sub-10-fs optical pulses, the use of a thin (≤ 25-μm) frequency doubling crystal is necessary to minimize the added dispersion and phase mismatch between the fundamental and the second-harmonic frequencies. Phase mismatch, in particular, can lead to a spectral filtering effect that can significantly distort the measured autocorrelation function. By use of the two-photon induced free-carrier generation in semiconductors, second-order autocorrelation measurements of sub-10-fs pulses should be obtained. A significant advantage of incorporating a semiconductor photodiode into correlation measurements is that the desired two-photon response and the transformation of light into electric current are combined into a single solid-state device.

Correlation techniques can be classified in a number of ways. The first, crosscorrelation [21, 22], is when one or more separated signals are correlated. The second is autocorrelation where an incoming beam of pulses is split into two. One beam travels through an optical path with a fixed length, the other through a path that includes an optical delay line. An optical delay line simply consists of a reflector mounted on a motorized translation stage. Both beams are focused in a nonlinear crystal such as BBO (β-barium borate), KDP (potassium dihydrogen phosphate) in order to produce second harmonic radiation. These crystals have the necessary properties of being strongly birefringent (necessary to obtain phase matching). Phase matching in the crystal is used to produce a beam at the second-harmonic frequency in which one photon has been taken from one beam and one from the other.

Using this method, two beams must overlap in time and space. Both beams originate from the same source, a single Ti: sapphire beam. This single beam is passed through a beam-splitter that reflects 50% and transmits 50% as seen below.

The portion of the beam that is allowed through the splitter unimpeded is then reflected from a single mirror that then reflects it towards the crystal. This beam's path is a set path that must remain constant in length throughout the experiment. The second beam path is not constant in length. After reflection, the second beam is reflected on a series of mirrors that direct it to a reflector that is mounted on a translation stage. A retroreflector uses a series of angled mirrors to reflect an incoming beam in the opposite direction as shown in Figure 3.5.1.

3.5.1. Intensity Autocorrelator

The intensity autocorrelation was the first attempt to measure an ultra-short pulse's intensity versus time. Early on (1960's), it was realized that there existed no shorter event that could be used to measure an ultra-short pulse than itself, and the autocorrelation is what results when a pulse is used to measure **.** It involves splitting the pulse into two, variably delaying one with respect to the other, and spatially overlapping the two pulses in some instantaneous non-linear optical medium**,** such as a second-harmonic-generation (SHG) crystal. A second harmonic crystal will produce "signal light" with a field envelope that is given by:

$$E(t) = E_1(t) = E_2(t) \qquad (3.9.1)$$

Where $E(t) = E_0(t)\, e^{i(\omega t+\varphi)}$

The second harmonic radiation generated in the crystal is proportional to

$$E_{2\omega}(t) \propto [E(t) + E(t-\tau)]^2 \qquad (3.9.2)$$

The second harmonic (2ω) pulse generated by the crystal is incident on a slow detector whose output current is integrated over a length of time compared to the optical pulse duration.

The output signal $A_d(\tau)$ generated by the detector is then given by

$$A_d(\tau) = \int_{-\infty}^{+\infty} [E_{2\omega}(t)]^2 \, dt \qquad (3.9.3)$$

$$= W_{2\omega}(1 + 2G^{(2)}(\tau) \qquad (3.9.4)$$

$W_{2\omega}$ is the second harmonic pulse energy and $G(\tau)$ is the autocorrelation function of the pulse intensity, which can be expressed as follows :

$$W_{2\omega} = \int_{-\infty}^{+\infty} E^4(t) \, dt \qquad (3.9.5)$$

and

$$G^{(2)}(\tau) = \frac{\int_{-\infty}^{+\infty} E^2(t)E^2(t-\tau)dt}{\int_{-\infty}^{+\infty} E^4(t)} \qquad (3.9.6)$$

The recorded signal $A_d(\tau)$ can also be expressed in terms of intensity as

$$A_d(\tau) = 1 + 2\frac{\int_{-\infty}^{+\infty} I(t)I(t-\tau)dt}{\int_{-\infty}^{+\infty} I^2(t)dt} \qquad (3.9.7)$$

In the case of a well- behaved ultra-short coherent light pulse of duration τ, we have $\tau = 0$, $A_d(\tau = 0) = 3$, $A_d(\tau \geq \infty)$, $A_d(\tau) = 1$. Equation (3.9.6) represents the autocorrelation signal when all of the second harmonic radiation is recorded by the **p**hotomultiplier tube (PMT). It is possible to design the autocorrelator in such a way that only the second harmonic radiation generated by the combined action of the two beams is

recorded (Figure.3.5.1). This type of autocorrelator is termed background free and the recorded signal is proportional to the output signal generated by the detector.

$$A_d(\tau) = \frac{+\int_{-\infty}^{+\infty} I(t)I(t-\tau)dt}{\int_{-\infty}^{+\infty} I^2(t)dt} \qquad (3.9.8)$$

In the case of the background free autocorrelators, the recorded signal has a peak to background ratio of 1 to 0 since for $\tau = 0$, $A_d(\tau) = 1$, and when τ is large enough so that no overlap between $E_1(t)$ and $E_2(t)$ exists, $A_d(\tau) = 0$.

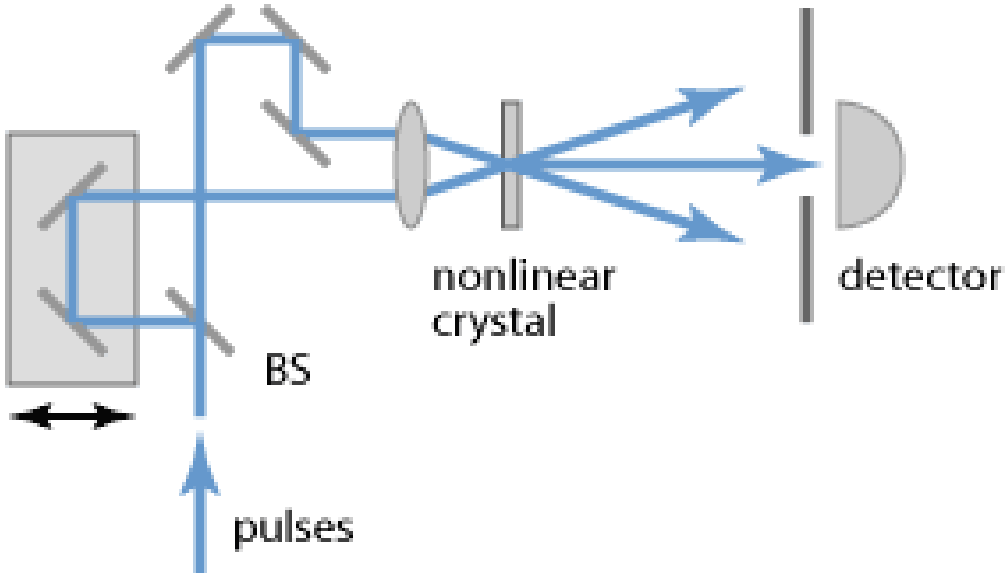

Figure 3.5.1 Experimental layout of an intensity autocorrelator. BS = beam splitter.

Figure 3.5.1 shows experimental layout for an intensity autocorrelator using second harmonic generation. A pulse is split into two, one is variably delayed with respect to the other, and the two pulses are overlapped in a second harmonic crystal. The second harmonic pulse energy is measured versus delay, yielding the autocorrelation trace.

In the case of the background free autocorrelators, the recorded signal has a peak to background ratio of one to zero since for $\tau = 0$, $A_d(\tau) = 1$, and when τ is large enough so that no overlap between $E_1(t)$ and $E_2(t)$ exists, $A_d(\tau) = 0$.The output is the intensity autocorrelation. No phase information is contained within intensity correlation and so does not reveal whether the pulse is chirped or not.

3.5.2 Interferometric Autocorrelator

A better method for detecting chirp is the measurement of an interferometric autocorrelation and is taken by overlapping the two input beams. The correlation signal oscillates at frequencies corresponding to the laser fundamental and second harmonic .Since the second-harmonic intensity is proportional to the square of the incident intensity, the detected second-harmonic intensity as a function of delay.

$$(A_i\,\tau) = \int_{-\infty}^{+\infty} |\{[E_0(t)\exp[i(\omega t + \varphi t)] + E_0(t-\tau)\exp i[\omega(t-\tau) + \varphi(t-\tau)]\}^2|^2\,dt \qquad (3.9.9)$$

Information regarding chirp is present with interferometric autocorrelation. The presence of chirp will distort the autocorrelation. If the time delay is set to zero in equation (3.9.9), the intensity is given by

$$A_i(0) = \int_{-\infty}^{+\infty} 2^4\ E_0(t)\,dt \qquad (3.9.10)$$

The autocorrelation signal corresponds to the coherent superposition of the two electric fields and the recorded signal is maximal. The second order autocorrelation is capable of distinguishing between transform-limited and chirped pulses. A second harmonic crystal is used to measure the second order autocorrelation function. If the time delay is set at half the light period, the two electric fields add destructively and the

resulting signal is almost zero . As a result of the constructive and destructive addition of the two fields every half period, the recorded signal is bounded by the pulse envelope (see Fig.3.5.2). In the case of chirped pulses, the center of the pulse contains different frequencies than the wings of the pulse. The constructive and destructive interference between the two fields lasts as long as the time delay is smaller than the coherence time of the pulse after which the interferometric autocorrelation merges with the intensity autocorrelation.

Assuming a linearly chirped Gaussian pulsewith unity amplitude

$$E(t) = \exp(-t^2/2T^2)\cos(\omega t + bt^2/T^2) \qquad 3.9.11$$

The interferometric autocorrelation can be written

$$A_i(\tau) = 1 + 4\exp[-(3+4b^2)\tau^2/8T^2]\cos(\omega t)\cos(b^2\tau^2/2T^2)$$
$$+\exp[-(1+4b^2)\tau^2/2T^2]\cos(2\omega t) + 2\exp(-\tau^2/2T^2) \qquad 3.9.12$$

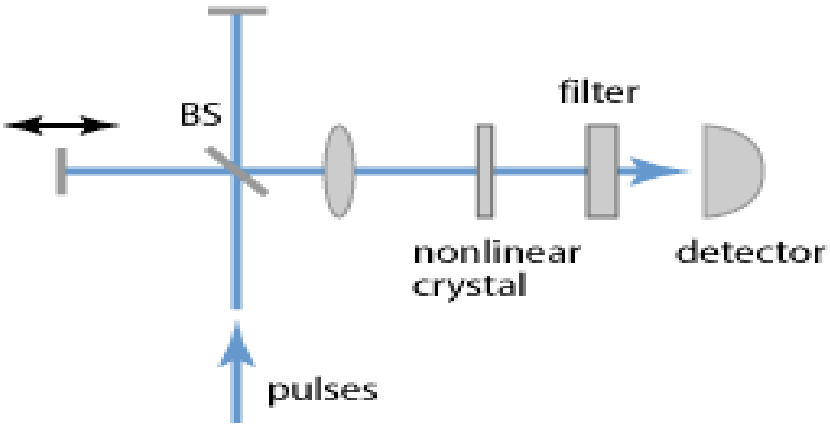

Figure 3.5.2.1shows the setup of an interferometric autocorrelator. BS = beam splitter.

Numerical calculations were carried out using eq.3.9.10 assuming a Gaussian pulse with FWHM of 10fs where the corresponding spectrum is centered at 800nm and for different values of the chirp parameter b. Figure 3.5.2 shows the interferometric

autocorrelation of a Gaussian pulse for three values of the dimensionless chirp parameter b: a) b=0, b) b=1 ,c) b=1.5. The dashed line is the envelope function and is calculated by replacing $\omega\tau$ in equation equation (3.9.11) by 2π for the upper envelope and π for the lower envelope.

When the pulse has no chirp (b=0) all the fringes in the interferometric autocorrelation are resolved since the field is coherent throughout the pulse. As the chirp parameter increases ($b \neq 0$) the field becomes incoherent at the wings of the pulse, and no interference is possible at the wings. The signal merges with the intensity autocorrelation for time delays exceeding the coherence length of the pulse as illustrated in Figure 3.5.2.

In the calculations it was assumed that the pulse possessed linear chirp. The situation varies unpredictably if more complicated forms of phase distortions are present in the pulse. The interferometric autocorrelation provides information on the presence of chirp but gives no indication of the shape of the chirp. In the case of an unchirped pulse, the interferometric autocorrelation can be used to estimate the pulse width by assuming a form of the pulse and by fitting the upper and lower envelope of the autocorrelation.

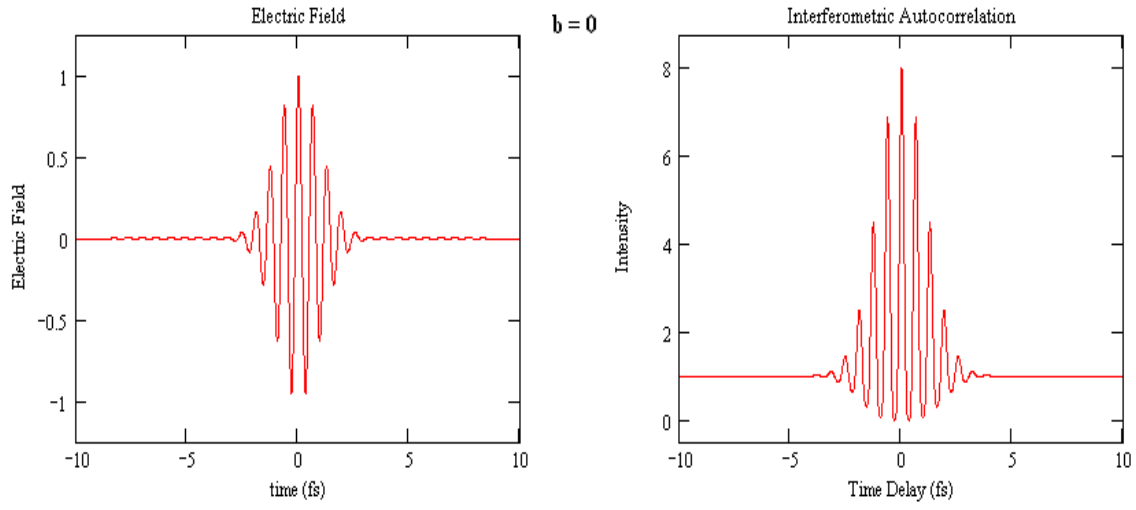

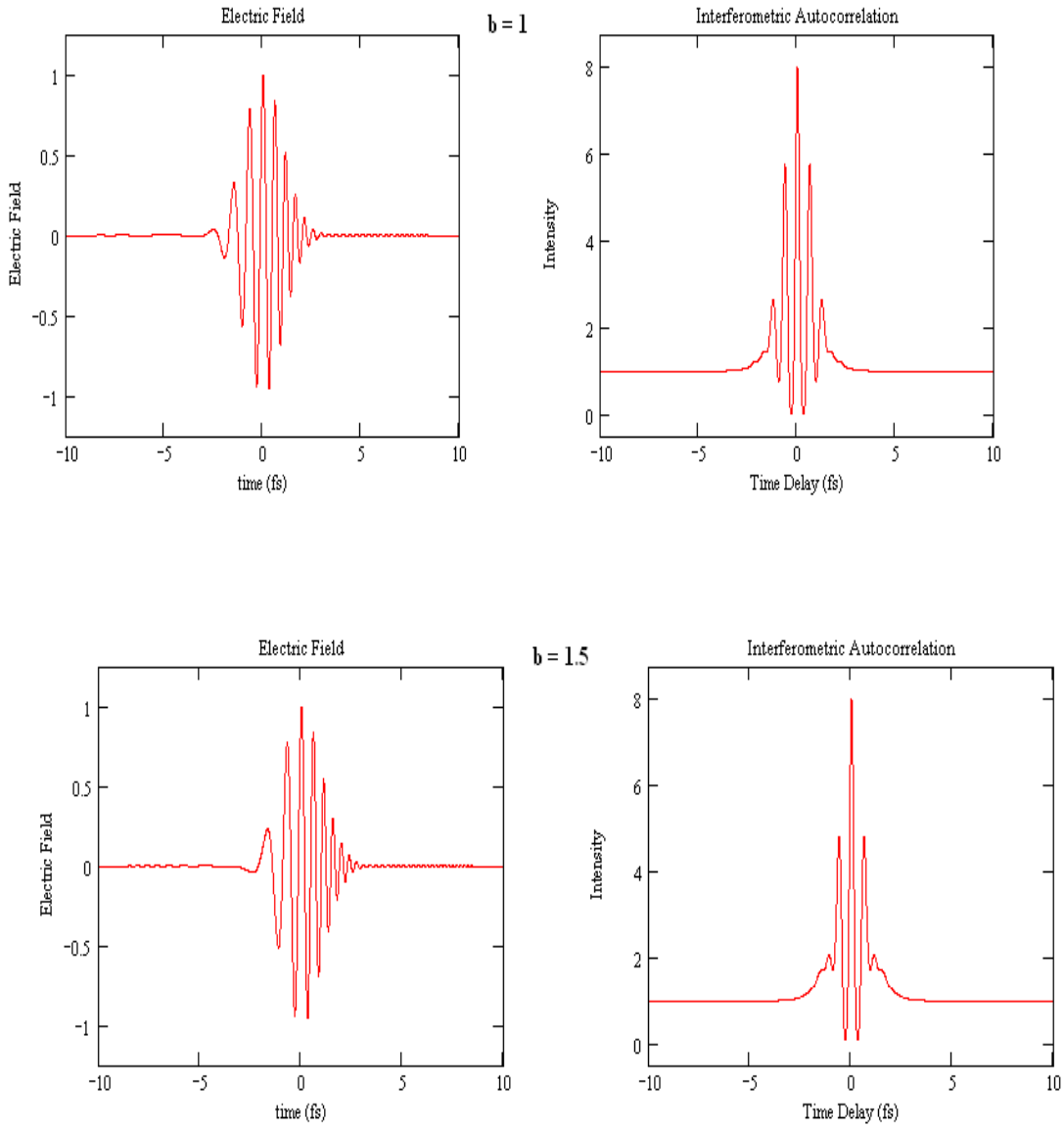

Figure 3.5.3 Interferometric autocorrelation of Gaussian pulses with FWHM of 10 fs for different values of the chirp parameter b: a) b=0, b) b=1, c) b=1.5.

3.5.4 Two-photon Absorption Autocorrelation

Aside from second-harmonic generation, one can use other nonlinear processes that do not require phase matching for second-order autocorrelation measurements. By use of two-photon-induced free-carrier generation in semiconductors, second-order

autocorrelation measurements of picoseconds and 100-fs pulses were obtained. A significant advantage of incorporating a semiconductor photodiode into autocorrelation measurements is that the two-photon response and the transformation of light into electric current are combined into a single solid-state device.

The most common method to measure ultra-short laser pulse duration is the intensity autocorrelation based on second harmonic generation (SHG) by a nonlinear crystal and photodetector. However, this measurement has many shortcomings. First, the SGH process requires phase matching, so the nonlinear crystal has to be angle-tuned for different wavelengths, and it is particularly difficult to phase-match to ultraviolet (UV) laser pulses. Second, to measure the duration of very short pulses (such as sub-20 fs) it is necessary to use a very thin nonlinear crystal (<100μm) to avoid added dispersion and phase mismatching between the fundamental and SHG pulses. Such a thin nonlinear crystal is expensive and produces a weak second harmonic signal which may require a sensitive detector. The laser pulse autocorrelator based on two-photon absorption (TPA) using large band gap semiconductor photodetector avoids the problems encountered with the autocorrelator based on SHG mentioned above. Several types of semiconductor photodetectors have now been found to be able to measure the ultra-short pulse duration. However, the materials used have a relatively small band gap, only laser pulses in near infrared and visible are detectable. Furthermore, most reports only demonstrate measurement of pulse duration of a couple of hundred femtoseconds, although the measurement of extremely short laser pulses of 6 fs has been demonstrated in a GaAsP photodiode at around 800 nm.

The two-photon absorption autocorrelation technique [23,24,25] is perhaps the simplest of a wide variety of autocorrelation methods

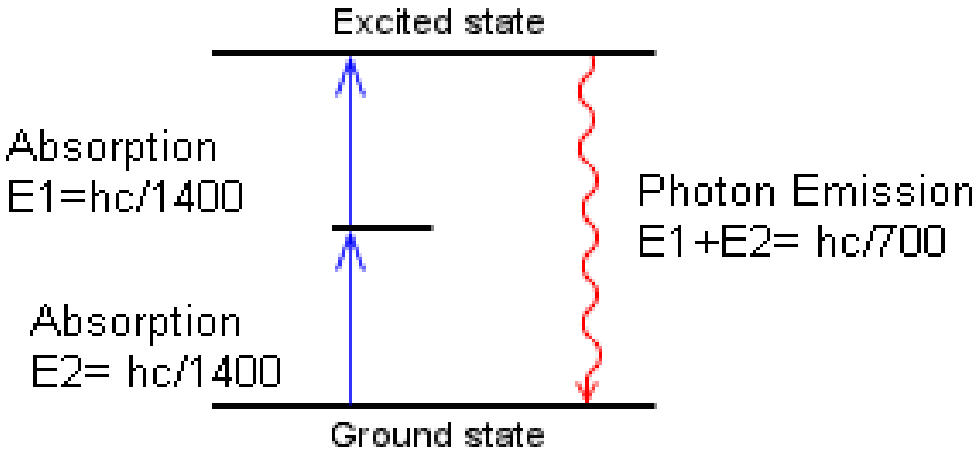

Figure 3.5.4 (a) shows a two-photon absorption scheme.

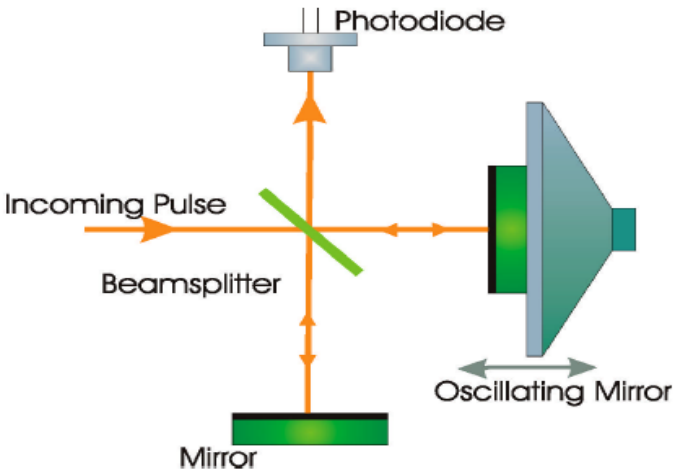

Figure 3.5.4(b) shows a two-photon absorption auto-correlator.Reproduced from Ref [26].

Figure 3.5.4 is a schematic of a two-photon absorption autocorrelator. The incident incoming pulse is split into two equal intensity components, both of which are directed down paths of equal optical lengths and are recombined on the detector. One pulse is reflected from a static mirror and the other from an oscillating mirror that introduces a delay causing the pulses to be scanned across each other and monitored at the detector. For this autocorrelator setup to work, the detector must have a quadratic response to the incident intensity. This was first achieved by using second harmonic crystals but these are expensive, difficult to align, and consideration needs to be made about their phase matching bandwidths. The same quadratic response can be achieved by the use of semiconductor materials such as LEDs or simple photodiodes. These provide a much simpler and cheaper alternative as the two-photon absorption in a semiconductor exhibiting this necessary quadratic response. An incident photon of greater energy than the semiconductor bandgap energy, E_g, will be absorbed linearly with respect to incident power. However, if the incident intensity of photons is high enough, as in the high peak of an ultra-short pulse, then photons of energy $1/2E_g<E<E_g$ can undergo a relatively efficient two-photon absorption process. The photocurrent produced from this has the desired quadratic response to the incident intensity.

If the two-photon detector is calibrated for a relatively slow frequency response, then a time-averaged intensity autocorrelation is recorded. This is defined as

$$G_i(\tau) = 1 + 2g(\tau) \qquad (3.9.11)$$

$$g(\tau) = \frac{\int_{-\infty}^{\infty} I(t)I(t-\tau)dt}{\int_{-\infty}^{\infty} I\left(t\right)^2 dt} \qquad (3.9.12)$$

It can be seen from the previous two equations that no function of phase are included. Therefore, there exists no information about the chirp on the pulse in the autocorrelation trace. Also, for the autocorrelation to provide valid information, the correct contrast ratio must be achieved. For values of $\tau = 0, \pm\infty$ the respective values of 1 and 3 for G_i (τ) are found. So for the two-photon intensity autocorrelation to provide accurate information, a contrast ratio of 3:1 must be achieved.

The advantages of measurement methods that involve TPA are that phase matching is not required and that the spectral response can accommodate broad-bandwidth pulses. In addition, autocorrelators based on TPA are insentitive to the polarization of the incident pulse.

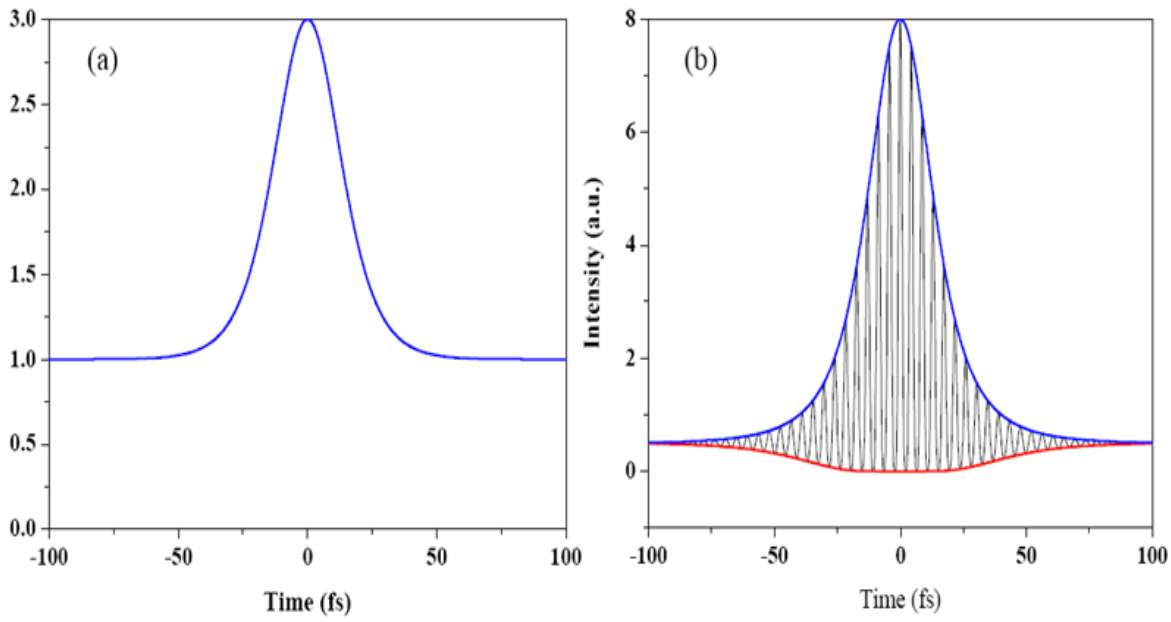

Figure 3.5.4(c):(i) Representative two-photon autocorrelation trace in intensity (ii) Representative two-photon Interferometric autocorrelation trace in intensity. Reproduced from Ref [26].

The FWHM of the autocorrelation trace does not directly provide the pulse duration of the ultra-short pulse. To calculate the pulse duration, a conversion factor has to be used. This factor depends on the assumed pulse shape and this relation takes the form.

$$\Delta\tau_p = \frac{\Delta t}{k} \qquad 3.9.13$$

Here k is the conversion factor, which for a $sech^2$ pulse shape is 1.542 or for Gaussian pulse shapes is 1.414. It has been shown that relative TPF profiles are to a large extent complementary to measurements of nonlinear enhancement, and that together they form a powerful tool for studying the structure of mode-locked laser signals. The pulse itself cannot be retrieved unless assumptions on the pulse shape are made. Moreover, despite its simplicity the method encounters quantitative difficulties in that the contrast between overlap and non-overlap parts is sensitive to many experimental parameters.

In recent years, two-photon absorption (TPA) semiconductor photoconductive devices have emerged as an attractive way for autocorrelation measurements of sub-10-fs laser pulses. Since the first demonstration of autocorrelation by use of this technique, many commercially available devices in different materials have been examined. In order to measure the duration of ultra-short laser pulses, various autocorrelation techniques have been developed. Measurements have been made by means of second harmonic generation (SHG), two-photon fluorescence and two-photon absorption in commercial photodiodes. Using TPA rather than SHG has several advantages;one being that TPA is polarization-independent and non-phasematched, simplifying alignment. Its simplicity is its major advantage over the second harmonic systems described previously. This technique is also an intensity-autocorrelation system. Two-photon absorption works to

convert the optical signal at fundamental wavelength directly into the photocurrent. This process is a non-resonant nonlinear effect that occurs for photons with (hν) less than the semiconductor energy gap E_g but greater than $\frac{E_g}{2}$. When using TPA for intensity autocorrelation measurements, very little single-photon absorption occurs for photons with hν less than E_g, but greater than $\frac{E_g}{2}$. An electron in the valence band of a semiconductor absorbs two photons, which give it enough energy for promotion to the conduction band. Hence, the photons must have a minimal energy of half the band-gap energy, so two could move an electron from the top of the valence band to the lowest level of the conduction band. The wavelength limit of this is when the photon energy is equal to the bandgap energy, so the photons are absorbed directly.

The basic optical configuration of the autocorrelators is similar to that of an interferometer. An incoming pulse train is split into two beams of equal intensity. An adjustable optical delay is inserted into one of the arms. The two beams are then recombined within a nonlinear material (semiconductor) for Two Photon Absorption (TPA). The incident pulses directly generate a nonlinear TPA photocurrent in the semiconductor, and the detection of this photocurrent as a function of interferometer optical delay between the interacting pulses yields the pulse autocorrelation function.

3.6 Gaussian Pulses

An optical pulse with a carrier frequency w_0, a complex Gaussian envelope and linear chirp is written in the form

$$E(t) = E_0(t) \exp[-at^2] \exp[i(\omega_0 t + bt^2)] \qquad (3.9.14)$$

The instantaneous intensity I (t) of the Gaussian pulse can be written

$$I(t) = E(t)\,E^*(t) = I_0 \exp[-2at^2] \quad . \quad (3.9.15)$$

Notice the chirp parameter, b, is not contained in the intensity profile. To find FWHM, we set $I(t_1) = I_0/2$ where $t_1 = \Delta t_p$ and Δt_p are defined as FWHM of the pulse .

At $t = t_1$ One obtains

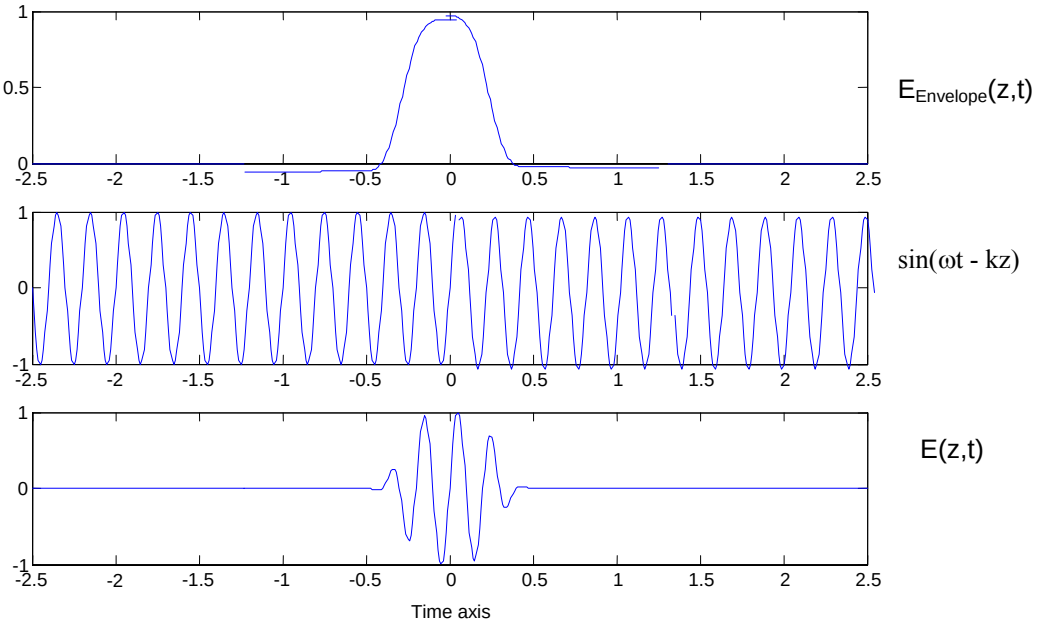

Fig.3.6.1 shows that E (z,t) is formed by multiplying together the top two signals.

$$\frac{1}{2} = \exp[-(2at_1^2)] \quad . \quad (3.9.16)$$

Taking natural logarithm of both sides:

$$-\ln 2 = -\ln \exp[-(2at^2)] = -2at_1^2$$

where

$$t_1 = \frac{\Delta t_p}{2} \quad (3.9.17)$$

and

$$\ln 2 = 2a \left(\frac{\Delta t_p}{2}\right)^2 \quad . \qquad (3.9.18)$$

$$\text{Finally, the pulse width } \tau_p = \left(\frac{2\ln 2}{a}\right)^{1/2} \qquad (3.9.19)$$

For a Gaussian pulse envelope function, $E_0(t) = \exp(-at^2)$

With $$\int_{-\infty}^{+\infty} E_0^4(t)\,dt = \int_{-\infty}^{+\infty} \exp(-4at^2)\,dt = \left(\frac{\pi}{4a}\right)^{1/2} \qquad (3.9.20)$$

$$\int_{-\infty}^{+\infty} E_0^2(t)\,E_0^2(t-\tau)\,dt = \left(\frac{\pi}{4a}\right)^{1/2} \exp(-a\tau^2) \qquad (3.9.21)$$

$$E_0^3(t)\,E_0(t-\tau) = E_0(t)\,E_0^3(t-\tau) = \exp(-3/4a\tau^2) \qquad (3.9.22)$$

The intensity autocorrelation of Gaussian pulses can be evaluated using eq (3.9.19) and eq (3.9.21).

$$I(\tau) = \frac{\int_{-\infty}^{+\infty} E_0^2(t)E_0^2(t-\tau)dt}{\int_{-\infty}^{+\infty} E_0^4(t)dt} \qquad (3.9.23)$$

In a similar fashion

$I(t_1) = I_0/2$ and at $t = \tau_1$ one obtains $\frac{1}{2} = \exp[-a\tau_1^2]$ (3.9.24)

Taking the natural logarithm of both sides $\ln 1 - \ln 2 = -a\tau_1^2$ where $\tau_1 = \frac{\Delta\tau_p}{2}$

(3.9.25)

$$\ln 2 = a\left(\frac{\Delta\tau_p}{2}\right)^2 \qquad (3.9.26)$$

The autocorrelation function is also a Gaussian pulse with a FWHM given by

$$\Delta\tau_p = \left(\frac{4\ln 2}{a}\right) \qquad (3.9.27)$$

Comparing the relationship between the FWHM of the autocorrelation function and the FWHM of the intensity of the optical pulse, we get the relationship between the measured and the actual pulse widths, $\frac{\Delta\tau_p}{\Delta t_p} = \sqrt{2}$ (3.9.28)

The intensity autocorrelation provides information on the duration of the optical pulses but reveals no information on the presence of any phase distortions like linear chirp in the optical pulse. Some information of the phase characteristics of the pulse can be found if the pulse width measurements are accompanied with the measurements of the spectrum. Mathematically, the spectrum of the pulse can be found by taking the Fourier transform.

A Gaussian pulse with chirp can be written as

$$E(t) = E_0(t)\exp[-at^2]\ \exp[I(\omega_0 t + bt^2)]\ . \qquad (3.9.29)$$

Combining the linear and quadratic terms in time of (eq 3.9.14)

$$E(t) = E_{0\ \exp[}\, i\omega_0 t - (a - ib)t^2 \quad . \qquad (3.9.30)$$

Defining γ = a-i b

The field amplitude becomes $E(t) = E_0(t)\ \exp[-\gamma t^2]\exp[i\omega_0 t]$ (3.9.31)

The spectral distribution of such a pulse is obtained by taking a Fourier transform

$$E(w) = \frac{1}{2\pi}\int_{-\infty}^{+\infty} E(t)\exp[-(i\omega t)dt \qquad (3.9.32)$$

$$E(w) = \frac{1}{2\pi}\int_{-\infty}^{+\infty} E_0(t)\ \exp[-(\gamma t^2)\exp[(i\omega_0 t)]\exp[-(i\omega t)] \qquad (3.9.33)$$

$$E(w) = \frac{1}{2\pi}\int_{-\infty}^{+\infty} E_0(t)\exp[-(\gamma t^2)]\exp[i(\omega-\omega_0)t]dt \qquad (3.9.34)$$

$$\text{Let } \beta = \omega_0 - \omega \quad \text{and} \quad \alpha = \gamma \qquad (3.9.35)$$

Using the Fourier transform pair

$$\int_{-\infty}^{+\infty} \exp[-(\alpha x^2 + \beta x)]dx\, dx = (\frac{\pi}{\alpha})^{1/2}\exp[\frac{\beta^2}{4\alpha}] \qquad (3.9.36)$$

Where the real part of α must be positive.

The Fourier transform of E (t) is given by

$$E(w) = E_0(t)\,(\frac{\pi}{\gamma})^{\frac{1}{2}}\exp[\frac{(\omega_0-\omega)^2}{4\gamma}] \qquad (3.9.37)$$

$$\text{Recall that } \gamma = a - ib \qquad (3.9.38)$$

$$\frac{1}{\gamma} = \frac{1}{a-ib} = \frac{a+ib}{a^2+b^2} \qquad (3.9.39)$$

$$\text{Substituting } \frac{1}{4\gamma} = \frac{a+ib}{4(a^2+b^2)} \qquad (3.9.40)$$

$$E(\omega) = E_0(t)\,(\frac{\pi}{\gamma})^{\frac{1}{2}}\exp[-\frac{1}{4}(\frac{a}{a^2+b^2})(\omega-\omega_0)^2 - i\frac{1}{4}(\frac{b}{a^2+b^2})(\omega-\omega_0)^2] \qquad (3.9.41)$$

The corresponding full width at half maximum (FWHM) of the power spectral density E (w) E* (w) is $E(w)\,E^*(w) = \left|E(\omega)\right|^2 = I(\omega)$. Note that the Fourier transform of the optical pulse is also a Gaussian function.

$$\text{At the half power point } \omega_1 = \frac{\Delta\omega}{2} \text{ and } I(\omega_1) = \frac{I_0}{2} \qquad (3.9.42)$$

$$\text{One obtains } \frac{1}{2} = \exp[-(\frac{\Delta\omega}{2})^2\frac{a}{2(a^2+b^2)}] \qquad (3.9.43)$$

Taking the natural logarithm of both sides, one gets

$$\ln 2 = \left(\frac{\Delta\omega}{2}\right)^2 \frac{a}{2(a^2 + b^2)} \qquad (3.9.44)$$

Multiplying both sides by 8 ($a^2 + b^2$) and dividing both sides by a, the FWHM of the spectrum is given

$$\Delta\omega_p = (8\ln 2)^{\frac{1}{2}} \left(\frac{a^2 + b^2}{a}\right)^{\frac{1}{2}} \qquad (3.9.45)$$

As $\omega = 2\pi f$, (3.9.46)

$$\Delta f_p = \frac{(2\ln 2)^{\frac{1}{2}}}{\pi} \left(\frac{a^2 + b^2}{a}\right)^{\frac{1}{2}} \qquad (3.9.47)$$

Recall that $\Delta t_p = \left(\frac{2\ln 2}{a}\right)^{\frac{1}{2}}$ (3.9.48)

Measurement of the FWHM of the spectrum reveals information about the chirp since the phase parameter b is present in the resulting equation. By taking the bandwidth-pulsewidth product, we get

$$\Delta f_p \Delta\tau_p = \frac{2\ln 2}{\pi} \left(1 + \frac{b^2}{a^2}\right)^{\frac{1}{2}} \qquad (3.9.49)$$

Expanding the square root, we finally have

$$\Delta f_p \Delta\tau_p = 0.44 \left(1 + \frac{b^2}{2a^2} + \ldots\right) \qquad (3.9.50)$$

For an optical pulse with no chirp, the bandwidth-pulse width product is 0.441. Bigger values for the bandwidth-pulse width product indicate the presence of chirp in the pulse but still give no information on the sign of the chirp.

In this chapter an outline of ultrashort pulse generation and characterization has been covered. The technique of autocorrelation, which provides a method for measuring the duration of these pulses, was also discussed.Some of the most commonly used

methods for mode-locking are reviewed.The basic theory of propagation of a Gaussian pulse through a dielectric medium is discussed.

3.7. References

1. A. G. Fox and T. Li. “Resonant modes in a maser interferometer”, *Bell Sys. Tech. J.* 40, 453 (1961).
2. A. G. Fox and T. Li, “Computation of optical resonator modes by the method of resonance excitation”, *IEEE J. Quantum Electron. QE-4,* 460 (1968).
3. Arnold L. Bloom, "Modes of a laser resonator containing tilted birefringent plates," *J. Opt. Soc. Am.* 64, 447-452 (1974)
4. G. Z. Baumann, "Mode behavior in laser resonators with zones of different indices of refraction," *Opt. Lett.* 9, 7-9 (1984).
5. N. McCarthy and M. Morin, "High-order transverse modes of misaligned laser resonators with Gaussian reflectivity mirrors," *Appl. Opt*. 28, 2189-2191 (1989).
6. S. Arahira et al., “Mode-locking at very high repetition rates more than terahertz in passively mode-locked distributed-Bragg-reflector laser diodes”, *IEEE J. Quantum Electron*. 32, 1211 (1996).
7. H. A. Haus, “A theory of forced mode locking”, *IEEE J. Quantum Electron. QE*-11, 323 (1975).
8. M. DiDomenico, “Small-signal analysis of internal (coupling type) modulation of lasers”, *J. Appl. Phys.* 35, 2870 (1964).
9. U. Morgner et al., “Sub-two cycle pulses from a Kerr-lens mode-locked Ti: sapphire laser”, *Opt. Lett.* 24 (6), 411 (1999).
10. D. E. Spence, P. N. Kean, W. Sibbett, “60-fsec pulse generation from a self-mode-locked Ti: sapphire laser”, *Opt. Lett*. 16 (1), 42 (1991).
11. T. Brabec et al., “Kerr lens mode locking”, *Opt. Lett.* 17 (18), 1292 (1992).

12. E. Cumberbatch, "Self-focusing in Non-linear optics", *J. Inst. Maths Applics* 6, 250 (1970).
13. Mori, W. B. et al. "Evolution of self-focusing of intense electromagnetic waves in plasma", *Phys. Rev. Lett.* 60, 1298 (1988).
14. F. Shimizu, "Frequency broadening in liquids by a short light pulse", *Phys. Rev. Lett.* 19 (19), 1097 (1967) (first demonstration of self-phase modulation).
15. R. R. Alfano and S. L. Shapiro, "Observation of self-phase modulation and small-scale filaments in crystals and glasses", *Phys. Rev. Lett.* 24 (11), 592 (1970).
16. R. H. Stolen and C. Lin, "Self-phase-modulation in silica optical fibers", *Phys. Rev. A* 17 (4), 1448 (1978).
17. L. F. Mollenauer and R. H. Stolen, "Soliton laser", *Opt. Lett.* 9 (1), 13 (1984).
18. F. M. Mitschke and L. F. Mollenauer, "Ultrashort pulses from the soliton laser", *Opt. Lett.* 12 (6), 407 (1987).
19. F. X. Kärtner et al., "Solitary pulse stabilization and shortening in actively mode-locked lasers", *J. Opt. Soc. Am. B* 12 (3), 486 (1995).
20. J. C. Diels and W. Rudolph, "Ultrashort Laser Pulse Phenomena", *2nd Ed.* (Academic, 2006).
21. S. Lochbrunner, P. Huppmann, and E.Riedle,"Crosscorrelation measurement of ultrashort visible pulses: comparison between nonlinear crystals and SiC photodiodes", *Optics Communications*, 184(1-4), 321-328, (2000).
22. J. A. Amstrong, "Measurement of picoseconds laser pulse widths", *Applied Physics Letter,* 31(10), 1444-1446, (2006).

23. D. T. Reid, M. Padgett, C. McGowan, W. E. Sleat, and W. Sibbett," Light-emitting diodes as measurement devices for femtosecond laser pulses", *Optics Letters*, 22(4), 233-235, (1997).

24. J. M. Roth, T. E. Murphy, and C. Xu, "Ultrasensitive and high-dynamic-range two-photon absorption in a GaAs photomultiplier tube", *Opt. Lett*. 27, 2076–2078 (2002).

25. D. T. Reid, W. Sibbett, J. M. Dudley, L. P. Barry, B. Thomsen, and J. D. Harvey, "Commercial semiconductor devices for two photon absorption autocorrelation of ultrashort light pulses", *Applied Optics*, 37(34), 8142-8144, (1998).

26. Alan McWilliam thesis' "Femtosecond Cr^{4+}:forsterite laser for applications in telecommunications and biophotonics ", p.90, November 2006.

27. Laser Fundamentals "Simple two-mirror laser cavity" graph reproduced from www.shorelaser.com.

CHAPTER 4: PICOSEOND AND FEMTOSECOND OPERATION OF CHROMIUM-DOPED CUNYITE LASER

4.1 Introduction

The generation of femsecond optical pulses has been an active area of research for many years and has opened up a wide range of applications from real monitoring of chemical reactions to ultra-high bit-rate optical communications.Without a doubt, the best results in terms of shortest pulse durations and highest average powers belong to the vibronic crystal-based Kerr-lens-mode-locked Ti:Sapphire laser that was first demonstrated in 1989. This particular laser, however, suffers from some practicalities that limit its applications outside major research laboratories; these include its peak emission wavelength at about 800 nm and its spectral coverage from 680 nm to 1050 nm, which limits penetration into biological tissue or is not well matched to telecommunications windows. Moreover femtosecond Ti: Sapphire lasers rely on rather expensive frequency doubled solid-state lasers. Recently, new gain media for the generating ultra-short laser pulses like Cr^{3+}: $LiSrAlF_6$ (LiSAF) or Cr^{4+}:Mg_2SiO_4 (Fosterite) had been reported that can be pumped by available cost-efficient laser diodes. However, the emission spectrum of Cr^{3+}: $LiSrAlF_6$ is very similar to Ti: Sapphire and Cr^{4+}:Mg_2SiO_4 has no laser emission above 1400 nm. At 1550 nm Erbium doped fiber lasers offer 100 fs to 200 fs laser pulses. But no ultrafast laser sources exist so far to fill the gap between 1400 nm and 1550 nm. The emission wavelength (800-1200nm) is not well matched to telecommunications windows. Recently tunable solid state lasers have emerged as new gain media for the generation and amplification of ultra-short pulses. The Cr^{4+}:Ca_2GeO_4 (Cunyite) can

generate sub-100fs pulses due to its wide emission spectrum. The shortest pulsewidth obtained so far was 233 fs.

In this chapter we discuss the generation of femtosecond laser pulses from Cr^{4+}:Ca_2GeO_4 (Cunyite). The basic theory of Gaussian pulse propagation through a dispersive medium and effects of pulse broadening and pulse compression [1,2,3,4,5] will be theoretically applied to the crystal. Section 4.6 describes the experimental setup and how 233 fs laser pulses are generated from the self-mode-locked Cunyite laser.

4.2 Propagation of Gaussian Pulses in a Dispersive Medium

The shape of a short intense optical pulse propagating in a dispersive medium can become distorted by the interplay between group-velocity dispersion (GVD) and light-induced index-of-refraction change in the medium (Shen [1984]; Boyd [1992]). These effects play an important role in the generation and propagation of ultrashort pulses as recorded in Martinez et al., 1984. The goal in this section is to determine the effects of a dispersive medium on a light pulse.

Consider a Gaussian pulse entering a dispersive medium at z=0. The pulse is represented by.

$$E_0(0,t) = e^{-a_0 t^2} e^{i\omega_0 t + ib_0 t^2} = \exp(-\Gamma_0 t^2 + i\omega_0 t) \qquad (4.2.1)$$

$$\text{Where } \Gamma_0 \equiv a_0 - ib_0 \qquad (4.2.2)$$

The pulse is represented by its two components: the fast oscillating function $\exp(i\omega_0 t)$ and a slow varying envelope function $\exp(-a_0 t^2 + ib_0 t^2)$.The frequency distribution of the Gaussian pulse is the Fourier transform of E (0,t) and is given by

$$\check{E}_0(0,\omega) = \exp\left(-\frac{(\omega-\omega_0)^2}{4\Gamma_0}\right) \qquad (4.2.3)$$

After propagating a distance z inside the dispersive medium, the pulse spectrum can be written as

$$\check{E}(z,w)=\check{E}(0,\omega)\exp(-ik(\omega)z) \qquad (4.2.4)$$

Where k(ω) is the propagation constant of the light in the medium , which is a function of frequency.

A medium is called "dispersive" when its propagation constant, k, is a function of frequency. The propagation constant can be developed as a power series about the central frequency ω_0 using the Taylor series expansion.

$$k(\omega) = k(\omega_0) + \left.\frac{dk}{d\omega}\right|_{\omega_0}(\omega-\omega_0) + \frac{1}{2}\left.\frac{d^2k}{d\omega^2}\right|_{\omega_0}(\omega-\omega_0)^2 + \frac{1}{6}\left.\frac{d^3k}{d\omega^3}\right|_{\omega_0}(\omega-\omega_0)^3 + ... \qquad (4.2.5)$$

Where $k(\omega) = k_0$ is the mean wavevector magnitude of the optical pulse,

$k_1 = \left.\frac{dk}{d\omega}\right|_{\omega=\omega_0} = \frac{1}{v_g} = \frac{n_g}{c}$ is the inverse of the group velocity,

and $k_2 = \left.\frac{d^2k}{d\omega^2}\right|_{\omega=\omega_0} = \frac{d(\frac{1}{v_g})}{d\omega} = \frac{1}{c}\frac{dn_g}{d\omega}$ is a measure of the dispersion in the group velocity.

For a specific frequency, the propagation constant in the dispersive medium is given by

$$k(\omega_0) = \frac{\omega_0 n(\omega_0)}{c}. \qquad (4.2.6)$$

Where $n(\omega_0)$ is the refractive index of the medium for frequency ω_0 and c is the speed of light in free space .The derivatives of the propagation constant with respect to frequency can be expressed in terms of the index of refraction. Using eq. 4.2.6 the first, second, and third derivatives are given by

$$\frac{\partial k}{\partial \omega} = \frac{n}{c_0} + \frac{\omega}{c_0}\frac{\partial n}{\partial \omega} \qquad (4.2.7)$$

$$\frac{\partial^2 k}{\partial \omega^2} = \frac{2}{c_0}\frac{\partial n}{\partial \omega} + \frac{\omega}{c_0}\frac{\partial^2 n}{\partial \omega^2} \qquad (4.2.8)$$

$$\frac{\partial^3 k}{\partial \omega^3} = \frac{3}{c_0}\frac{\partial^2 n}{\partial \omega^2} + \frac{\omega}{c_0}\frac{\partial^3 n}{\partial \omega^3} \qquad (4.2.9)$$

The derivatives of the refractive index with respect to frequency (left side) can be changed to derivatives of the refractive index with respect to wavelength by using

$$\omega = \frac{2\pi c}{\lambda} \qquad (4.2.10)$$

$$\frac{\partial n}{\partial \omega} = -\frac{\lambda^2}{2\pi c_0}\frac{\partial n}{\partial \lambda} \qquad (4.2.11)$$

$$\frac{\partial^2 n}{\partial \omega^2} = \frac{\lambda^3}{2\pi c_0^2}\frac{\partial n}{\partial \lambda} + \frac{\lambda^4}{2\pi^2 c_0^2}\frac{\partial^2 n}{\partial \lambda^2} \qquad (4.2.12)$$

$$\frac{\partial^3 n}{\partial \omega^3} = -\frac{3\lambda^4}{4\pi^3 c_0^3}\frac{\partial n}{\partial \lambda} - \frac{3\lambda^5}{2\pi^3 c_0^3}\frac{\partial^2 n}{\partial \lambda^2} - \frac{\lambda^6}{8\pi^3 c_0^3}\frac{\partial^3 n}{\partial \lambda^3} \qquad (4.2.13)$$

The derivatives of the propagation constant with respect to frequency can be calculated by substituting eq 4.2.(11-13) in eq 4.2.(7-9).

$$\frac{\partial k}{\partial \omega} = \frac{n}{c_0} - \frac{\lambda}{c_0}\frac{\partial n}{\partial \lambda} \qquad (4.2.14)$$

$$\frac{\partial^2 k}{\partial \omega^2} = \frac{\lambda^3}{2\pi c_0^2}\frac{\partial^2 n}{\partial \lambda^2} \qquad (4.2.15)$$

$$\frac{\partial^3 k}{\partial \omega^3} = -\frac{\lambda^5}{4\pi^2 c_0^3}\frac{\partial^3 n}{\partial \lambda^3} \qquad (4.2.16)$$

Notice that the frequency spectrum is a Gaussian distribution peaked at ω_0. The field at a distance z is obtained by substituting the expression for k(ω) in the equation of Ě(z,ω). We obtain

$$\check{E}(z,\omega) = \check{E}(0,\omega)\exp\{-iz[k(\omega_0) + \left.\frac{dk}{d\omega}\right|_{\omega_0}(\omega-\omega_0) + \left.\frac{1}{2}\frac{d^2k}{d\omega^2}\right|_{\omega_0}(\omega-\omega_0)^2]\} \qquad (4.2.17)$$

The notation in eq. 4.2.17 can be simplified by setting

$$k = k(\omega_0) \qquad (4.2.18)$$

$$k_1 = \left.\frac{dk}{d\omega}\right|_{\omega_0} \qquad (4.2.19)$$

$$k_2 = \left.\frac{d^2k}{d\omega^2}\right|_{\omega_0} \qquad (4.2.20)$$

After substituting for eq. 4.2.18-20, the last equation becomes

$$\check{E}(z,\omega) = \check{E}(0,\omega)\exp\{-iz[k + k_1(\omega-\omega_0) + \frac{k_2}{2}(\omega-\omega_0)^2]\} \qquad (4.2.21)$$

$$\check{E}(z,\omega) = \exp\{-[ikz + ik_1z(\omega-\omega_0) + \frac{1}{4\gamma(z)}(\omega-\omega_0)^2]\} \qquad (4.2.22)$$

Where $$\frac{1}{4\gamma(z)} = \frac{1}{4\Gamma_0} + i\frac{k_2 z}{2} \; or \; \frac{1}{\gamma(z)} = \frac{1}{\Gamma_0} + 2ik_2z \qquad (4.2.23)$$

The pulse in the time domain can be estimated by taking the Fourier transform of $\check{E}(z,\omega)$.

$$E(z,\omega) = \int_{+\infty}^{-\infty} \check{E}(z,\omega)e^{i\omega t}d\omega \qquad (4.2.24)$$

$$E(z,t) = \int_{+\infty}^{-\infty} \exp\{-[ikz + ik_1(\omega-\omega_0) + \frac{1}{\gamma(z)}(\omega-\omega_0)^2 - \omega t]\}d\omega \qquad (4.2.25)$$

Which by changing the variable to (ω - ω_0),

$$\mathrm{E}(z,t) = \exp[i(\omega_0 t - kz)] \int_{+\infty}^{-\infty} \exp\{-\frac{(\omega-\omega_0)^2}{4\gamma(z)} + i(\omega-\omega_0)(t-k_1 z)\} d(\omega-\omega_0) \qquad (4.2.26)$$

$$\mathrm{E}(z,t) = \sqrt{4\pi\gamma(z)}\exp[i\omega_0(t-\frac{z}{v_g})]\exp[-\gamma(z)\left(t-\frac{z}{v_g}\right)^2] \qquad (4.2.27)$$

$where\, \tau = (t-\frac{z}{v_g})$ and carrying out the integration yields

$$\mathrm{E}(z,t) = \sqrt{4\pi\gamma(z)}\exp[i(\omega_0 t - kz)]\exp[-\gamma(z)(t-k_1 z)^2] \qquad (4.2.28)$$

The central frequency ω_0 is seen to travel at a phase velocity given by $v_p(\omega_0) = \frac{\omega_0}{k(\omega_0)}$

The resulting equation of the Gaussian pulse after traveling a distance z in the dispersive medium is still Gaussian and is similar to the input pulse. It is characterized by a fast oscillating function which is delayed by a phase given by

$$\frac{k(\omega_0)}{\omega_0} z \qquad (4.2.29)$$

$$v_p(\omega_0) = \frac{\omega_0}{k(\omega_0)} = \text{(Phase Velocity)} \qquad (4.2.30)$$

Phase velocity is the velocity needed to keep up with a maximum of the fast oscillating field. The slower envelope function is delayed by an amount of $k_1 z$. The envelope of the pulse seems to move at a group velocity given by

$$v_g(\omega_0) = \frac{1}{k_1} = \left.\frac{1}{\frac{dk}{d\omega}}\right|_{\omega_0} = \text{(Group Velocity)} \qquad (4.2.31)$$

Group velocity is the velocity that the pulse propagates in the dispersive medium. Group velocity can be considered as the speed that the energy of the pulse propagates.

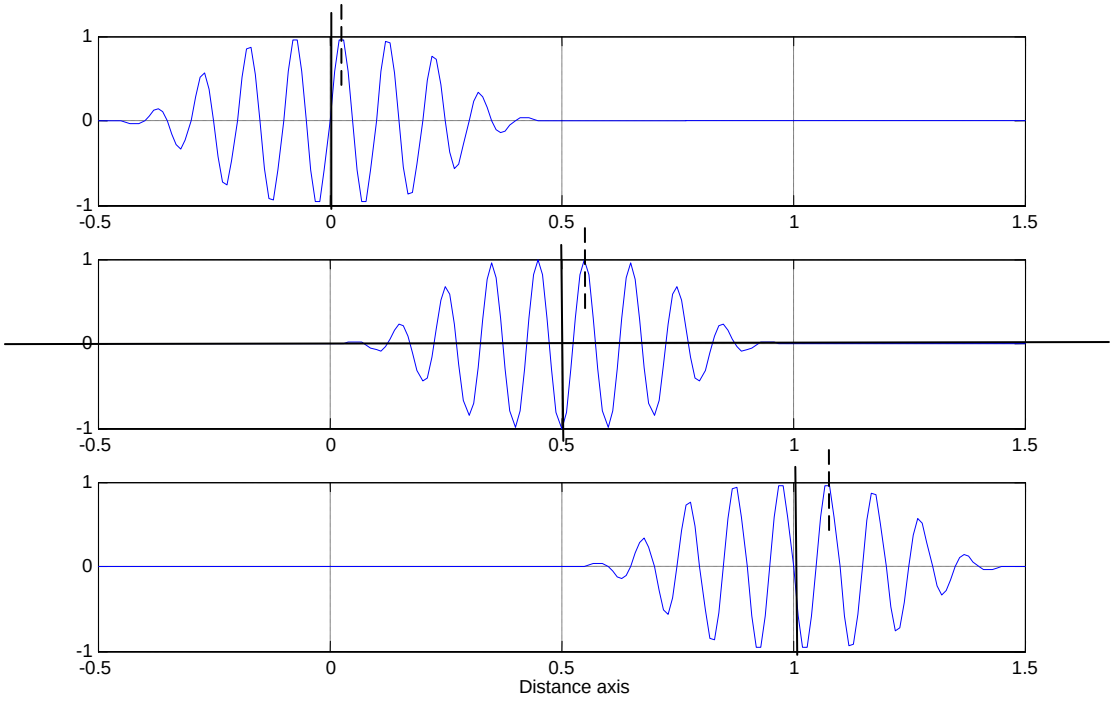

Figure 4.2.1 (Group velocity) shows three instances in time of the modulated wave. A solid line is drawn through the centre of the envelope, whilst a dashed line is drawn through a peak in the carrier. Note that subsequent "snapshots" of the modulated wave show that the peak of the carrier has propagated a greater distance than the envelope. Hence the carrier has propagated faster than the envelope. Now the movement of the solid line represents the group velocity and the dotted line the phase velocity. The importance of the group velocity is that it is the speed in which the information content of the modulated waveform is moving.

The envelope function is also affected by the complex variable $\gamma(z)$ given by eq. 4.2.23. If $k_2 = 0$, then the pulse will propagate indefinitely without any change to its

temporal envelope. This is called "zero dispersion" wavelength. Third order dispersion effects become significant when generating pulses of sub-100-fs. Therefore this needs to be compensated for. The third order dispersion of a material is given

$$\frac{\partial^3 k}{\partial \omega^3} = \frac{1}{c_0}\left(\frac{3d^2 n}{d\omega^2} + \omega\frac{d^3 n}{d\omega^3}\right) \qquad (4.2.32)$$

If k_2 is non zero, then there will be a variation of the group velocity as a function of frequency which is the so called Group Velocity Dispersion (GVD). Group velocity dispersion gives rise to phenomena such as pulse broadening, pulse compression, pulse reshaping. The pulse shape will no longer remain unchanged and will, in general, spread as the pulse travels. The spreading of the pulse can be accounted for by noting that the group velocity v_g may not be the same for each frequency component of the laser pulse. Group velocity dispersion is, responsible for pulse broadening, related to group velocity by

$$k_2 = \left.\frac{d^2 k}{d\omega^2}\right|_{\omega_0} = \left.\frac{d(\frac{1}{v_g})}{d\omega}\right|_{\omega_0} \qquad \text{(GVD)} \qquad (4.2.33)$$

The initial pulse width, defined as the full width at half maximum intensity, is given by

$$\tau_p(0) = \sqrt{\frac{2\ln 2}{a_0}} \qquad (4.2.34)$$

Similarly, the pulse width at z is given by

$$\tau_p(z) = \sqrt{\frac{2\ln 2}{a(z)}} \qquad (4.2.35)$$

The function a(z) can be estimated using eq.4.2.23

$$\frac{1}{\gamma(z)} = \frac{1}{a(z) - ib(z)} = \frac{1}{\Gamma_0} + 2ik_2 z \qquad (4.2.36)$$

By solving eq. (4.2.36), the expression for the function a(z) and b(z) can be approximated

$$a(z) = \frac{a_0}{(1 + 2k_2 z b_0)^2 + (2k_2 z a_0)^2} \qquad (4.2.37)$$

$$b(z) = \frac{b_0(1 + 2k_2 z b_0) + 2k_2 z a_0^{\,2}}{(1 + 2k_2 z b_0)^2 + (2k_2 z a_0)^2} \qquad (4.2.38)$$

If the input pulse has no chirp ($b_0 = 0$), then the pulse width of the output pulse at z is

$$\tau_p(z) = \sqrt{\frac{2\ln 2}{a(z)}} = \sqrt{\frac{2\ln 2}{a_0}[1 + (2k_2 a_0)^2]} \qquad (4.2.39)$$

where $a_0 = \dfrac{2\ln 2}{\tau_p^{\,2}(0)}$

Substituting for a_0 from eq. 4.2.33, the pulse width after propagating a distance z can thus be expressed as $\tau_p(z) = \tau_p(0)\sqrt{[1 + (\frac{4k_2 z \ln 2}{\tau_p^{\,2}(0)})^2]}$ (4.2.40)

From the above expression, it is obvious that the pulse width of the output pulse depends on the GVD (k_2), the distance traveled (z), and the pulse width of the input pulse.

Consider the propagation of a frequency-chirped laser pulse through a dispersive medium. One can determine the distance after which the pulse will shorten .Considering eq4. 2.39, the pulse width is inversely dependent on a(z) and the pulse width will be minimal when a(z) is maximal. When b(z) = 0, the pulse width is minimum. Using either of these conditions, the distance that will make the pulse width minimum is given by

$$z_{b(z=0)} = \frac{-b_0}{2k_2(a_0^2 + b_0^2)} = \frac{-b_0}{2k_2[(\frac{2\ln 2}{\tau_p^2(0)})^2 + b_0^2]} \qquad (4.2.41)$$

Now let's consider an un-chirped pulse, b=0, going into a dispersive medium. After a distance z, the width of the pulse is given by

$$\tau_p^2(z) = \tau_p^2(0) + (\frac{4k_2 z \ln 2}{\tau_p^2(0)})^2 = \tau_p^2(0)[1 + (\frac{z}{z_D})^2] \qquad (4.2.42)$$

The dispersion length, z_D, is called the "Rayleigh length" and is defined as the distance traveled in the dispersive medium after which the pulse will increase by a factor $\sqrt{2}$ and is given by

$$z_D = \frac{\tau_p^2(0)}{4k_2 \ln 2} \qquad (4.2.43)$$

The group velocity dispersion is often characterized by $D \equiv L^{-1}\frac{dT}{d\lambda}$ where T is the pulse transmission time through a dispersive material of length L. This constant D measures the variation in the time it takes for a pulse to transmit through a dispersive material as a function of the different frequencies. The units of D are picoseconds or femtoseconds of delay per nanometer of bandwidth per centimeter of distance traveled in the dispersive medium. The dispersion constant is related to the second derivative of the propagation constant by the relation

$$D = -\frac{2\pi c_0}{\lambda^2}\frac{d^2k}{d\omega^2} \qquad (4.2.44)$$

With this new definition, the pulse width expression from eq.4.2.39 can be written

$$\tau_p(z) = \tau_p(0)\sqrt{1 + (\frac{2\ln 2}{\pi c_0}\frac{Dz\lambda^2}{\tau_p^2(0)})^2} \qquad (4.2.45)$$

Discussions on pulse propagation are usually carried out using the total phase of a light pulse. The equivalent expression to eq. (4.2.1) describing a Gaussian light pulse before entering a dispersive medium (z=0) can be written as

$$E(0,t)=E_0 e^{i\Phi(t)} e^{at^2} \qquad (4.2.46)$$

The expression describing the pulse after propagating a distance z in the dispersive medium is, using the same procedure that resulted in eq.4.2. 4, given by

$$\check{E}(z,\omega)=\check{E}(0,\omega)e^{i\Phi(\omega)} \qquad (4.2.47)$$

The phase shift suffered by a light pulse after propagation through an optical system is a function of the frequency and is denoted as Φ (ω). The phase Φ (ω) can be expressed as a series using the Taylor series expansion around the center frequency of the pulse ω_0 as

$$\Phi(\omega) = \Phi(\omega_0) + \left.\frac{d\Phi}{d\omega}\right|_{\omega_0} (\omega-\omega_0) + \frac{1}{2}\left.\frac{d^2\Phi}{d\omega^2}\right|_{\omega_0} (\omega-\omega_0)^2 + \frac{1}{6}\left.\frac{d^3\Phi}{d\omega^3}\right|_{\omega_0} (\omega-\omega_0)^3 + \ldots. \qquad (4.2.48)$$

Where, $\Phi(\omega_0) = \Phi_0 -$ is a constant phase shift, $\tau_0 = \left.\frac{d\Phi}{d\omega}\right|_{\omega_0}$ - the system delay time

for the carrier frequency ω_0 i.e. the time it takes the frequency ω_0 to transverse the dispersive system to quadratic phase of the delay line.

$\left.\frac{d^3\Phi}{d\omega^3}\right|_{\omega_0}$ - Cubic phase of the delay line

In his paper "Optical Pulse Compression with Diffraction Gratings" Treacey showed that the relation between the phase, Φ, and the optical path, P, traveled by the pulse is given by

$$\Phi(\omega) = \frac{\omega P}{c_0} \qquad (4.2.49)$$

The derivatives of phase with respect to frequency in eq. 47 can be written as a function of the optical path.

$$\tau_0 = \frac{d\Phi}{d\omega} = \frac{d(\frac{\omega P}{c_0})}{d\omega} = \frac{1}{c_0}(\omega \frac{dP}{d\omega} + P) \qquad (4.2.50)$$

$$\frac{d^2\Phi}{d\omega^2} = \frac{2}{c_0}\frac{dP}{d\omega} + \frac{\omega}{c_0}\frac{d^2P}{d\omega^2} \qquad (4.2.51)$$

$$\frac{d^3\Phi}{d\omega^3} = \frac{3}{c_0}\frac{d^2P}{d\omega^2} + \frac{\omega}{c_0}\frac{d^3P}{d\omega^3} \qquad (4.2.52)$$

Eq. 4.2.50-52 can be written as derivatives of the optical path, P, with respect to wavelength, λ.

$$\omega = \frac{2\pi c_0}{\lambda} \qquad (4.2.53)$$

The equivalent expressions for eqs.4.2.48 and 4.2.49 are

$$\Phi = \frac{2\pi P}{\lambda} \qquad (4.2.54)$$

$$\frac{d\Phi}{d\omega} = \frac{P}{c_0} - \frac{\lambda}{c_0}\frac{dP}{d\lambda} \qquad (4.2.55)$$

Using eq.4.2.52 then followed by eqs. 4.2.49-52 one can express the derivatives of the optical path with respect to wavelength. Modifying equation.4.2.51 requires a few steps. We first use the chain rule for the second derivative of phase with respect to frequency

$$\frac{d^2\Phi}{d\omega^2} = \frac{d^2\lambda}{d\omega^2}\frac{d\Phi}{d\lambda} + (\frac{d\lambda}{d\omega})^2\frac{d^2\Phi}{d\lambda^2} \qquad (4.2.56)$$

The derivatives of phase with respect to wavelength can be written as

$$\frac{d\Phi}{d\lambda} = \frac{d(\frac{\omega P}{c_0})}{d\lambda} = -\frac{2\pi}{\lambda^2}P + \frac{2\pi}{\lambda}\frac{dP}{d\lambda} \qquad (4.2.57)$$

$$\frac{d^2\Phi}{d\lambda^2} = \frac{4\pi}{\lambda^3}P - \frac{4\pi}{\lambda^2}\frac{dP}{d\lambda} + \frac{4\pi}{\lambda}\frac{d^2P}{d\lambda^2} \qquad (4.2.58)$$

Using eq. 4.2.52 the derivatives of wavelength with respect to frequency can be expressed as

$$\frac{d\lambda}{d\omega} = -\frac{\lambda^2}{2\pi c_0} \qquad (4.2.59)$$

$$\frac{d^2\lambda}{d\omega^2} = \frac{\lambda^3}{2\pi^2 {c_0}^2} \qquad (4.2.59)$$

Substituting equations.4.2.57-4.2.60 in eq. 4.2.56 results in

$$\frac{d^2\Phi}{d\omega^2} = \frac{\lambda^3}{2\pi^2 {c_0}^2}(-\frac{2\pi}{\lambda^2}P + \frac{2\pi}{\lambda}\frac{dP}{d\lambda}) + \frac{\lambda^3}{2\pi^2 {c_0}^2}(\frac{4\pi}{\lambda^3}P - \frac{4\pi}{\lambda^2}\frac{dP}{d\lambda} + \frac{4\pi}{\lambda}\frac{d^2P}{d\lambda^2}) \qquad (4.2.60)$$

The last expression can be rewritten as

$$\frac{d^2\Phi}{d\omega^2} = \frac{\lambda^3}{2\pi {c_0}^2}\frac{d^2P}{d\lambda^2} \qquad (4.2.61)$$

In a similar fashion, the cubic phase can be evaluated. Following the same steps outlined above, the cubic phase can be written as

$$\frac{d^3\Phi}{d\omega^3} = \frac{d^3\Phi}{d\lambda^3}(\frac{d\lambda}{d\omega})^3 + 3\frac{d^2\Phi}{d\lambda^2}\frac{d\lambda}{d\omega}\frac{d\lambda^2}{d\omega^2} + \frac{d\Phi}{d\lambda}\frac{d^3\lambda}{d\omega^3} \qquad (4.2.62)$$

$$\frac{d^3\Phi}{d\omega^3} = -\frac{\lambda^4}{4\pi^2 {c_0}^3}\left[3\frac{d^2P}{d\lambda^2} + \lambda\frac{d^3P}{d\lambda^3}\right] \qquad (4.2.63)$$

The dispersion constant, D, can also be expressed in terms of the optical path, P, using the following procedure. Treacy also showed that the time it takes a light pulse to transverse an optical system is related to the phase by

$$T=\frac{\partial\Phi(\omega)}{\partial\omega} \qquad (4.2.64)$$

Where $\Phi(\omega)$ is the phase function and is given by

$$\Phi(\omega)=\frac{\omega P}{c_0} \qquad (4.2.65)$$

The time T is found by substituting eq.4.2.65 in eq.4.2.64

$$T=\frac{d(\frac{\omega P}{c_0})}{d\omega}=\frac{1}{c_0}(\omega\frac{dP}{d\omega}+P) \qquad (4.2.66)$$

$$\text{Using } \lambda=\frac{2\pi c_0}{\omega} \text{ and } d\omega=-\frac{2\pi c_0}{\lambda^2}d\lambda \qquad (4.2.67)$$

Eq.4.2.66 can be written as a function of wavelength

$$T=\frac{1}{c_0}(P-\lambda\frac{dP}{d\lambda}) \qquad (4.2.68)$$

$$\frac{dT}{d\lambda}=-\frac{\lambda}{c_0}\frac{d^2P}{d\lambda^2} \qquad (4.2.69)$$

Substituting the expression for T in the definition of the group velocity dispersion as defined in the equation below

$$D=\frac{1}{L}\frac{dT}{d\lambda} \qquad (4.2.70)$$

results in the following expression

$$D=-\frac{\lambda}{Lc_0}\frac{d^2P}{d\lambda^2} \qquad (4.2.71)$$

Next consider a light pulse crossing a dispersive medium of thickness, l_m. The optical path of this system is

$$P = l_m n_m \qquad (4.2.72)$$

where n_m is the index of refraction of the dispersive medium. The second derivative of P with respect to wavelength is

$$\frac{d^2 P}{d\lambda^2} = l_m \frac{d^2 n_m}{d\lambda^2} \qquad (4.2.73)$$

Substituting equation.4.2.73 in eq. 4.2.61, the quadratic phase induced on the light pulse is given by

$$\frac{d^2 \Phi_m}{d\omega^2} = \frac{\lambda^3 l_m}{2\pi c_0^{\,2}} \frac{d^2 n_m}{d\lambda^2} \qquad (4.2.74)$$

We can use the same procedure to obtain the cubic phase induced on the pulse as a result of propagating through the dispersive medium.

$$\frac{d^3 \Phi}{d\omega^3} = -\frac{\lambda^4}{4\pi^2 c_0^{\,3}} [3 \frac{d^2 n_m}{d\lambda^2} + \lambda \frac{d^3 n_m}{d\lambda^3}] \qquad (4.2.75)$$

The analysis presented here provides the base for discussion of phase distortion compensation in the Cr^{4+}:Ca_2GeO_4 (Cunyite) laser.

4.3. Dispersion management

To get a stable self mode-locking operation a Kerr-lens has to be formed inside the laser cavity. Usually the Kerr-lens is built up inside the laser crystal. Since the optical pulse must not disperse (or its envelope stretched in time) to retain the Kerr-lens effect it is necessary to keep the overall round-trip dispersion very close to zero. In our experimental setup dispersive mirrors are used to compensate the dispersion [5,6] of the laser crystal.

4.3.1. Dispersion measurement on Cunyite crystals

Due to the low gain and low thermal properties of Cunyite, the length of the crystal should be large enough to avoid intense local up-heating in the center. In this thesis a 4.5 mm long crystal is used. This is significantly longer than in the case of a Ti: sapphire crystal, which is typically 2 mm long. The longer crystal has therefore a larger GDD (Group Delay Dispersion) and TOD (Third Order Dispersion) and is the dominant source of positive GDD and TOD in the resonator.

In order to design a compact laser setup comprising only chirped mirrors for intracavity dispersion compensation, precise information about the dispersion data of all components is required. White-light interferometry is one of the most common method used to analyze dispersion curves. The apparatus used is a Michelson interferometer illuminated by a white-light source (tungsten halogen lamp). The setup is shown in Fig.4.3.1 where a low dispersion gold mirror is placed in "the reference" arm and the crystal to be measured in the "sample" arm. When one of the mirrors is tilted around a horizontal axis while the other mirror is vertical, horizontal interference fringes are generated by each spectral component of the white-light source at the exit plane of the interferometer. A transmission grating and an achromatic lens are used to create the spectrally dispersed image of a vertical section of the superimposed "white light" interference fringes on a CCD array; the section is created by a vertical slit. The interference patterns corresponding to different wavelengths are linearly dispersed in the horizontal direction.

Most approaches for the measurement of the group-delay dispersion (GDD) of laser crystals have been based on a white light interferometer that contains the dispersive

element in one arm, keeping the other arm as a reference. The cross-correlation pattern reveals the wavelength-dependent optical path difference between the two arms.

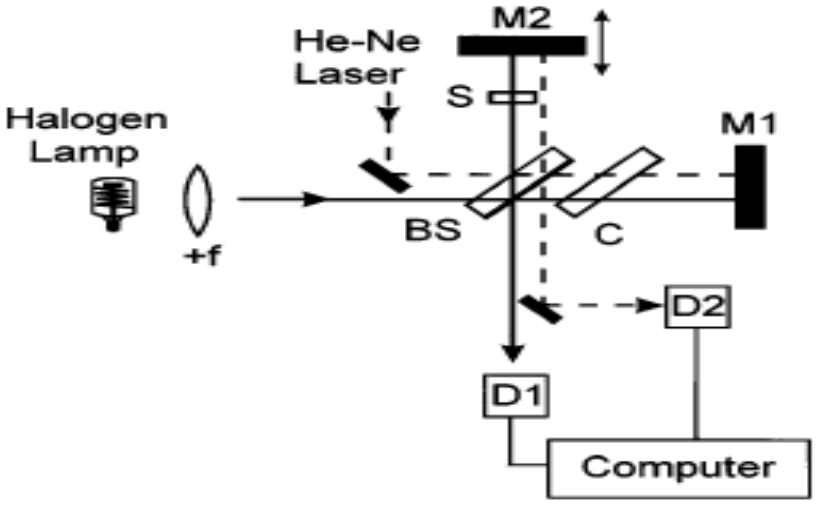

Figure 4.3.1(a) Experimental setup for recording white-light interferograms. White light and helium-neon laser fringes are measured simultaneously with detectors D1 and D2 and stored in a computer. The helium-neon fringes were used to determine by what distance mirror M2 is moved. Figure reproduced from Ref [7].

Thus, to effectively control the dispersion of a laser resonator, it is important to know the GDD and TOD of Cunyite over the respective spectral range. Several groups already reported about phase and group delay dispersion of Cr^{4+}:Ca_2GeO_4 (Cunyite) crystal using different measurement methods. The most recent measurement by Diddams et al. based on white-light interferometry demonstrated that its GDD measurement is in good agreement with the previous results. For our cavity design, we use this data which is believed to be the most reliable data. The dispersion (characteristics) of broadband Cunyite crystals is characterized in the wavelength range from 1006 to 1600nm.

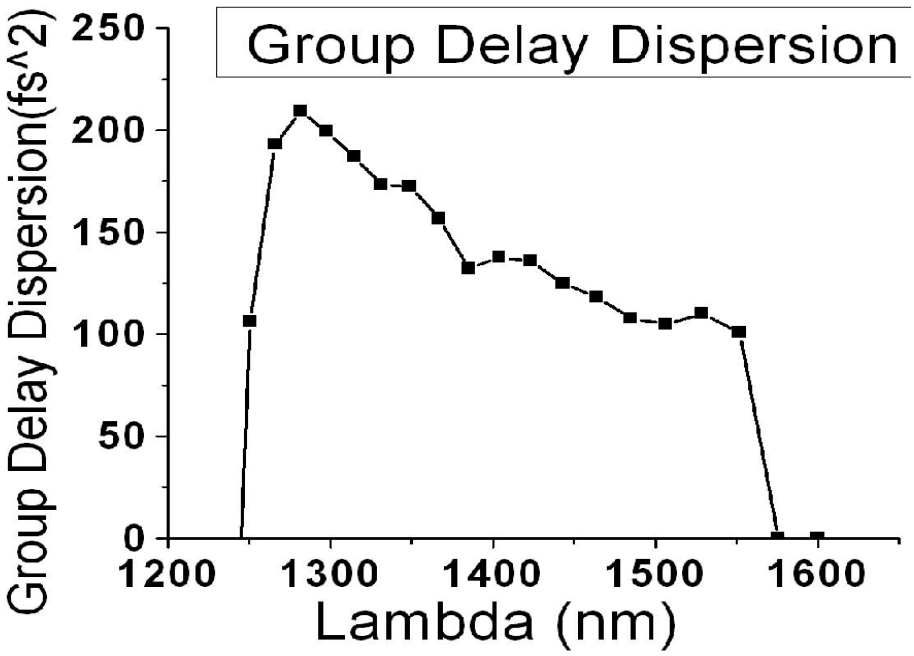

Figure 4.3.1(b) shows the measured group delay dispersion of the 3 mm Cunyite crystal with Fourier transform of the white-light interferometric cross correlation.

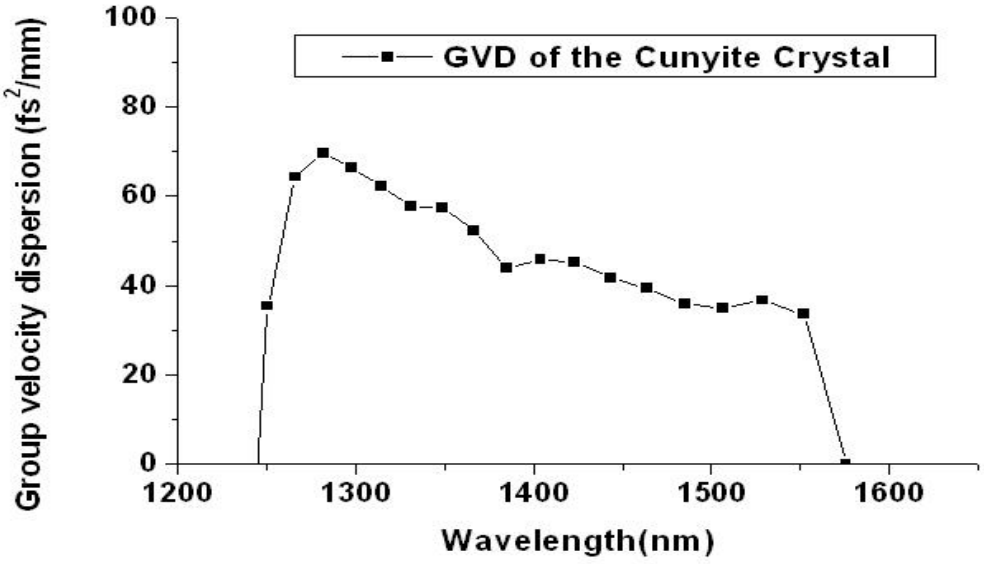

Figure 4.3.1(c) Measured group velocity dispersion per mm of the Cunyite crystal

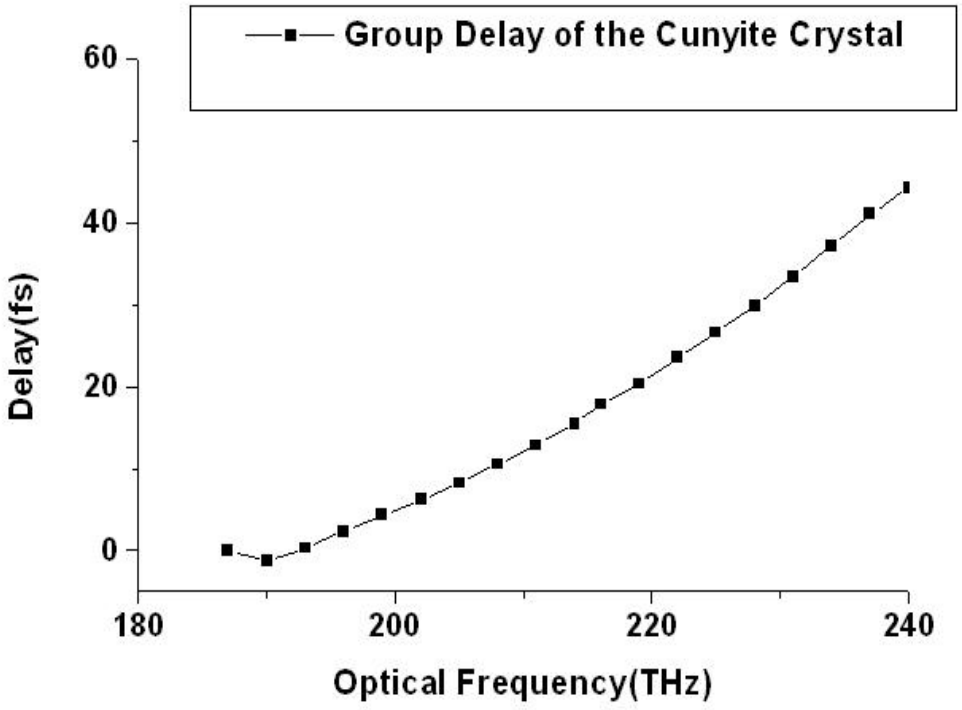

Figure 4.3.1(d) Measured group delay of Cunyite crystal with Fourier transform of the white-light interferometric cross correlation.

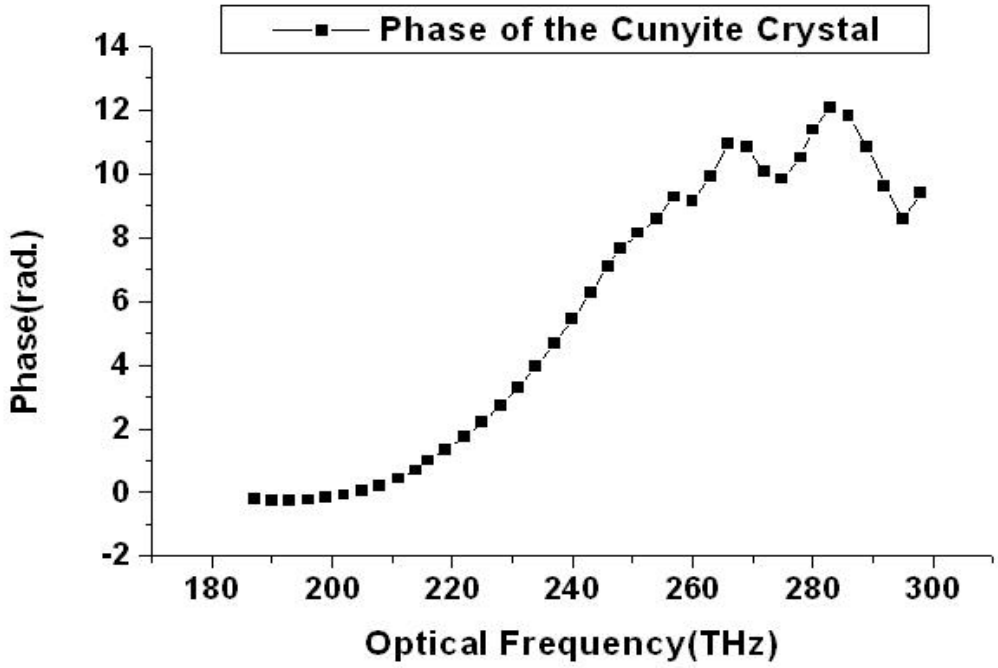

Figure 4.3.1(f) Measured phase of the Cunyite crystal using Fourier transform of the white-light interferometric cross correlation.

The data which is used to calculate the group delay dispersion, the group velocity dispersion, the group delay and the phase of the Cr^{4+}:Ca_2GeO_4 (Cunyite) crystal can be found in Appendix C.

4.4. Glass Slabs – A simple method for dispersion compensation

Another method that can be possibly used for intracavity GVD compensation in a femtosecond Cr^{4+}: Ca_2GeO_4(Cunyite) laser operating at 1450 nm is the introduction of a simple glass plate made of BK7, fused silica, quartz, etc. The GVD of some glasses become negative at longer wavelengths. Table 4.3.5 lists the zero-GVD of the BK7, fused silica, quartz glasses, as well as their negative GVD values at 1550 nm.

Glass	Zero-GVD wavelength	GVD at 1550nm
BK7	1322nm	-24.75 fs^2 /mm
Fused Silica	1273nm	-27.98 fs^2 /mm
Quartz	1279nm	-31.12 fs^2 /mm

Table 4.4.1(a) lists the zero-GVD of the BK7, fused silica, quartz glasses, as well as their negative GVD values.

Therefore, it is feasible to compensate the positive GVD from the Cunyite crystal with a glass plate at a wavelength longer than ~1350nm. For instance,compensating the GVD of a 1-mm Cr^{4+}: Cunyite crystal at 1450nm needs about 5-mm fused silica.

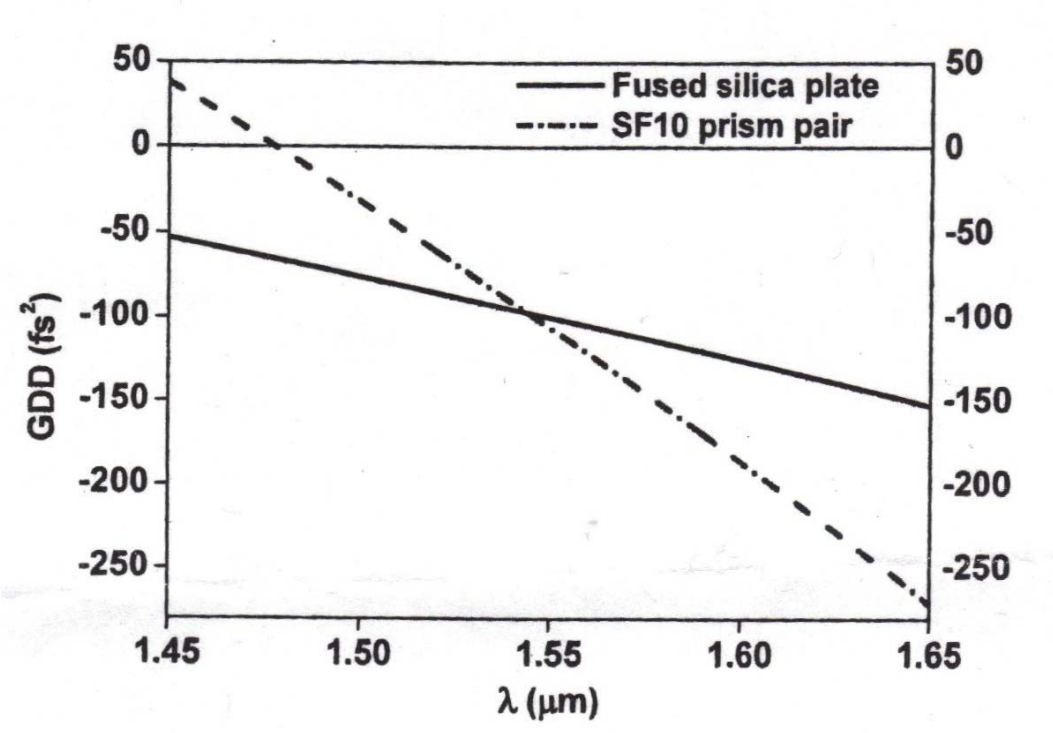

Figure 4.4.1(a) fused silica plate and SF10 prism pair GDD compensation'scomparison.

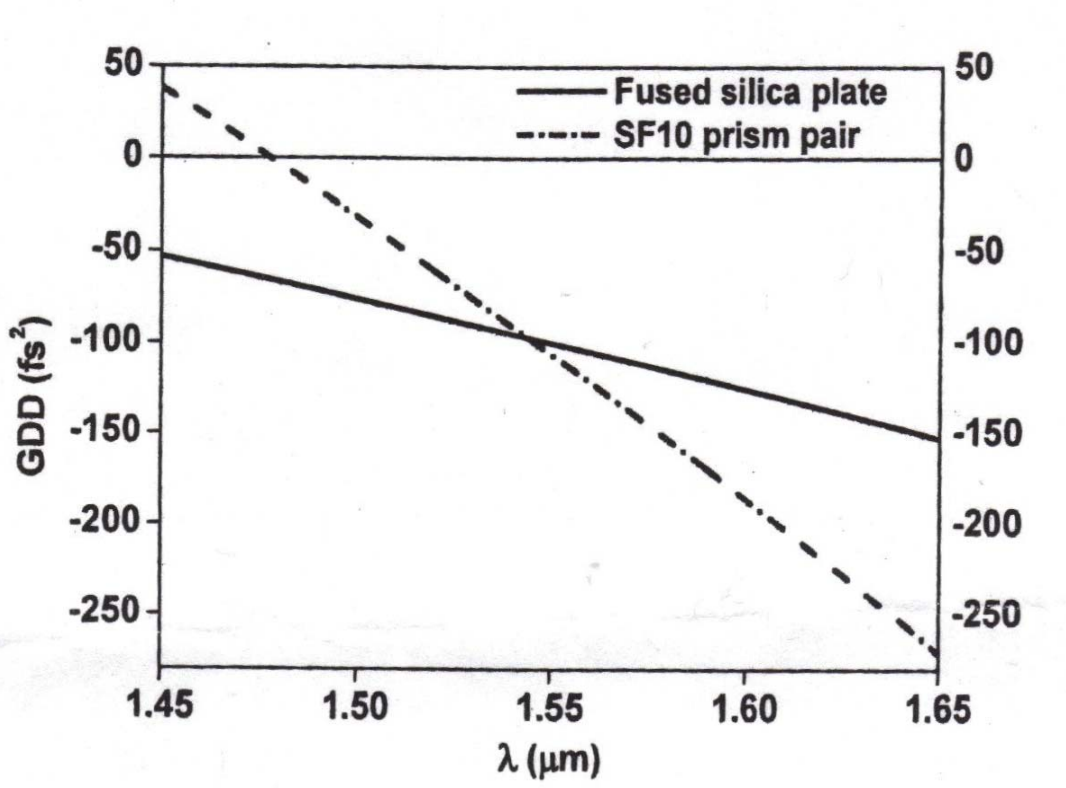

Figure 4.4.1(b) shows the GDD of a prism pair versus distance (L) between the two prisms.

The most important advantages of using a glass plate for GVD compensation are simplicity and low cost. A glass plate even with high polishing quality $\left(\frac{\lambda}{10}\right)$ and a very small wedge (<10) is at least several times cheaper than a pair of prisms or a pair of gratings. It can be placed under Brewster angle to minimize insertion losses.

4.5 Pulse Compression Using DCM's

Chirped mirrors are the most popular method of controlling group velocity dispersion in a laser cavity. Chirped mirrors [9,10,11,12] have proved to be essential devices for the production of ultra-short pulses directly from the oscillator, and more generally for many aspects of femto-second laser sources. Because of the dominant role

of soliton- like pulse shaping in ultra-short pulse solid-state lasers, femto-second pulse generation relies on net negative, i.e. anomalous intracavity group-delay dispersion (GDD). Solid-state gain media introduce a certain amount of frequency dependent positive (normal) dispersion in the cavity, which dispersion must also be balanced by anomalous dispersion. Brewster-angled prism pairs built into the laser cavity were the only low loss sources of broadband negative GDD until the use of negative dispersion or phase correcting dielectric laser mirrors was initiated.

These dielectric mirrors consist of alternating pairs of transparent high-index and low-index layers. A Bragg mirror reflects light when all the Fresnel reflections at the high/low index interfaces constructively add up. Chirping the mirror structure therefore allows the generation of a wanted group delay,GD(ω). Currently, only chirped mirrors can compensate for the limiting third-order dispersion in addition to second-order dispersion over a large bandwidth. Chirped mirrors have advantages over the prisms and gratings: (1) High efficiency. Chirped mirrors can have a reflection rate as high as that of normal dielectric mirrors e.g.reaching 99.8 percent (2) Large compensation bandwidth. Chirped mirrors can produce a nearly constant negative GDD over a large spectral range with very little oscillation around the target design (3) Simple arrangement. Chirped mirrors can be used just like normal dielectric mirrors. Ultra-short pulsed laser systems with chirped mirrors can be arranged very simply and compactly when compared with the systems using prisms or gratings.

Chirped mirrors have an important drawback. The impedance mismatch of the chirped mirror structure to the ambient medium (air) causes unwanted spectral oscillations around the target function. The oscillation amplitude increases dramatically

with mirror bandwidth. This problem can be solved by the so-called double-chirped mirrors (DCM).The impedance of the chirped mirror section is matched to the low-index or high-index material of the coating, which is then matched to the ambient air by an additional antireflection (AR) coating on top of the chirped mirror as shown in figure as

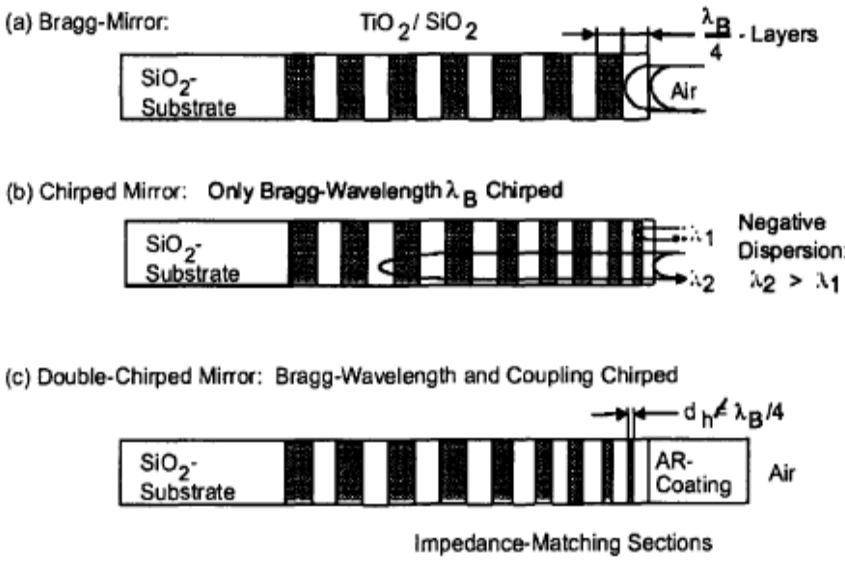

Figure 4.5.1(a) Standard Bragg mirror (b) Simple chirped mirror (c) Double chirped mirror.

When the dispersion is anomalous (negative), a longer wavelength travels a longer optical path and therefore has a higher group delay. However, this simple chirped mirror shown in Fig.4.5.1 (b) has a strong oscillation in group delay and GDD as a function of wavelength due to the impedance mismatch between ambient medium and the mirror stack as well as within the stack [13]. To avoid this problem, impedance matching sections are added, and this is called a Double-Chirped Mirror (DCM) shown in Figure 4.5.1(c).

The double-chirped mirrors (DCMs) consist of 48 SiO_2 and TiO_2 layers and were fabricated by ion-beam sputtering on fused silica substrates. Figure 4.5.1(f-i) shows the designed and calculated GDD with fitted curve for Cr^{4+}: Ca_2GeO_4 DCMs. The negative dispersion is well controlled from 1350nm to 1550nm range. The short wavelength is limited by the pump window at 1064nm.

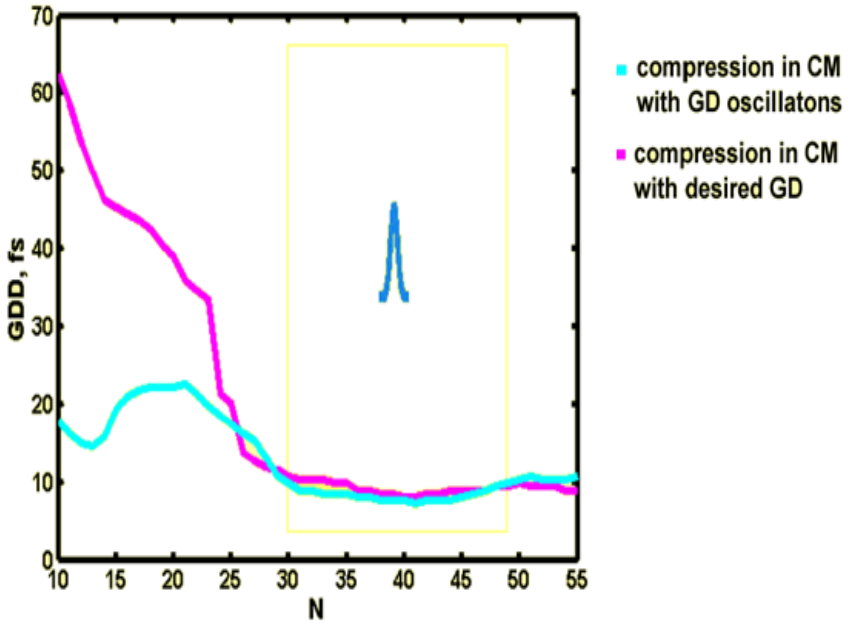

Figure 4.5.1 (d) shows the laser pulse compression in CM (red line) with GD oscillations and the compression in CM (green line) with desired GD.Figure reproduced from Ref [8].

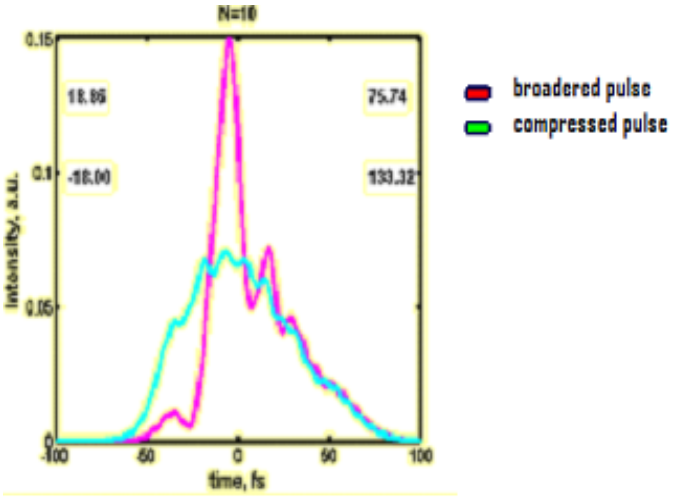

Figure 4.5.1(e) shows the difference between a broadened pulse with pedestals and a compressed pulse with Gaussian shape.Figure reproduced from Ref [8].

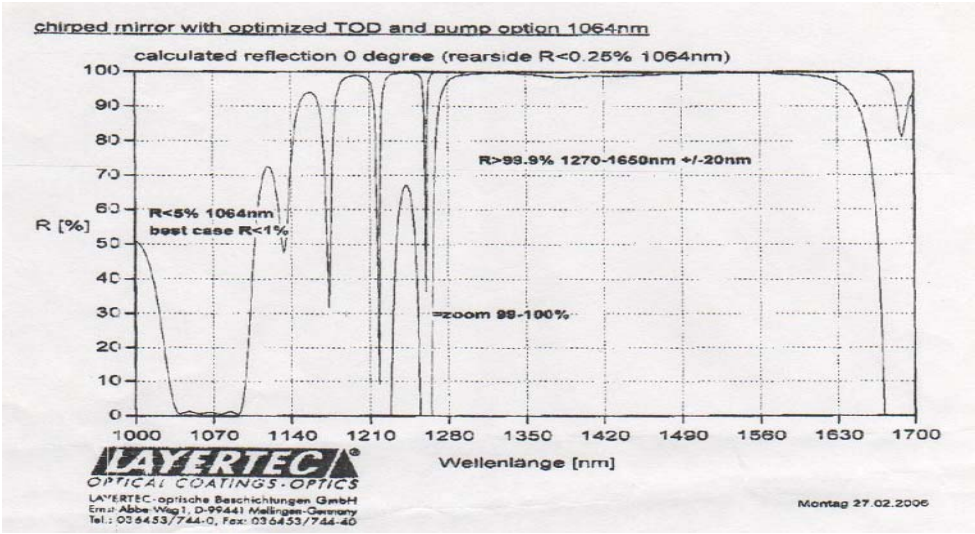

Figure 4.5.1(f) Reflectance's calculations of the Layertec chirp mirrors. (GVD= -50 fs^2).

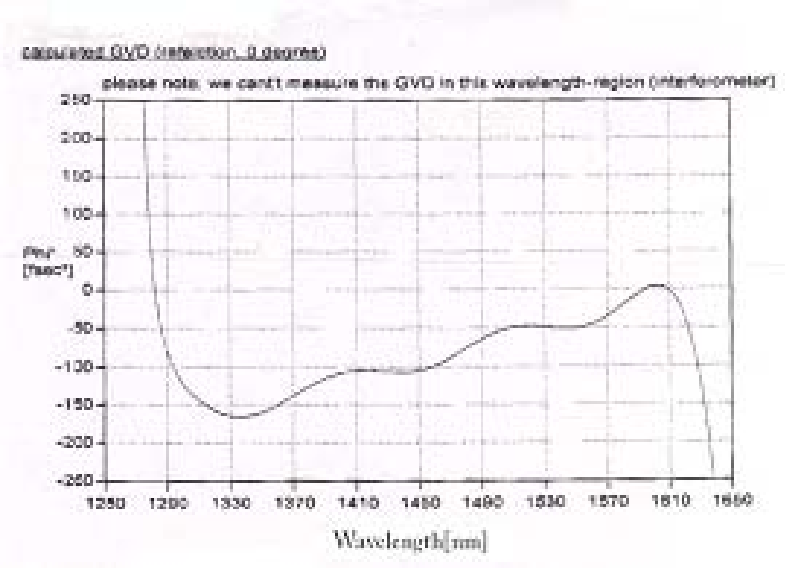

Figure 4.5.1 (g) Group velocity dispersion (-50 fs^2) calculations of the Layertec chirp mirrors.

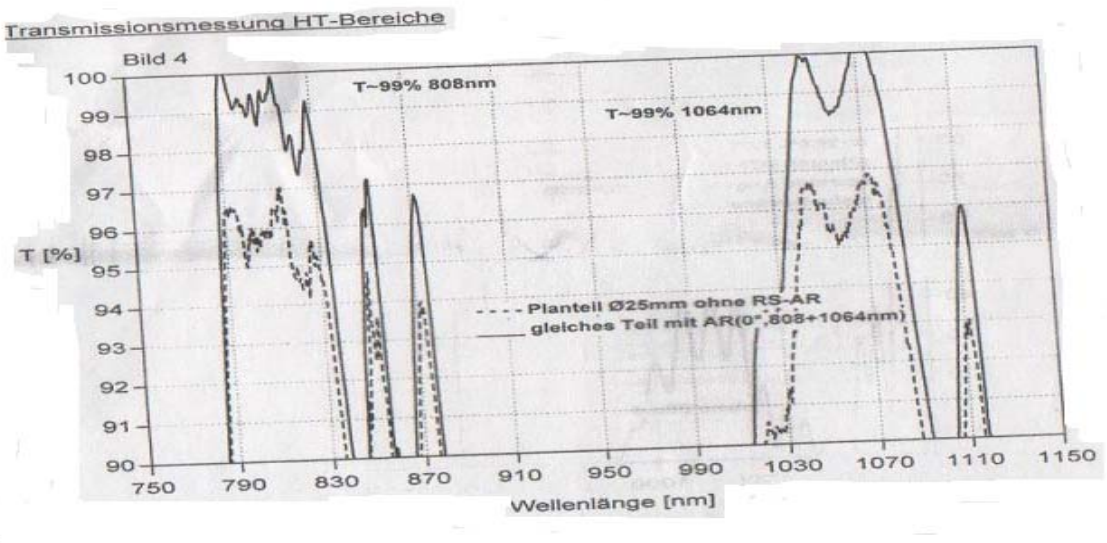

Figure 4.5.1(h) Transmission of the Layertec chirped mirrors.

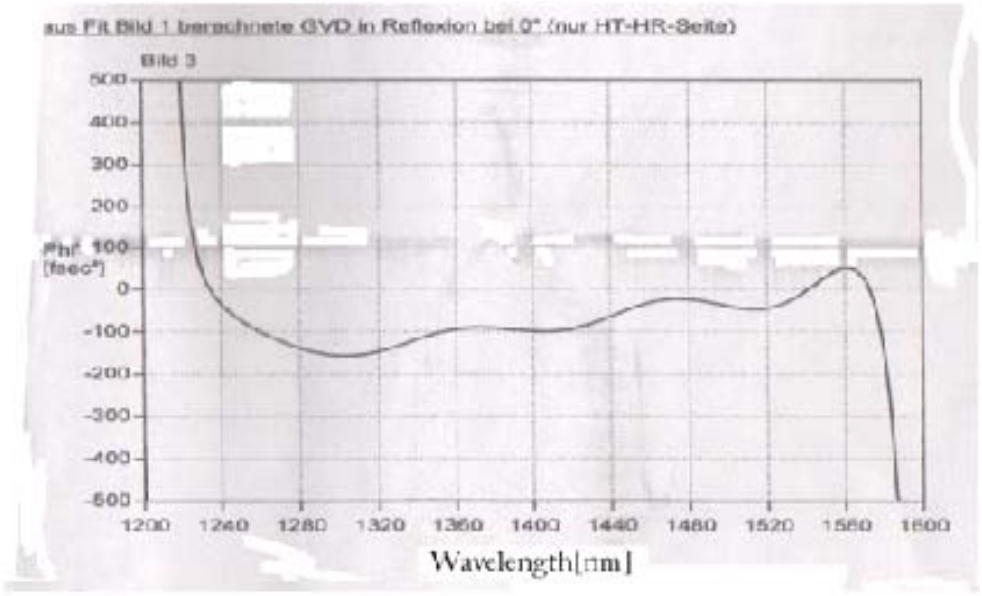

Figure 4.5.1(i) Group velocity dispersion (-100 fs^2) of the Layertec chirp mirrors.

Two pairs of chirped mirrors (M4-M7) were placed on the OC (M8) side. To estimate the net dispersion of the cavity, the negative group-velocity dispersion (GVD) contribution coming from the chirped mirrors with approximately-800fs^2 per bounce at 1450nm andCr^{4+}: Ca_2GeO_4 (GVD=+200 fs^2 at1430nm) gain medium was taken into account. The calculated dispersion of Cunyite using a fit to the measured reflection data is shown in Figure 4.5.1(f-i) above .The estimated total round-trip cavity dispersion is approximated to be – 800 fs^2 at 1430nm.

4.6. Broadband SESAM for self-starting Mode-locking

A possible alternative to KLM is passive mode-locking with a real saturable absorber, e.g. with a (SESAM). It is also possible to combine KLM and a SESAM [13, 15,16] to achieve self-starting mode-locking and very short pulses. As the light oscillates in the cavity, this preferential transmission leads to amplification of the high intensity spikes, causing the laser to mode-lock after many oscillations. This is one of the most

successful techniques for passively mode locking a laser. But as the name suggests, a semiconductor saturable absorber mirror (SESAM) necessarily absorbs some radiation causing some heating of the absorber at higher energies. The most dominant passive mode-locking schemes involve a semiconductor saturable absorber mirror (SESAM) as the passive element. There are a number of different SESAM designs commercially available in the market. To mode lock the laser, we used saturable absorber mirrors provided by the Chemistry Department at the City College of New York.

For passive mode-locking using saturable absorbers, two possible devices are typically used: a semiconductor saturable absorber mirror (SESAM) or a saturable Bragg reflector (SBR) [14,17]. Both provide an intensity-dependent reflectivity to administer the necessary loss/gain modulation and therefore the intense pulses in mode-locked operation are favored over the continuous-wave. Both devices exhibit similar characteristics, with layers of high and low index semiconductor materials to act as a Bragg reflector with a saturable absorber layer near the top of the device. The saturable absorber provides the modulation for mode-locking to take place. Initially noise spikes in the laser act to bleach the saturable absorber before building up into the mode-locked pulse train.

Any difference between the two devices can be found in the semiconductor layer structure and also the growth technique and post processing of the device. Generally, the absorber layer for a SESAM has been grown at lower temperature than that of a semiconductor Bragg reflector (SBR); this affects the spectral and temporal responses of the device with SESAMs displaying a much broader profile than SBRs where the spectral and temporal characteristics tend to be sharply peaked. With advances in epitaxial growth

techniques such as molecular beam epitaxy (MBE), these devices can be grown with greater precision. The range of research in which SESAMs or SBRs are used for mode-locking shows the versatility of these devices and the range of wavelengths and pulse durations, from pico-second to sub-10 femto-seconds, over which self-starting can be initiated and maintained.

There are five important macroscopic properties of semiconductor saturable absorbers that determine the operation of a passively mode-locked laser. These are impulse recovery time τ_A, modulation depth ΔR, nonsaturable losses ΔR_{NS}, saturation fluence F_{sat}, and the spectral bandwidth, $\Delta\lambda$.

The impulse recovery time τ_A is the time the device takes to recover after an intense incident pulse has saturated the device. A suitable recovery time is essential for the appropriate mode-locking mechanism. For fast saturable absorption mode-locking, this must be in the order of the pulse duration. For solitonic mode-locking the impulse recovery time can be up to ten times the duration of the pulse.

The modulation depth ΔR is the maximum change in reflectivity of the device between a low intensity incident pulse and a high intensity pulse that bleaches the absorber. To become bleached the incident pulse needs a fluence (defined as energy density per unit area) much larger than the saturation fluence of the absorber. The larger the modulation depth is, the shorter the duration of the pulse that can be supported and the greater the likelihood of a self-starting operation. Since larger modulation depth is the contributing factor of Q-switching instabilities,a balance must be found. To alter the modulation depth the reflectivity of the front surface can be altered, or the thickness of the absorber. Typically the modulation depth ΔR is 1-2%.

Non-saturable losses ΔR_{NS}, are any losses that are present after an intense pulse has bleached an absorber. These losses include a less than 100% reflectivity of the Bragg stack, scattering loss and residual absorption. The design and growth of the device influences the amount of nonsaturable losses present. Absorbers grown at low temperatures tend to display a significantly higher nonsaturable loss than a high temperature growth device such as a typical SBR. For use in low gain systems, such as the laser described in this thesis, the nonsaturable losses were kept as low as possible.

Saturation fluence, F_{sat} is defined as the energy density per unit area, and is a measure of the minimum energy density per unit area upon the saturable absorber required to fully saturate it. This property should ideally be kept as small as possible so that the device can be operated while fully saturated, minimizing any residual losses and allowing access to the available modulation depth. With high saturation fluence,Q-switched mode-locking is more likely to take place, and the possibility of damaging the structure is increasingly likely with higher fluence.

Another property of the saturable absorber is its spectral bandwidth. This is the range of wavelengths that are reflected from the Bragg stack and as such this places certain constraints on the minimum pulse duration that can be produced. The spectral bandwidth of the device can be determined from the index contrast between the layers of the Bragg stack and from the thickness of these layers. This property of the system along with the gain bandwidth of the gain crystal will determine the range of wavelengths over which lasing can be sustained. From this ,the minimum pulse duration can be determined.

In this project, semiconductor saturable absorber mirrors were used to initiate mode-locking. An outline of ultra-short pulse generation and characterization is given.

The effects of the propagation of an ultra-short pulse through a dielectric material were described and ways of exploiting these effects in various mode-locked techniques were discussed.

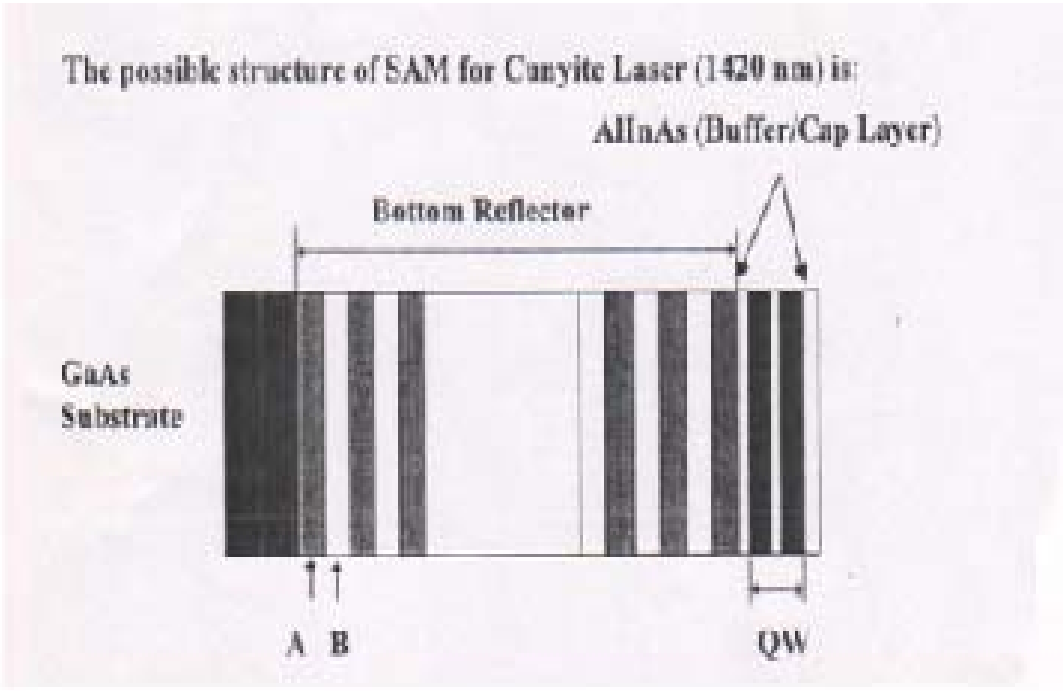

Figure 4.6.1 Basic layer structure of the homegrown semiconductor saturable absorber mirror.

4.7 Experimental results

4.7.1 Continuous-wave Performance of Cr^{4+}: Ca_2GeO_4 (Cunyite) Laser

For CW operation, a 4-mirror cavity resonator was used. Instead of a SESAM and a focusing mirror,a flat high reflective mirror was used as an end mirror. Since the fluorescence of Cr^{4+}:Ca_2GeO_4 (Cunyite) is quite weak, a short cavity with almost the same length was constructed. The final arm lengths used for (CW) lasing were L_1= 60 cm and L_2 = 45 cm .The cavity was designed so that the laser mode was of comparable size

inside the crystal for mode matching purposes. With this arrangement, this laser provided a continuous wave (CW) output in the 1430 nm spectral region with a minimum lasing threshold of 1W .The performance of the laser with the available output coupler was evaluated, as shown in Fig. 2.6.1.The slope efficiency of the laser with the available output coupler was calculated. For the 2.5% output coupler the slope efficiency was calculated to be 4.6%.

The cavity was designed so that the laser mode was of comparable size inside the crystal for mode matching purposes. Fig.4.5.2 shows the CW laser performance using 1%,2%, and 5% transmission OCs. The CW output wavelength was ~ 1430 nm for all OCs. The corresponding threshold pump power and the slope efficiency with respect to pump power were 0.5W, 1W, 1.5W and 3.125%, 4.58%, 3.75% respectively. The best laser power performance was obtained with the 2.5% OC shown in Fig. 2b. Using this 2.5% output coupler, the laser produced up 240mW of output power with 5W pump power. The threshold pump power and the corresponding slope efficiency for this mirror were 70 mW and 4.6%.

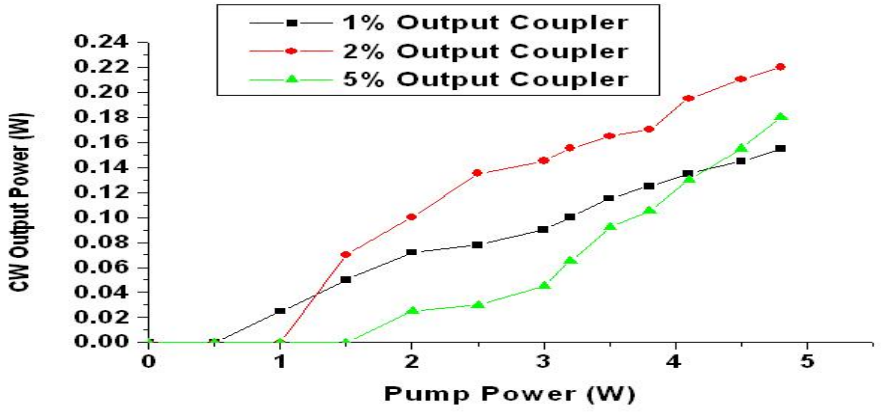

Figure.4.7.1. (Color on line) CW efficiency curves for the Nd:YAG pumped Cr^{4+}: Ca_2GeO_4 (Cunyite) laser taken with the 1% , 2.5% , 5% OCs.

Transmission	Slope Efficiency	Threshold (W)
T=1%	2.4%	0.5
T=2.5%	4.6%	1
T=5%	4.2%	1.5

Table 4.7.1 summarizes the CW efficiency curves and corresponding threshold pump power for the Cr^{4+}: Ca_2GeO_4 (Cunyite) laser taken with the 1%,2%,5% OCs.

The second feature of the laser to be characterized is its frequency tunability. This was achieved by placing a fused silica prism in the long arm (HR) of the cavity.This acted to disperse the intracavity modes enabling discrete wavelengths to be selected by changing the angle of the output coupler. The tunability of the laser with the 1% output coupler in place is shown in Fig. 4.6.b.It can easily be seen that the Cunyite laser was tunable between 1340nm and 1460nm. For these measurements the spectrum was monitored with an Ando spectrum analyzer with measurements taken every 2nm.

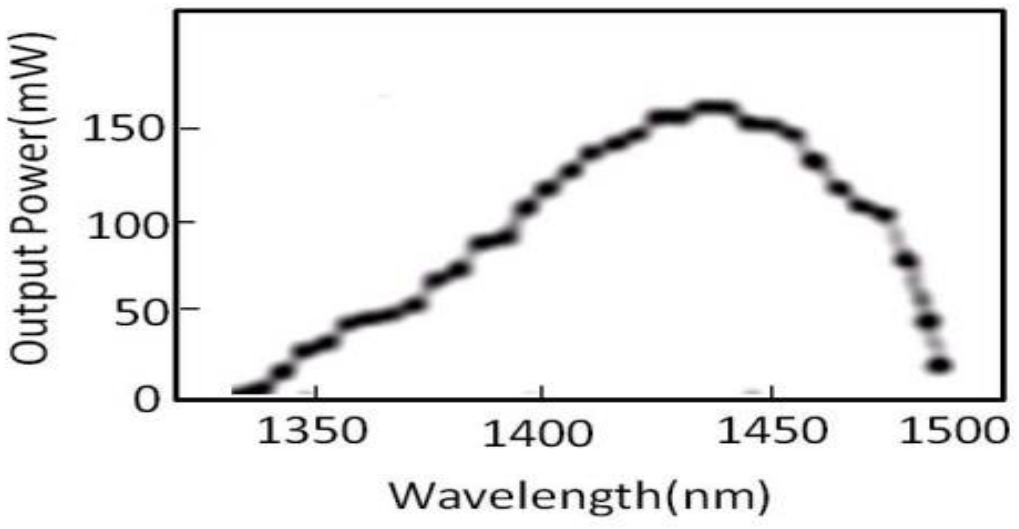

Fig4.7.1 b tuning range with 1% output coupler.Reproduced from Ref. [19].

4.7. 2 Passively Mode-Locked Performance of Cr^{4+}: Ca_2GeO_4 (Cunyite) Laser

The most complicated way to achieve mode-locking is by using passive mode-locking mechanisms. In this technique, the light in the cavity is used to cause a change in some intra-cavity element, which will then itself produce a change in the intra-cavity light. Fig.4.5.1shows the schematic diagram of the experimental arrangement for the self-starting passively mode-locked operation of the Cr^{4+}:Ca_2GeO_4 (Cunyite) laser. A 10-W Quasi-CW Nd: YAG laser operating at 1064nm was focused with a 3.85cm input lens (L) to pump the astigmatically compensated Cr^{4+}:Ca_2GeO_4 X -cavity consisting of two curved high reflectivity mirrors (M1andM2, R=50mm), a SESAM (M7) instead of a flat end high reflectivity mirror, a flat broadband output coupler (M6) in combination with several chirped flat dielectric mirrors (M4-M5) used for dispersion compensation. The total cavity length was 67cm, with asymmetric HR and OC arm lengths of 40 and 60cm, respectively. The separation between the mirror and the SESAM was ~ 5.5 cm.

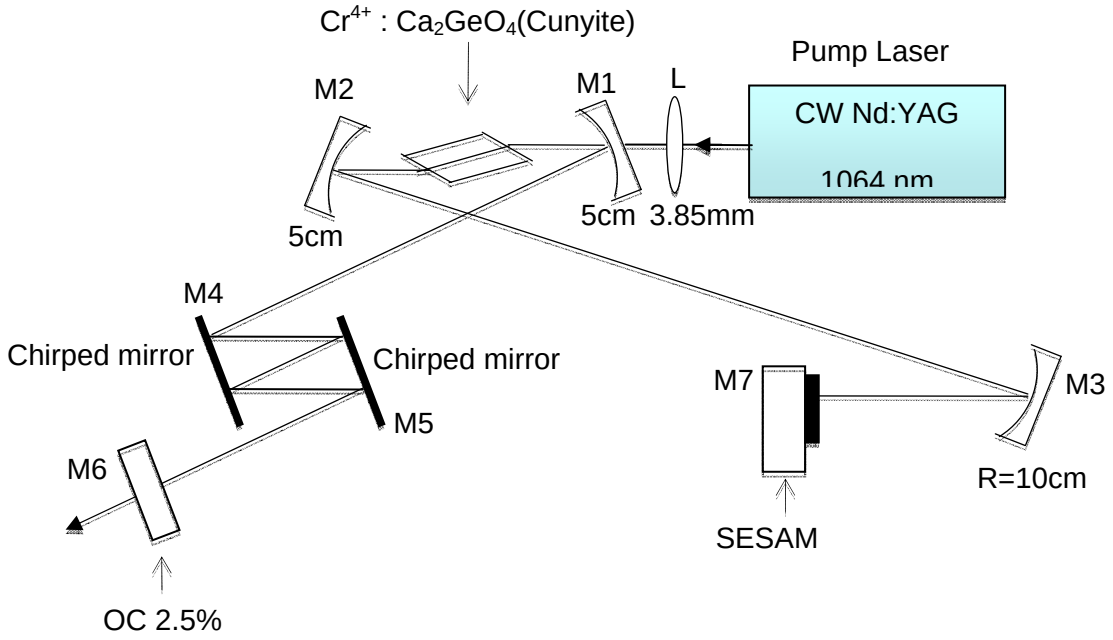

Fig.4.7. 2(a) Schematic of the Nd-YAG: pumped mode-locked Cr^{4+}: Ca_2GeO_4 (Cunyite) laser. The pump beam is focused onto a 4.5 mm-thick highly doped Cr^{4+}: Ca_2GeO_4 (Cunyite) crystal (absorption coefficient of $1cm^{-1}$ at 1064 nm). M1 and M2: Dichroic, curved high reflectance mirrors with R=5cm; M4 andM5: Chirped dispersive mirrors; M6: 2.5% broadband output coupler. M3: curved high reflectance mirror focusing the beam onto the SESAM; M7: SESAM mirror attached with thermal conductive paste to the center of a copper heatsink with 12.7 mm diameter.

In self-starting mode-locked operation [18], a pair of chirped mirrors (M4andM5) with group velocity dispersion (GVD) of approximately-100fs^2 per bounce was used to provide negative dispersion. The estimated total round-trip cavity dispersion was approximately -200fs^2. A SESAM (M7) was used to initiate and sustain mode locking.The SESAM had a a low level of non-saturable loss ~0.5%, a 2% saturable absorption at 1064nm, a 1% depth of modulation,a reflectivity of 99%,a bandwidth of 100nm ,an intracavity saturation fluence of 100 μJ/cm^2,and a carrier lifetime of 20-ps.The laser beam was focused onto the SESAM by a concave mirror (M3, ROC=100mm) The

incident angle on the SESAM-focusing mirror was as small as possible for the best operation. The beam size upon the SESAM was calculated to be 170μm.The separation between the mirror (M3) and the SESAM was 6.5 cm. With the SESAM in the cavity, the mode-locking became self-starting when the separation between the SESAM (M7) and the curved mirror (M3) was optimized.

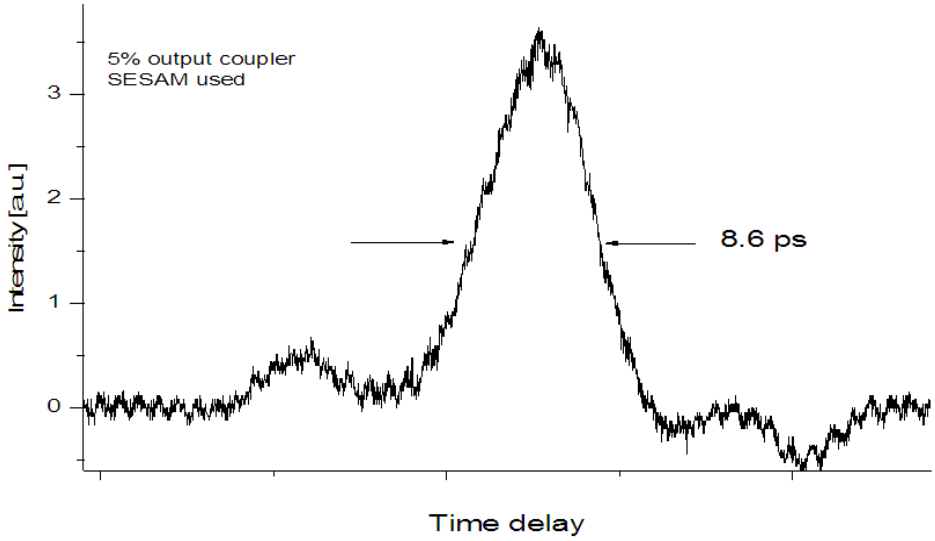

Figure 4.7.2(b) Autocorrelation trace of the 8.6ps pulses recorded .The pulse width was measured to be 5ps by assuming a $sech^2$ pulse profile.

Further optimization of the cavity resulted in a significantly wider spectra measurements of 5.2 nm. The reduction of the pulse width from 5ps to 365 fs indicated that dispersion-compensated mirrors are responsible for the shortening of the pulses.

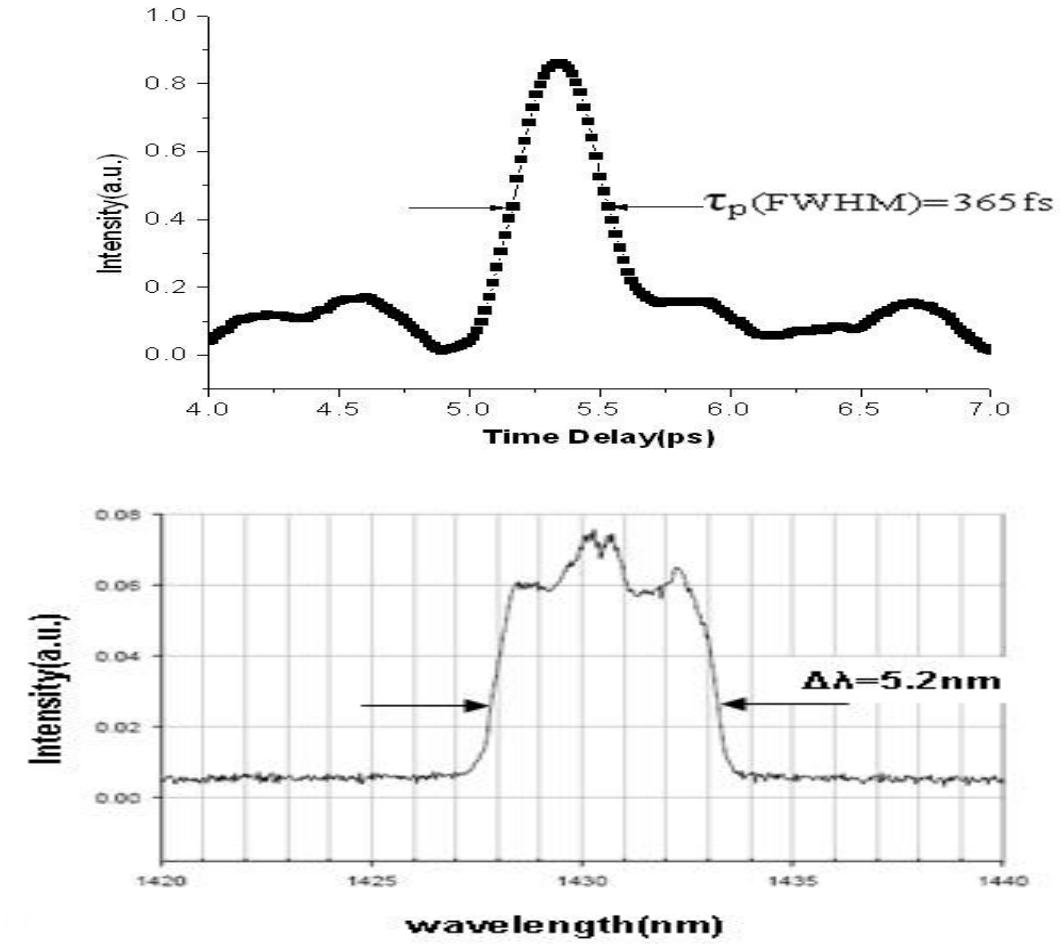

Figure 4.7.2(c) :(i)Autocorrelation trace of the 550fs pulses recorded (the pulse width was measured to be 365fs by assuming a $sech^2$ pulse profile) (ii) Spectrum of the mode-locked pulses (the spectral width of the pulses was measured to be 5.2nm)

The shortest autocorrelation width obtained with this setup is 450 fs which corresponds to a pulse width of 223 fs assuming a hyperbolic secant shape.The measurements do not last long enough to survive any spectra measurements.

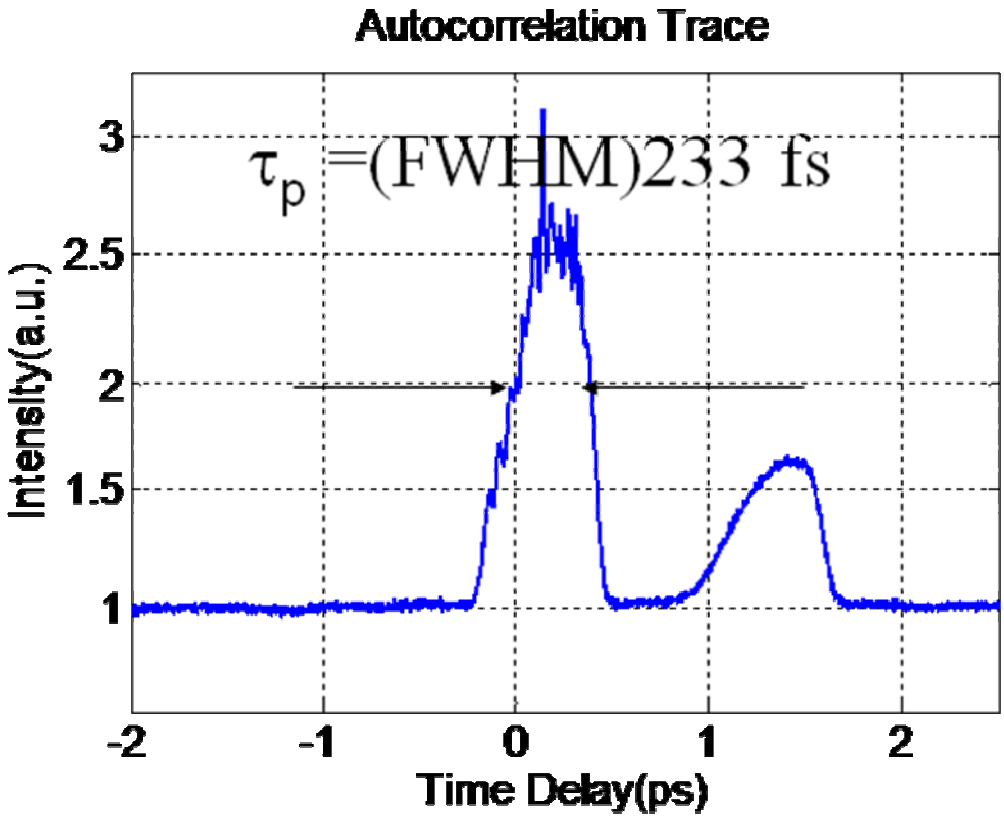

Figure 4.7.2 (d) Autocorrelation trace of the 450fs pulses recorded .The pulse width was measured to be 233fs by assuming a $sech^2$ pulse profile.

The pulsewidths measured in the preliminary self-starting passively mode-locking experiments are much longer than expected. However, the results presented are not surprising considering the amount of anomalous dispersion to be compensated. Using a higher output power CW mode-locked Nd: YAG in combination with an improved cavity design significantly shortens the pulse width to 5 picoseconds. Further improvement of the pulse width of the passively mode-locked Cunyite laser was achieved by replacing the Cr^{4+}:Ca_2GeO_4 (Cunyite) crystal (crystal) with a newer crystal. Crystal. In order to reduce the losses of the laser cavity, a 2.5% output coupler was used throughout the experiment.

Better thermal contact between the crystal and the aluminum block was achieved by wrapping the crystal in 1 mm thick indium foil.

Pulse-width measurements were carried out using a two-photon absorption auto-correlator. The autocorrelation trace of the pulse and the corresponding spectrum of the output pulses from the passively mode-locked Cr^{4+}: Ca_2GeO_4 (Cunyite) laser are shown in figure 4.7.2(a-d), respectively.

Table 4.7.2 calculated pulse duration from spectral bandwidth.

Spectral width FWHM (nm)	Center wavelength (nm) 1430 nm		Autocorrelation Width FWHM (fs) τac	Pulse Width FWHM (fs) τp	CB Numerical Constant
2		Gauss	1805.65	1276.98	0.441
		Sech	1407.42	912.13	0.135
3		Gauss	1203.77	851.32	0.441
		Sech	938.27	608.08	0.135
4		Gauss	903.40	638.49	0.441
		Sech	703.70	456.06	0.135
5		Gauss	722.26	510.79	0.441
		Sech	562.96	364.85	0.135

Table 4.7.2 compares different τac and τp widths assuming Gaussian-fit, Hyperbolic secant –fit.

4.8 Multiple Pulsing

Visible sidebands corresponding to net anomalous dispersion are characteristic to the output spectrum of a soliton mode-locked laser. The sidebands arise from the interaction between the soliton field and the non-solitonic dispersive waves. For certain frequencies, the two waves become phase matched, which results in the formation of narrow peaks superimposed on the smooth soliton spectrum. Generally they are an undesired effect that is a signature of soliton pulse losses but they are useful in determining the net cavity GVD [20].

Consider the case of anomalous dispersion, i.e., $\alpha < 0$ and $k < 0$. For large enough values of k, the total chirp becomes non-monotonic and has a reverse sign (as compared with that of the linear chirp) over a central part of the pulse Figure 1d. This behavior implies that the central part compresses whereas the outer parts of the pulse broaden. Consequently, only part of the pulse compresses efficiently, and a pedestal is formed. At higher pump powers, nonlinear effects cause wave breaking [21] which leads to multiple pulse operation. Thus, the wave breaking and pedestal formation are analogous phenomena and relate directly to the non-monotonic character of SPM and dispersion-induced chirp variation.

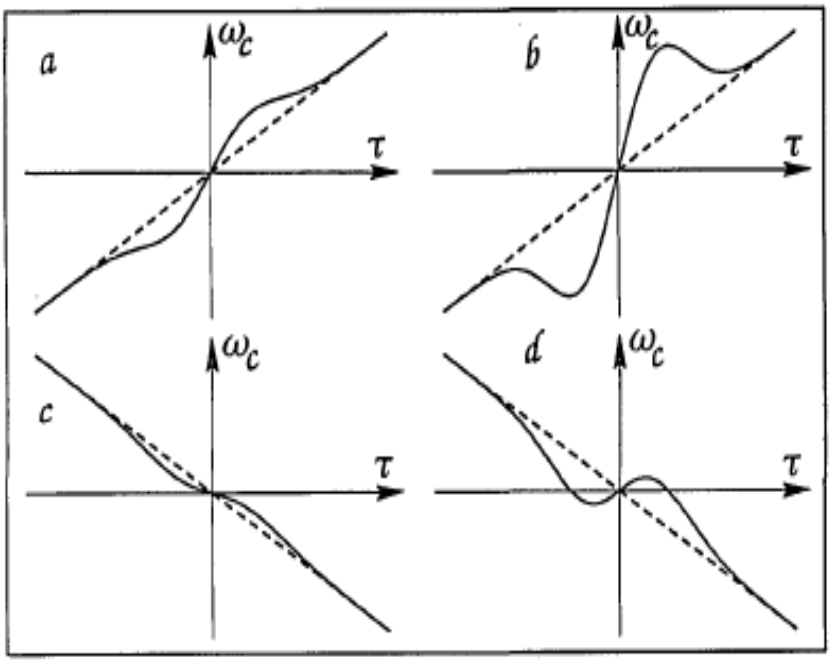

Figure 4.8.1Qualitative plot of the initial chirp variation: (a) normal dispersion, weak nonlinearity,(b) normal dispersion, strong nonlinearity, (c) anomalous dispersion, weak nonlinearity, (d) anomalous dispersion, strong nonlinearity.Reproduced from Ref [ ].

4.9 Conclusion

Self-starting operation of the chromium-doped Ca_2GeO_4 laser was demonsrated. Cr: Cunyite laser has been established as a source of femto-second pulses tunable in the near infrared at 1430 nm. Self-starting passively mode-locking techniques were successfully engineered and implemented leading to the generation of pulse width autocorrelation profile 550 fs pulses with 70 mW output power after adjusting the cavity.

Transform-limited 365fs will be scaled down to shorter pulses with higher damage- threshold SESAM. Sub-100-fs with the implementation of intracavity group-dispersion compensation will be pursued in the near future. Further progress to directly amplify these femto-second pulses is undergoing, which may lead to a reliable high-

energy light source. The performance of the Cr^{4+}: Ca_2GeO_4 (Cunyite) laser could be improved further by using quartz plates and a semiconductor saturable absorber mirror which exhibits a high modulation depth and low non-saturable losses.

Is there further room for extending the bandwidth of the Cr: Cunyite laser we built? The answer is yes. The first issue is the optimization of the SESAM. Higher modulation depth by optimization of absorbing layer thickness combined with broader reflectivity of mirror structure will significantly improve the bandwidth. A new Saturable GaInNAs Bragg Reflector design is currently made available.

The second issue is further characterized the thermal loading inside the laser crystal. Since the resonator condition is critical for critical modelocking, these thermal effects have strong influence on lasers. Because such thermal effects pose serious problems in power scaling and resonator stability, it is of paramount importance to determine accurately the amount of heat generation in the gain media in order to design the most optimum resonator configurations.

Further optimization of the Cr: Cunyite laser by SESAM is expected as a promising solution to get sub-100fs optical pulses in the 1.4μm spectral range in the near future.

4.10 References

1. A. Seas'thesis,"Generation of ultrashort pulses from chromium doped forsterite laser", pp130-148(1993).
2. Lectures' notes on laser optics from Professor Alfano's at the physics department of City College of New York (2005).
3. Richard. Barakat,"Ultrashort optical pulse propagation in a dispersive medium,"*J. Opt. Soc. Am. B* 3, 1602-1604 (1986).
4. M. Trippenback, T. C. Scott, and Y. B. Band,"Near-and-Far Field Propagation of Beams and Pulses in Dispersive Media", *Opt. Lett.*, 22(579),1997.
5. I. Walmsley, L. Waxer, and C. Dorrer, "The role of dispersion in ultrafast optics", *Review of Scientific Instruments,* 72(1), 1-29 (2001).
6. O. E. Martínez *et al.*, "Negative group-velocity dispersion using refraction", *J. Opt. Soc. Am. A*1(10),1003 (1984).

7 .S. Diddams and J.C.Diels,"Dispersion measurement with white-light interferometry,"*J. Opt.Soc. Am. B* 13,1120-1129(1996).

8 .S.O.Yakushev,I. A.Sukhoiva, O.V.Shulika, V.V.Lysak, S.I.Petrov "Simulation of interaction of the femtosecond laser pulses with chirped mirror",pp.(6-9-10).

9. F. X. Kaertner, N. Matuschek, T. Schibli, U. Keller, H. A. Hauls, C. Heine, R. Morf, V. Scheuer, M. Tilsch and T.Tschudi, "Design and fabrication of double-chirped mirrors", *Opt. Lett.* 22,831-833(1997).
10. F. X. Kaertner, U. Morgner, R. Ell, T. Schibli, J. G. Fujimoto and E. P. Pippen, V. Scheuer, G. Angelow, T. Tschudi, "Ultrabroaband double-chirped mirror pairs for generation of octave spectra" , *J. Opt. Soc. Am.* B 18, 882-885 (2001).

11. G. Tempea *et al.*, "Dispersion control over 150 THz with chirped dielectric mirrors", *IEEE J. Sel. Top. Quantum Electron* 4 (2),19(1998).

12. N. Matuschek *et al.*,"Theory of double-chirped mirrors", *IEEE J. Sel. Top. Quantum Electron* 4,197(1998).

13. I. D. Jung, F. X. Kartner, L. R. Brovelli, M. Kamp and U. Keller, " Experimental-verification of soliton mode-locking using only a slow saturable absorber", *Opt. Lett.*, 20(18), 1892-1894 (1995).

14. S. Tsuda,W. H. Knox, S. T. Cundiff,W.Y. Jan, J. E. Cunningham,"Mode-locking ultrafast solid-state lasers with saturable Bragg reflectors", *IEEE Journal of Selected Topics in Quantum Electronics*, 2(3), 454-464 (1996).

15. U. Keller, K. J. Weingarten, F. X. Kartner, D. Kopf, B. Braun, I. D. Jung, R. Fluck, C. Honninger, N.Matuschek and J.A. der Au," Semiconductor saturable absorber mirrors (SESAM's) for femto-second to nanosecond pulse generation in solid-state lasers", *IEEE Journal of Selected Topics in Quantum Electronics,* 2(3), 435-453 (1996).

16. B. Craig and A. Krueger, "Saturable Bragg reflectors simplify modelocking", *Laser Focus World* 36(8), 227-228 (2000).

17. S. N. Tandon, J. T. Gopinath, T. R. Schibli, G. S. Petrich, L. A. Kolodziejski, F. X. Kaertner, and E.P. Pippen, "Saturable Absorber with Large Area Broadband Bragg Reflectors for Femto-second Pulse Generation", CLEO 2003, Baltimore, MD (2003).

18. K. Weingarten, F. Kartner, D. Knopf, B. Braun, I. Jung, C. Honninger, N. Matuschek, J. Aus der Au, "Semiconductor saturable absorber mirrors (SESAMs) for

femtosecond to nanosecond pulse generation pulse generation in solid- state lasers", *IEEE JSTQE* 2,435 (1996).

19. IUSL Triennial Progress Report (City College of New York, July 1, 2003 - June 30, 2006) pp. 43.

20. M. L. Dennis and I. N. Dulling III, "Experimental study of sideband generation in femtosecond fiber lasers", *IEEE J. Quantum Electron* 30(6), 1459-1477 (1994).

21. D. Anderson, M. Desaix, M. Lisak, and M. L. Quiroga-Teixeiro, "Wave breaking in nonlinear optical fibe", *J. Opt. Soc. Am. B,* 9, 1358 (1992).

CHAPTER 5: SUMMARY AND FUTURE DIRECTIONS

5.1. Summary

The research efforts presented in this thesis pioneered the generation of ultrashort pulses using the chromium-doped cunyite laser. As a result Cr^{4+}: Ca_2GeO_4 (Cunyite) laser has been established as a reliable source of femtosecond and sub-10-fs pulses tunable in the near infrared. Self-starting passively mode-locking was successfully engineered and implemented leading to the generation of 224 fs pulses from the Cr^{4+}:Ca_2GeO_4 (Cunyite) laser.

This research treated the development of Nd: YAG pumped femtosecond Cr^{4+}:Ca_2GeO_4 (Cunyite) lasers based on chromium-doped solid-state materials and the investigations of their dynamics. The work concentrates on the development of stable laser oscillator capable of generating pulses as short as 224-fs. Different chromium-doped Cunyite materials were tested as a gain medium. Early attempts to generate mode-locked pulses led to the generation of 60 ps using a quantum-well-based semiconductor saturable absorber mirror. Further experiments resulted in the generation of the shortest sub-picosecond (223 fs) pulses to date from the Cr^{4+}:Ca_2GeO_4 (Cunyite) laser. The output power was 40 mW and the repetition rate 100 MHz. The mode-locked laser was tuned in the spectral range of 1390-1475nm.

Improvements in crystal growth and fabrication of semiconductor saturable absorber mirrors (SESAM) with higher modulation and lower nonsaturable losses will lead to larger output power and the generation of sub-100-fs pulses.

5.2. Future Directions

5.2.1 Additional Kerr-lens Mode-locked Cr^{4+}:Ca_2GeO_4 (Cunyite) laser

Femtosecond pulses can be generated from the Chromium-doped Cunyite laser without the assistance of a SESAM mirror. The laser shown in Fig. 5.2.1 is designed to achieve Kerr-lens mode-locking. Femtosecond pulses will be generated from the Chromium-doped Cunyite laser by adjusting the length of the Cunyite laser to match the frequency of the pumping CW modelocked Nd: YAG laser.

Femtosecond pulse formation in a broadband solid-state Cunyite laser relies on the cavity round trip time decreasing with the optical frequency near the gain line center [(negative group delay dispersion)] because of the strong self-phase modulation[1] inherent in the Cunyite crystal. Negative dispersion will be introduced by a new set of high reflectivity dielectric mirrors that provide the feedback necessary for oscillation. Because of the reduced mirror dispersion the number of reflections off the dispersive mirrors per round trip has been increased from four to eight. This will result in a more balanced distribution of the negative group delay dispersion (GDD) in the cavity reducing the discretenees of solitonlike shaping. The chirped mirrors are designed to have a group velocity dispersion (GVD) of -130 fs^2 and a reflectivity of at least 99.9 percent over the spectral range 1.3μm to 1.6 μm. Using multiple reflections from these mirrors, as much as four times the GVD of one chirped mirrors in the cavity can be provided. To estimate the net dispersion of the cavity the negative group-velocity dispersion (GVD) contribution.The estimated total round-trip cavity dispersion was approximated –950 fs^2 at 1450nm.

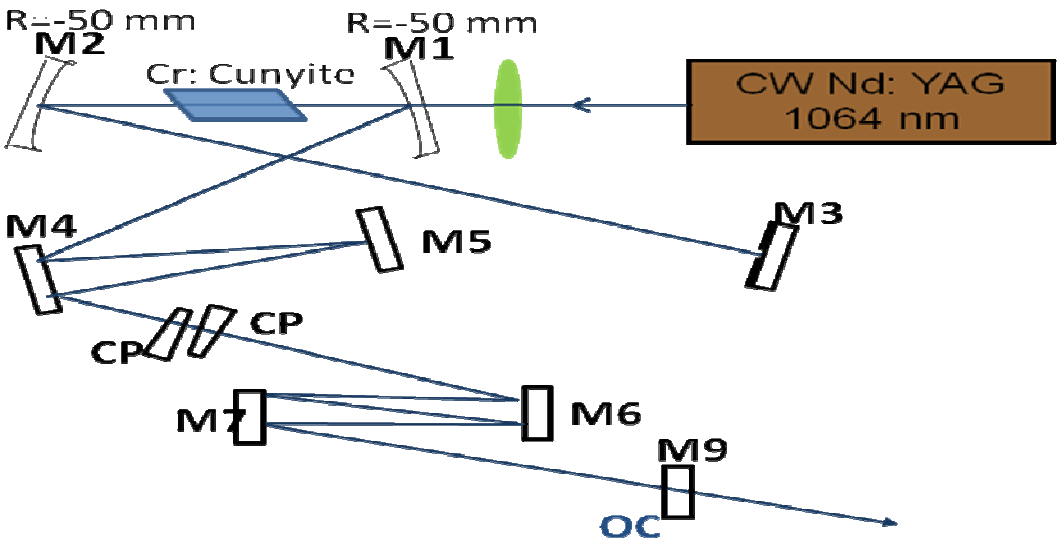

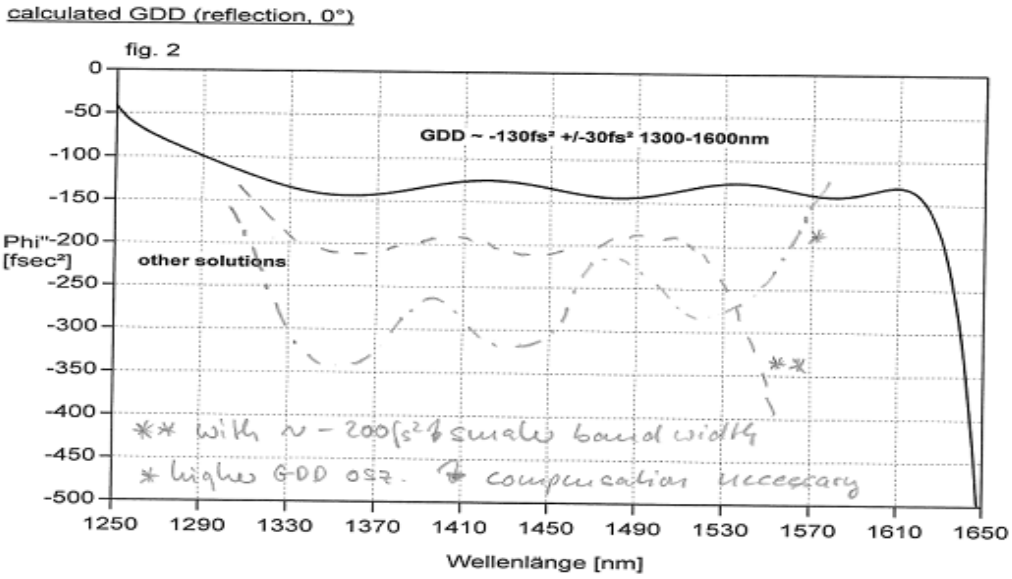

Figure 5.2.1a Schematic of laser setup of a mirror-dispersion-controlled KLM Cr^{4+}:Ca_2GeO_4 laser. The pump beam is focused by a 38.5mmlens onto a 3.8-mm thick highly doped Cr^{4+}:Ca2GeO4 crystal. (M1,M2) single-stack quarter-wave dichroic mirrors highly transmitting at the pump wavelengths with radii of curvature of 5cm; (M3-M7) chirped dispersive mirrors;OC,1% broadband output coupler; CP: wedged .compensating glass plate, (b) GDD of the chirped dispersive mirrors.

5.2.2. Improved Self-Starting Passively Mode-Locked Cr^{4+}: Ca_2GeO_4 (Cunyite) Laser with Double Chirped Mirrors

Another enabling technology for applications is the exploitation of optimized semiconductor saturable absorber mirrors (SESAMs)[2] as intracavity elements to passively initiate and maintain the pulse with a greater degree of fewer cavity constraints than apply in Kerr-lens mode-locking. Favorable characteristics of our newest SESAM mirror are the low nonsaturable losses, low saturation fluence, fast recovery for absorption and a high modulation depth.

The SESAM mode-locked Cunyite laser demonstrates superior stability to a purely Kerr-lens mode-locked one. Kerr-lens mode-locking (KLM), although it has been widely used to produce femtosecond laser pulses, is generally not self-starting. The starting and the stabilization of the mode-locking are more difficult to achieve in chromium-ion-doped crystal families, particularly in Cr^{4+}:Ca_2GeO_4 (Cunyite) since the host crystals require low-temperature to prevent thermal fluctuations.

The estimated total round-trip cavity dispersion was approximated – 1000 fs^2 at 1450 nm. Sub-100fs will be generated by self-starting passively modelocking.

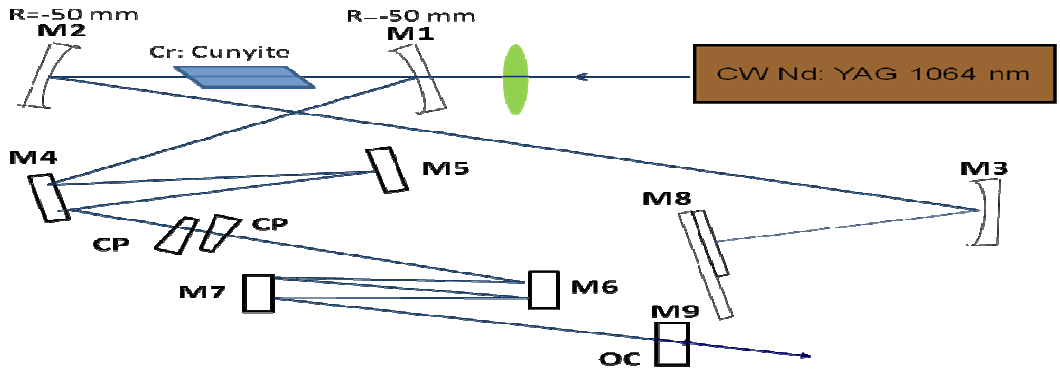

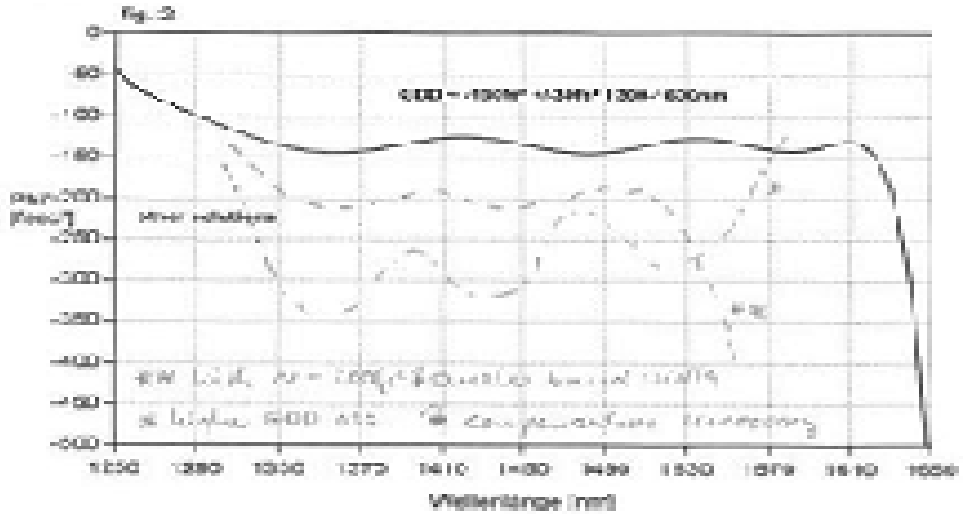

Figure 5.2.2 Schematic of the laser setup of a mirror-dispersion-controlled KLM Cr^{4+}:Ca_2GeO_4 laser with GDD of the chirped dispersive mirrors. The pump beam is focused by a 38.5mm lens onto a 3.8 mm thick highly doped Cr^{4+}:Ca_2GeO_4 crystal. M1-M3, single-stack quarter-wave dichroic, curved folding mirrors highly transmitting at the pump wavelengths with radii of curvature of 5cm; M4-M7chirped dispersive mirrors; M8 - a GaInNAsSb SESAM mirror; (M7),OC -3% broadband output coupler; CP: wedged compensating glass plate. (b) GDD of the chirped dispersive mirrors.

5.3 Femtosecond Cr^{4+}:Ca_2GeO_4 (Cunyite) for Applications in Telecommunications and Biophotonics

A specific area of research needed for successful future developments of ultrafast Cunyite lasers that can be suitable for data-communications or biophotonics relates to device designs that offer more compact and rugged laser configurations.

5.3.1 Applications of ultra-short lasers in the 1300 nm spectral region

When considering femtosecond pulses at 1300 nm there are two fields for which this wavelength regime is particularly suited; these are telecommunications and biophotonics. In the field of telecommunications [3] the wavelengths are chosen based on how well they propagate in optical fibers.

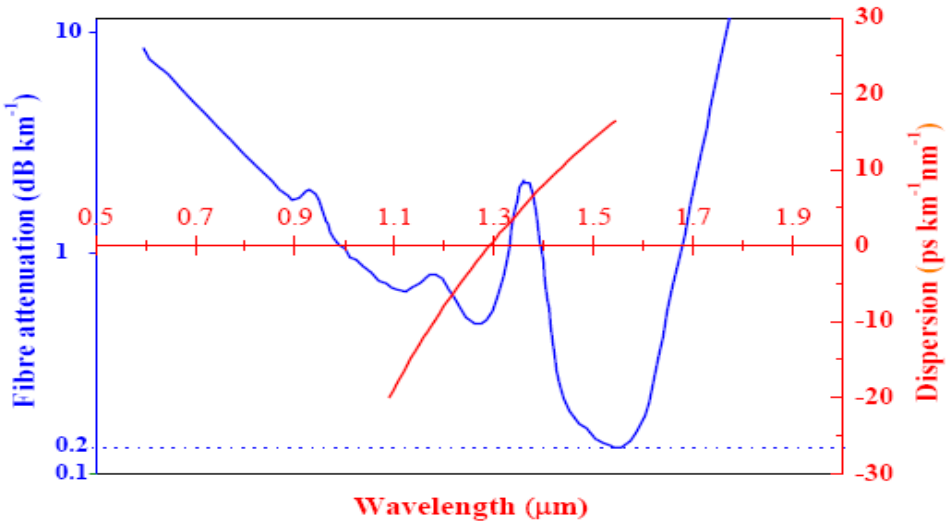

Figure 5.3.1Attenuation and dispersion for a typical optical fiber showing a minimum at 1550nm.

The graph shows that a minimum of attenuation exists around 1550 nm. Thus this is the wavelength regime that current long range (transoceanic) networks use and where the well-developed optical amplifiers are found. However, if pulses have to be used successfully then the dispersion characteristics of the fiber have to be considered. In the spectral region around 1300nm there is negligible dispersion; therefore these pulses will not broaden significantly as they propagate in an optical fiber. This is of particular importance in systems where dense wavelength division multiplexing (DWDM) is to be

used [4], since as the pulse travels down an optical fiber it will broaden in time if this is not counteracted at that moment.

A second area in which pulses around 1400nm are desirable is in the field of biophotonics [5]. Fig. 5.3.2 shows that human skin has a transmission window centered approximately at 1400nm [4]. The major constituents in biological tissue that absorb radiation include water, melanin, and oxyhaemoglobin (HbO_2**)** for which the attenuation characteristics are shown. The graph shown that in the 1300 nm region there is minimum of absorption between these three components and, therefore, this spectral region is ideal for therapeutic or diagnostic applications in medicine [5].

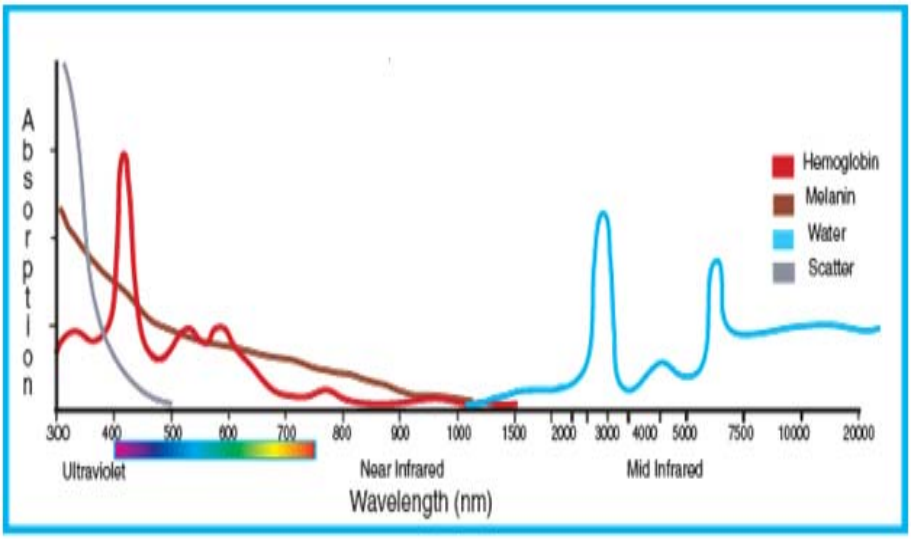

Figure 5.3.2 Infrared light is absorbed primarily by water, while visible and ultraviolet light are primarily absorbed by hemoglobin and melanin, respectively. As wavelength decreases toward the violet and ultraviolet, scatter or absorption from covalent bonds in protein limits penetration depth in this range. (Figure reproduced from Shore Laser)[6]

The topic of photodynamic therapy is of particular interest [7]. This is where a photo-sensitizing agent is introduced into the tissue and illuminated by optical radiation, specifically laser radiation. This agent can be designed to fluoresce to aid in the diagnosis of disease, or to undergo a chemical change for therapeutic purposes. This technique is desirable for the diagnosis or treatment of a number of ailments, many of which require radiation that can penetrate deeply into the tissue.

The high peak powers generated from an ultrashort pulse laser allow for the additional possibility of 2-photon absorption techniques to be utilized. Due to absorption around 1400nm, minimal damage will be caused by the passage of light through tissue. A chemical or a dye that absorbs at half this wavelength could be introduced into the desired area of tissue. Then light from a femtosecond Cr^{4+}**:** Ca_2GeO_4 (Cunyite) laser, which operates in the 1400 nm spectral regime, would be absorbed where it is needed without causing any damage to the surrounding tissue.

The interaction of light with biological matter such as tissue, cells and intracellular bodies like chromosomes [10,11] is highly wavelength-dependent. It is often necessary to use complex optics to deliver the light and when, as is becoming more and more common, short pulses are used, there is an additional wavelength dependence added by the dispersion of the optical system. Precise intracellular microsurgery and in-depth penetration of light into tissue are both examples of processes that are made possible by utilizing the multi-photon interaction of short-pulse laser radiation with matter. The first can be used to accurately incise or ablate intra-cellular components, hence affecting the manner in which the cell functions, and the second to image deep within tissue [8,9]. In both cases it is important that as little absorption as possible occurs out of the focal

volume and it can be done by keeping single-photon absorption to a minimum. Hence, it is of great importance to select the wavelength of the laser with care, taking into account single-and multi-photon cross sections plus the dispersion characteristics of the optical system.

In multi-photon interactions, longer wavelength radiation requires more incident photons for ionization such that absorption cross-section is lower than at shorter wavelengths and the localization of the two-photon process is enhanced. Furthermore, the multi-photon absorption cross-section has been found to decrease in many biological tissues with longer wavelength and 1300 nm lies within a single-photon absorption window.

5.4 Conclusion

Chromium-doped Cunyite (Cr^{4+}:Ca_2GeO_4) is one of the most promising tunable solid-state materials for near-infrared. Since the first demonstrations of pulsed and cw lasing in Cr^{4+}:Ca_2GeO_4 (Cunyite), it has attracted significant attention from researchers. The lasing wavelength of Cr^{4+}:Ca_2GeO_4 (Cunyite) is centered at 1400nm and extends from1300 nm to 1600 nm, making it a complementary laser material for Ti: sapphire lasing wavelength (700-1100 nm) and Cr^{4+}: YAG lasing wavelength (1400-1600 nm).

The 1.3-1.6μm regime is a natural direction in which to apply the femtosecond Cr^{4+}:Ca_2GeO_4 (Cunyite) lasers because wavelength and frequency references in this regime are important for telecommunications, remote sensing, biomedical imaging and diagnostics applications,fiber sensing and semiconductor devices,glass-ceramics preparation suitable for fiberization and waveguide. Theoretically, the bandwidth of this crystal can support sub-11 fs pulses. The nonlinear refractive index of this material is

indeed sufficient to support Kerr-lens mode-locking. This is an indication that the Cr: cunyite laser can operate, similar to Cr^{4+}: Mg_2SiO_4 (forsterite) lasers in a self-mode-locked regime. The region near 1400 nm is important for several reasons.

First, light scattering in biological tissues at this wavelength is significantly reduced from scattering at 800nm (the center wavelength of the Ti: sapphire laser) and 1064 nm (the center wavelength of Nd: YAG, and absorption is significant lower at approximately 1400 nm (the center wavelength of Cr^{4+}:Ca_2GeO_4 (Cunyite)). Light in the mid-near infrared can penetrate deeply into biological tissues, capitalizes on absorption by adipose tissue and water. Wavelengths in the 1400nm range are less damaging to biological samples than other ultrafast lasers making Cr^{4+}: Ca_2GeO_4 (Cunyite) based femtosecond laser systems an ideal source of ultrashort pulses for biological and medical applications. This wavelength falls in the transparency window of most biological tissues allowing deep tissues penetration with minimal photo damaging and making it a valuable alternative source for multi-photon imaging.

Second, this wavelength is near the zero-dispersion wavelength of optical fibers and thus makes Cr^{4+}:Ca_2GeO_4 (Cunyite) potentially important for optical communications. The extremely broadband pulses around telecommunication wavelength of 1.5μm are highly demanded in numerous applications, such as optical telecommunications.

Cr^{4+}:Ca_2GeO_4 (Cunyite) is at the forefront of photonics. The main idea behind this research is that sub-100 fs pulses will be generated by adjusting the length of the Cunyite laser to match the frequency of the pump laser. Cr^{4+}:Ca_2GeO_4 (Cunyite) solid-state lasers, because of their wavelengths of operation, have a huge potential. This laser provides a

source that can be applied to several different areas of research. The versatility of this laser will allow for its continued development and probable commercialization.

5.5 References

1. O. E. Martínez and R. L. Fork, "Theory of passively mode-locked lasers including self-phase modulation and group-velocity dispersion", *Opt. Lett.* 9 (5), 156 (1984).
2. A. J. DeMaria, D. A. Stetser, and H. Heynau, "Self mode-locking of lasers with saturable absorbers", *Appl. Phys. Lett.* 8, 174 (1966).
3. Knox, W.H., "Ultrafast technology in telecommunications",*IEEE Journal of Selected Topics in Quantum Electronics,* 2000. 6 (6): p. 1273-1278
4. Dennis, T., Curtis, E.A., Oates, C.W., Hollberg, Gilbert S.L., "Wavelength References for 1300-nm Wavelength-Division Multiplexing*", Journal of Lightwave Technology, 2002*. 20 (5): p. 776-782.
5. Svanberg, S.,"Some applications of ultrashort laser pulses in biology and medicine", *Measurement Science & Technology, 2001*. 12 (11): p. 1777-1783.
6. Light-interactions with tissues "Water, hemoglobin, melanin, scatter, and absorption" graph reproduced from www.shorelaser.com.
7. Diamond I, Granelli S G, McDonagh A F, Nielsen S, Wilson C B and Jaenicke R "Photodynamic therapy of malignant-tumors ",*J.Opt.Soc.Am.* 64 534.
8. Fischer, P., A. McWilliam, C.T.A. Brown, K. Wood, M.MacDonald, W.Sibbett, and K. Dholakia, "Deep tissue penetration of radiation: modelling and experiments", Paper CL-4-Wed, European Conference on Lasers and Electro-Optics (ECLEO), Munich, Germany, 2005.
9. Cheong, W.F., P.S.A., and A.J.Welch, "A review of optical properties of biological tissues", *IEEE Journal of Quantum Electronics, 1990*. 26 (12): p. 2166-2185.

10. Konig K. Riemann I and Fritzsche W 2001 Nanodissection of human chromosomes with near-infrared femtosecond laser pulses *Opt. Lett*.26 819-21.

11. Laing H.Wright W H, Cheng S, He W and Bems M W 1993 Micromanipulation of chromosomes in Ptk2 cells using laser microsurgery (optical scalpel) in combination with laser- induced optical force (optical tweezers) *Exp. Cell Res.* 204 110-20**.**

APPENDIX

APPENDIX A : Mirror Coatings of Four-Mirror Cavity Design

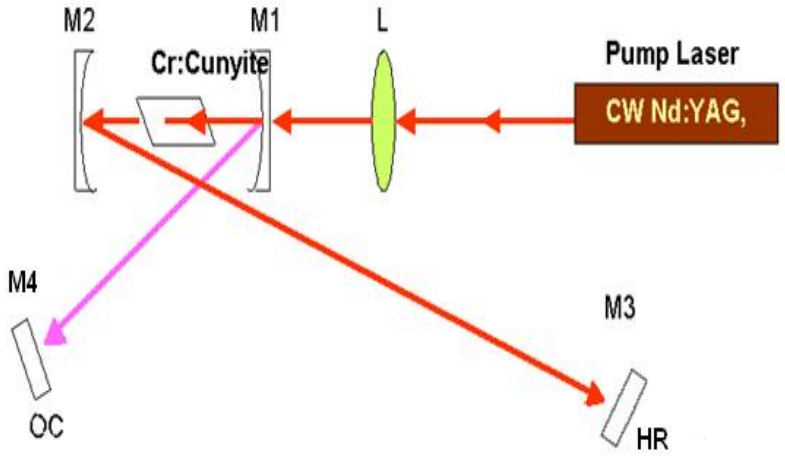

Fig.A1. Schematic of a Cr^{4+}: Ca_2GeO_4 (Cunyite) typical four-mirror astigmaticallycompensatedcavity showing the beam mode size. The experimental arrangement is shown above. The Brewster -cut Cunyite crystal is placed in a four - mirror X-fold astigmatically compensated cavity.

M1: Dichroic,curved mirror,1/2-inch with R>99.9% @ 1420 nm and T>90% @ 1064nm, **M2**, curved mirror, ½-inch with R> 99.9% @ 1064/1420nm, both high reflecting. ROC=50 mm**M3**, 1-inch flat mirror,R>99.9% @ 1064/1420 nm, high reflecting at both wavelengths**M4-O,**1-inch flat mirror , R> 99.9% @1064nm and T =5% @ 1420nm .

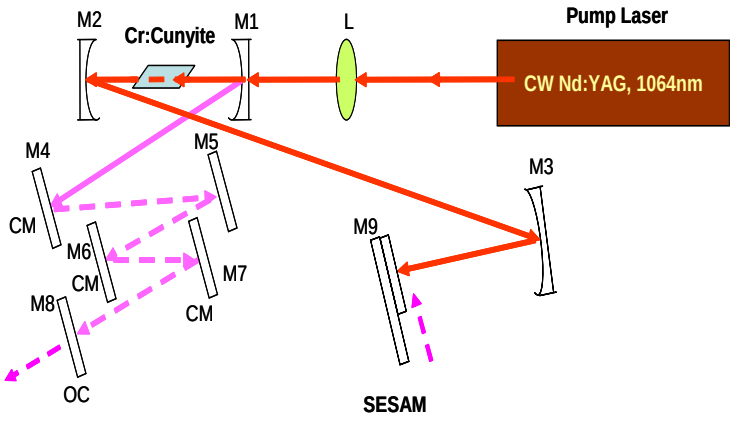

Fig. A2. Schematic of the experimental setup: L, focusing lens; M1 and M2: Dichroic, curved high reflectors with R=50cm; M4-M7: Chirped dielectric laser mirrors; OC (M8),output coupler: T = 2.5%.

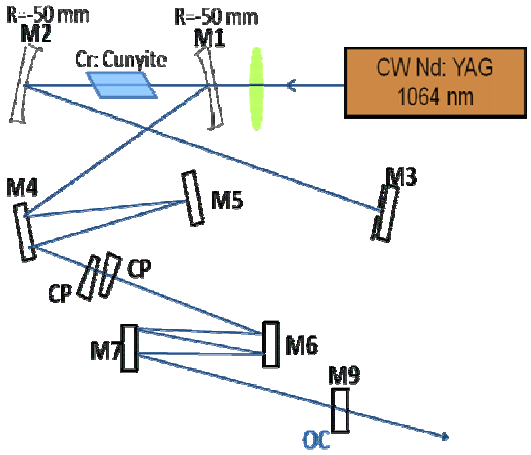

Fig.A. 3 Schematic laser setup of a mirror-dispersion-controlled KLM Cr^{4+}:Ca_2GeO_4 laser. The pump beam is focused by a 38.5mmlens onto a 3.8-mm thick highly doped Cr^{4+}:Ca_2GeO_4 crystal. (M1,M2) single-stack quarter-wave dichroic mirrors highly transmitting at the pump wavelengths with radii of curvature of 5cm; M3-M7chirped dispersive mirrors; OC, 1% broadband output coupler; CP: wedged .compensating glass plate.

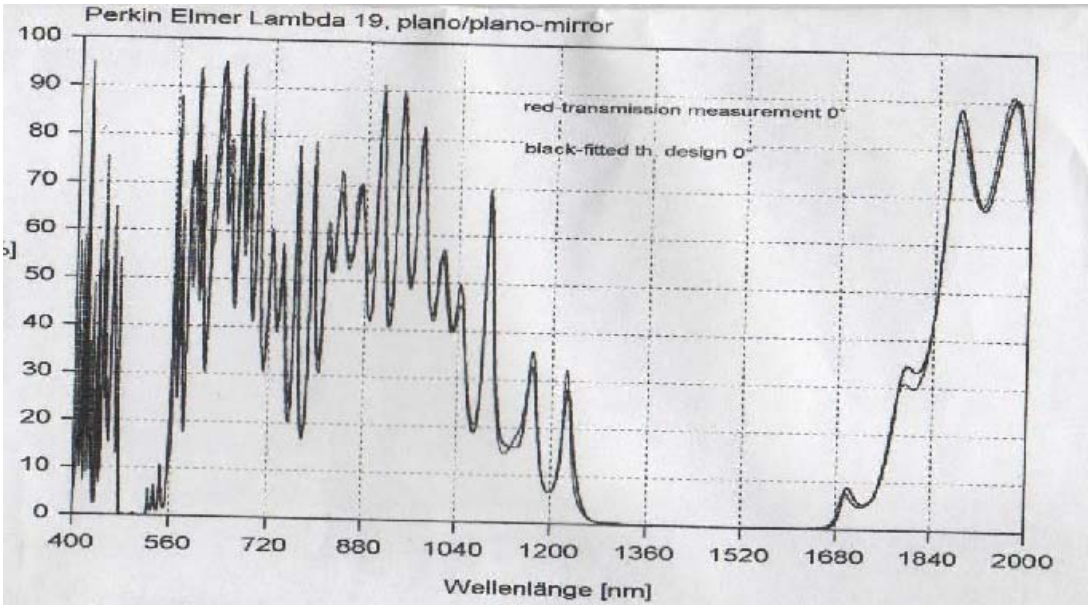

Fig.B1. Transmission of dielectric coating on chirped Mirror M1-M8 versus wavelength.

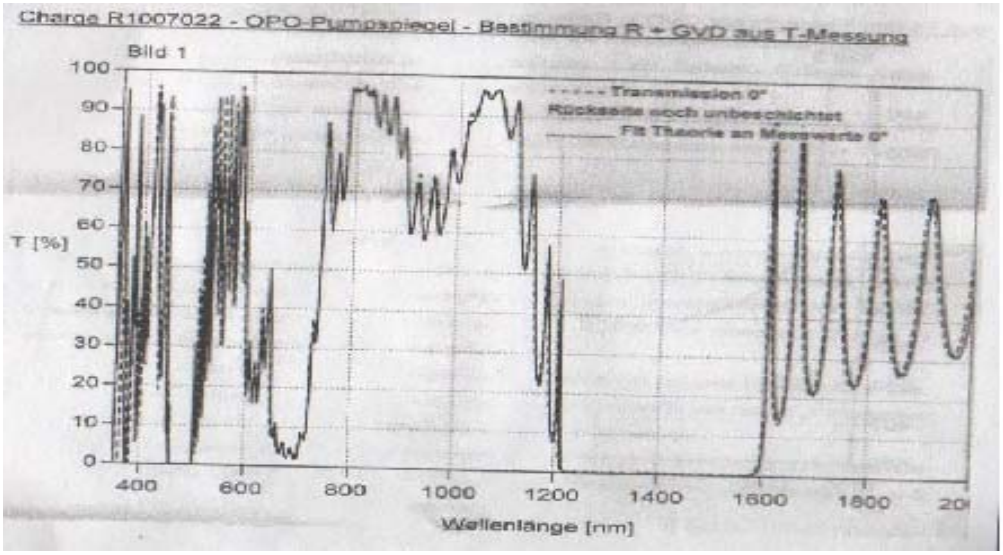

Fig.B2. Transmission of dielectric coating on a new set of chirped Mirror M1-M8 versus wavelength.

Appendix C:

The data used to calculate the group delay dispersion, the group velocity dispersion, the group delay and the phase of the Cr: Cunyite crystal (Chapter 4.3.1)

Freq (Hz)	Lambda (nm)	Phase (rad)	Group Delay (fs)	Group Delay Dispersion (fs^2)
1.87E+14	1600	-0.210003	0	0
1.90E+14	1575.55	-0.245592	-1.33218	0
1.93E+14	1551.83	-0.258689	0.28237	100.937
1.96E+14	1528.81	-0.235272	2.35671	110.101
1.99E+14	1506.47	-0.17256	4.30618	104.93
2.02E+14	1484.77	-0.077896	6.19155	107.658
2.05E+14	1463.69	0.0537198	8.24072	118.136
2.08E+14	1443.2	0.223274	10.509	124.857
2.11E+14	1423.27	0.437787	12.8038	135.88
2.14E+14	1403.89	0.691209	15.4749	137.613
2.16E+14	1385.03	1.00334	17.8331	132.043
2.19E+14	1366.67	1.34295	20.3006	156.614
2.22E+14	1348.78	1.74526	23.5568	172.474
2.25E+14	1331.36	2.20387	26.604	172.991
2.28E+14	1314.39	2.71754	29.879	186.864
2.31E+14	1297.84	3.29584	33.4332	199.299
2.34E+14	1281.7	3.93941	37.1627	209.142
2.37E+14	1265.96	4.65401	41.0766	192.996
2.40E+14	1250.6	5.44062	44.216	106.293
2.43E+14	1235.61	6.26995	44.9613	-181.982
2.46E+14	1220.98	7.0838	37.5652	-438.518
2.48E+14	1206.69	7.64283	28.935	-340.31
2.51E+14	1192.73	8.14127	25.1281	52.329
2.54E+14	1179.08	8.56118	30.8474	-251.744
2.57E+14	1165.75	9.26864	15.9277	-367.443
2.60E+14	1152.71	9.14328	17.4186	914.064
2.63E+14	1139.97	9.90523	49.3336	228.087
2.66E+14	1127.5	10.9463	25.7544	-2013.43
2.69E+14	1115.3	10.8465	-24.2504	-1461.59
2.72E+14	1103.36	10.06	-27.6617	989.239
2.75E+14	1091.68	9.83552	11.9029	1905.11
2.78E+14	1080.24	10.495	41.9634	854.225
2.80E+14	1069.03	11.3691	43.1218	-811.365
2.83E+14	1058.06	12.0709	12.3108	-2100.33
2.86E+14	1047.31	11.8191	-33.6381	-1984.11
2.89E+14	1036.78	10.8416	-60.2015	-782.765
2.92E+14	1026.46	9.6189	-62.2454	1486.24

2.95E+14	1016.34	8.56674	-5.8845	1703.18
2.98E+14	1006.41	9.40384	0	0

Lambda (nm)	GDD (fs^2)	GDD/Length (fs^2/mm)
1600.0	0.0	0.0
1575.6	0.0	0.0
1551.8	100.9	33.6
1528.8	110.1	36.7
1506.5	104.9	35.0
1484.8	107.7	35.9
1463.7	118.1	39.4
1443.2	124.9	41.6
1423.3	135.9	45.3
1403.9	137.6	45.9
1385.0	132.0	44.0
1366.7	156.6	52.2
1348.8	172.5	57.5
1331.4	173.0	57.7
1314.4	186.9	62.3
1297.8	199.3	66.4
1281.7	209.1	69.7
1266.0	193.0	64.3
1250.6	106.3	35.4
1235.6	-182.0	-60.7
1221.0	-438.5	-146.2
1206.7	-340.3	-113.4
1192.7	52.3	17.4
1179.1	-251.7	-83.9
1165.8	-367.4	-122.5
1152.7	914.1	304.7
1140.0	228.1	76.0
1127.5	-2013.4	-671.1
1115.3	-1461.6	-487.2
1103.4	989.2	329.7
1091.7	1905.1	635.0
1080.2	854.2	284.7
1069.0	-811.4	-270.5
1058.1	-2100.3	-700.1
1047.3	-1984.1	-661.4
1036.8	-782.8	-260.9
1026.5	1486.2	495.4
1016.3	1703.2	567.7
1006.4	0.0	0.0

BIBLIOGRAPHY

CHAPTER 1

1. T. Maiman, "Stimulated Optical Radiation inRuby", *Nature*, 187, 493-494 (1960).

2. R.C.Morris and C.F. Cline "Chromium-doped Beryllium Aluminate Lasers," U.S .Patent# 3,997,853.Dec14,1976.

3. M.L.Shand, J.C.Walling, "A tunable emerald laser"*IEEE J. Quant. Elec*, 18, 1829-1830 (1982).

4. Shand.M.L; Lai.S.T,"CW laser pumped emerald laser" *IEEE J. Quant. Elec* (ISSN 0018-9197), 20,p. 105-108, (1984).

5. S.A.Payne, L.L.Chase, L.K.Smith, W.L.Kway, and H.W.Newkirk "Laser performance of $LiSrAlF_6:Cr^{3+}$",*J. Appl. Phys.*,1851-1856 (1989).

6. S.A.Payne, L.L.Chase, and G.D.Wilke"Optical spectroscopy of the new laser materials, $LiSrAlF_6:Cr^{3+}$ and $LiCaAlF_6:Cr^{3+}$",*J. Luminesc Phys.*, vol 4,167-176 (1989).

7. Payne et al.,"$LiCaAIF_6:Cr^{3+}$: A Promising New Solid-State Laser Material," *J. Quant. Elect,*24(11), 2243-2252,1988.

8. Norman P. Barnes, "Transition-Metal Solid State Lasers," in *Tunable Lasers Handbook.*ed F. J. Duarte (San Diego: Academic Press, 1995).

9. C. H. Vilain, J. P. Foing and P. Schanne: *Dig. Conf. Advanced Solid-State Lasers*, *Opt. Soc. Am*. 99, 1995.

10. W. R. Rapoport and M. L. Shand: Solid State Commun, Elsevier, 84, 1992.

11. Shkadarevich, A. P., "Recent Advances in Tunable Solid State Lasers," *Opt. Soc. Amer.,* 5, 60-65, 198

12. A.J.DeMaria, W.H.Glenn Jr., M.J. Brienza, and M.E. Mack, " Picosecond laser pulses *", Proc. IEEE,* Vol. 57, pp. 2 (1969).

13. S.Chen, and J. Wang, "Self- starting issues of passive self-focusing mode-locking "*Optics Letters*, Vol. 16, 689, 1991.

14. T. Myint'sthesis"Optical spectroscopic properties of active ion doped transparent glasses", January 25, 2010.

15. A. Seas'thesis"Generation of ultrashort pulses from the chromium-doped forsterite laser"(1984).

CHAPTER 2

1. V. Petricevic,A. B. Bykov, J. M. Evans, and R. R. Alfano, "Room-temperature near-infrared tunable laser operation of (Cr^{4+}:Ca_2GeO_4) laser *Opt. Lett.* 21,1750-1752(1996).

2. B. Xu, J. M. Evans, V. Petricevic, S. P. Guo, O. Maksinov, M. C. Tamargo, and R. R. Alfano, "Continuous-wave and passively mode-locked operation of a cunyite (Cr^{4+}:Ca_2GeO_4) laser*," Appl. Opt.* 39, 4975-4978 (2000).

3. Michelet Jeanty, V. Kartazaev, M. Sharonov, A. Bykov,and R.R.Alfano,"Ultrafast laser pulses from the chromium-doped cunyite laser" Accepted at *Opt. Comm* , November 19, 2010.

4. Petricevic.V,Bykov. A. B.Evans J.M,Seas.A,Alfano R.R.Alfano"Room Temperature cw and Pulsed Near-Infrared Tunable Laser Operation of Cr4+: Ca_2 GeO_4",*CLEO 97,OSA Technical Digest Series*,11 (1997) 425.

5. J. M. Evans, V. Petričević, A. B. Bykov, A. Delgado, and R. R. Alfano, "Direct diode-pumped continuous-wave near-infrared tunable laser operation of Cr^{4+}:$^{+}$:Ca_2GeO_4 and Cr^{4+}:Mg_2SiO_4," *Opt. Express*, 22, 1171-1173(1997).

6. M.Yu .Sharonov,S. Owen, A.B. Bykov, W. B.Wang , R. R. Alfano, "Optical properties of Cunyite(Cr^{4+}:Ca_2GeO_4) crystals co-doped with Er^{3+} ions" *Optics Comm*, Volume 209,Issues 1-3, 1 August 2002, Page 209-216.

7. R.W.G.Wyckoff. Crystal structures Vol. 4,2ndEd.(Interscience, New York 1968).

8. M.F.Hazenkamp,U.Oetliker,H.U.Güdel,U.Kesper and D.Reinen,"Absorption and luminescence spectroscopy of Cr^{4+}-doped Ca_2GeO_4.A potential near infrared laser material", *Chemical Physics Letters*, Volume 233, Issue 4, 17 February 1995, Pages 466-470.

9. J. M. Evans, V. Petricevic, A.B. Bykov, and R. R.Alfano, "Continuous-wave all-solid-state laser operation of Cr^{4+}: forsterite and Cr^{4+}: Ca_2GeO_4 ," in *Diode Pumped Solid State Lasers: Applications and Issues,* Vol. 17 of 1998 OSA Trends in Optics and Photonics Series, M. W. Dowley, ed, (Optical Society of America, 1998), pp. 101.

10. T. Myint'sthesis"Optical spectroscopic properties of active ion doped transparent glasses", January 25, 2010.

11. Hazenkamp et al., "Optical Spectroscopy of Cr^{4+}-doped Ca_2GeO_4 and Mg_2SiO_4," *Phys. Rev.,* 53(5):2367-2377 (1996).

12. M.Yu .Sharonov,S. Owen, A.B. Bykov, W. B.Wang , R. R. Alfano, "Flux and characterization of Cr^{4+}: Ca_2GeO_4 crystals as a new near infrared tunable laser material", *Journal of Crystal Growth*,volume 211, Issues 1-4, 1 April 2000, Pages 295-301.

13. Güdel.H.U.Hazenkamp.M.F,Huber.G.Kück.S"Excited state absorption measurements and laser potential of Cr^{4+}-doped Ca_2GeO_4", *Applied Physics B,* vol. 64 6 p.647-650.

14. T. Ishii,K.Ogasawara,I. Tanaka, U.Kesper and H.Adachi,"Absorption First-Principle Calculation of peak energies and intensities in optical absorption spectrun of Cr^{4+}-doped Ca_2GeO_4", In advanced solid-state lasers, *OSA Technical Digest Series* (Optical Society of America,2000).

15. A. Sennaroglu, A. Askar, and F. M. Atay, "Quantitative study of laser beam propagation in a thermally loaded absorber" *J. Opt. Soc. Am.* B 14, 356-363 (1997).

16. A. Sennaroglu, "Analysis and optimization of lifetime thermal loading in continuous-wave Cr-doped solid-state lasers", *J. Opt. Soc. Am. B* 18,1578-1586 (2001).

17. A. Agnesi, E. Piccini, G.C. Reali, "Influence of thermal effects in Kerr-lens mode-locked femtosecond Cr^{4+}: forsterite lasers*", Opt. Comm.* 135, 77-82 (1997).

18. J. F. Power, "Pulsed mode thermal lens effect detection in the near field via thermally induced probe beam spatial phase modulation: a theory," Appl. Opt. 29, 52-63 (1990).

19. R. Paschotta, "Beam quality deterioration of lasers caused by intracavity beam distortions", *Opt. Express* 14 (13),6069(2006).

20. N. Hodgson and H. Weber,"Laser Resonators and Beam Propagation",Springer Series in Optical Sciences, Berlin (2005).

21. V. Magni,"Multielement stable resonators containing a variable lens", *J. Opt. Soc. Am. A* 4 (10),1962 (1987).

CHAPTER 3

1. A. G. Fox and T. Li. “Resonant modes in a maser interferometer”, *Bell Sys. Tech. J.* 40, 453 (1961).

2. A. G. Fox and T. Li, “Computation of optical resonator modes by the method of resonance excitation”, *IEEE J. Quantum Electron. QE-4,* 460(1968).

3. Arnold L. Bloom, "Modes of a laser resonator containing tilted birefringent plates," *J. Opt. Soc. Am.* 64, 447-452 (1974)

4. G. Z. Baumann, "Mode behavior in laser resonators with zones of different indices of refraction," *Opt. Lett.* 9,7-9(1984).

5. N.McCarthy and M. Morin, "High-order transverse modes of misaligned laser resonators with Gaussian reflectivity mirrors," *Appl. Opt*. 28, 2189-2191 (1989).

6. S. Arahira et al., “Mode-locking at very high repetition rates more than terahertz in passively mode-locked distributed-Bragg-reflector laser diodes”, *IEEE J. Quantum Electron*.32, 1211(1996).

7 .H.A.Haus,“A theory of forced mode locking”, *IEEE J. Quantum Electron. QE*-11,323 (1975).

8. M. DiDomenico,“Small-signal analysis of internal (coupling type) modulation of lasers”, *J. Appl. Phys.* 35, 2870 (1964).

9 .U. Morgner et al., “Sub-two cycle pulses from a Kerr-lens mode-locked Ti: sapphire laser”, *Opt. Lett.* 24 (6),411 (1999).

10 .D. E. Spence, P. N. Kean, W. Sibbett, “60-fsec pulse generation from a self-mode-locked Ti: sapphire laser”, *Opt. Lett*. 16 (1), 42(1991).

11. T. Brabec et al., “Kerr lens mode locking”, *Opt. Lett.* 17 (18), 1292 (1992).

12. E.Cumberbatch, "Self-focusing in Non-linear optics", *J. Inst. Maths Applics* 6, 250 (1970).

13. Mori, W. B. et al. "Evolution of self-focusing of intense electromagnetic waves in plasma", *Phys. Rev. Lett.* 60,1298 (1988).

14. F. Shimizu,“Frequency broadening in liquids by a short light pulse”, *Phys. Rev. Lett.* 19 (19), 1097 (1967) (first demonstration of self-phase modulation).

15. R. R. Alfano and S. L. Shapiro, “Observation of self-phase modulation and small-scale filaments in crystals and glasses”, *Phys. Rev. Lett.* 24 (11), 592 (1970).

16. R. H. Stolen and C. Lin, “Self-phase-modulation in silica optical fibers”, *Phys. Rev. A* 17 (4), 1448 (1978).

17. L. F. Mollenauer and R. H. Stolen, “Soliton laser”,*Opt. Lett.* 9 (1),13 (1984).

18. F. M. Mitschke and L. F. Mollenauer,“Ultrashort pulses from the soliton laser”, *Opt. Lett.* 12 (6),407 (1987).

19. F. X. Kärtner et al.,“Solitary pulse stabilization and shortening in actively mode-locked lasers”, *J. Opt. Soc. Am. B* 12 (3), 486 (1995).

20. J. C.Diels and W. Rudolph, “Ultrashort Laser Pulse Phenomena”, *2nd Ed.* Academic, 2006.

21. S. Lochbrunner, P. Huppmann, and E.Riedle,”Crosscorrelation measurement of ultrashort visible pulses: comparison between nonlinear crystals and SiC photodiodes”, *Optics Communications*, 184(1-4), 321-328, (2000).

22. J. A. Amstrong, “Measurement of picoseconds laser pulse widths”, *Applied Physics Letter,* 31(10), 1444-1446, (2006).

23.D. T. Reid, M. Padgett, C. McGowan, W. E. Sleat, and W. Sibbett," Light-emitting diodes as measurement devices for femtosecond laser pulses", *Optics Letters*, 22(4), 233-235, (1997).

24. J. M. Roth, T. E. Murphy, and C. Xu,"Ultrasensitive and high-dynamic-range two-photon absorption in a GaAs photomultiplier tube", *Opt. Lett*. 27, 2076–2078 (2002).

25. D. T. Reid, W. Sibbett, J. M. Dudley, L. P. Barry, B. Thomsen, and J. D. Harvey, "Commercial semiconductor devices for two photon absorption autocorrelation of ultrashort light pulses", *Applied Optics*, 37(34), 8142-8144, (1998).

26. Alan McWilliam thesis' "Femtosecond Cr^{4+}:forsterite laser for applications in telecommunications and biophotonics ", p.90, November 2006.26.Laser Fundamentals

27. "Simple two-mirror laser cavity" graph reproduced from www.shorelaser.com.

CHAPTER 4

1. A. Seas'thesis,"Generation of ultrashort pulses from chromium doped forsterite laser",pp130-148(1993).

2. Lectures' notes on "aser optics" from Professor Alfano's at the physics department of City College of New York (2005).

3. Richard. Barakat,"Ultrashort optical pulse propagation in a dispersive medium,"*J. Opt. Soc. Am. B* 3, 1602-1604 (1986).

4. M. Trippenback, T. C. Scott, and Y. B. Band,"Near-and-Far Field Propagation of Beams and Pulses in Dispersive Media", *Opt. Lett.*, 22(579),1997.

5. I. Walmsley, L. Waxer, and C. Dorrer, "The role of dispersion in ultrafast optics", *Review of Scientific Instruments,* 72(1), 1-29 (2001).

6. O. E. Martínez *et al.*, "Negative group-velocity dispersion using refraction", *J. Opt. Soc. Am. A*1(10),1003 (1984).

7 .S. Diddams and J.C.Diels,"Dispersion measurement with white-light interferometry,"*J. Opt.Soc. Am. B* 13,1120-1129(1996).

8 .S.O.Yakushev, I.A.Sukhoiva, O.V.Shulika, V.V.Lysak, S.I.Petrov "Simulation of interaction of the femtosecond laser pulses with chirped mirror",pp.(6-9-10).

9. F. X. Kaertner, N. Matuschek, T. Schibli, U. Keller, H. A. Hauls, C. Heine, R. Morf, V. Scheuer, M. Tilsch and T.Tschudi, "Design and fabrication of double-chirped mirrors", *Opt. Lett.*22, 831-833(1997).

10. F. X. Kaertner, U. Morgner, R. Ell, T. Schibli, J. G. Fujimoto and E. P. Pippen, V. Scheuer, G. Angelow, T. Tschudi, "Ultrabroaband double-chirped mirror pairs for generation of octave spectra" , *J. Opt. Soc. Am.* B 18, 882-885 (2001).

11. G. Tempea *et al.*, "Dispersion control over 150 THz with chirped dielectric mirrors", *IEEE J. Sel. Top. Quantum Electron* 4 (2),19(1998).

12. N. Matuschek *et al.*,"Theory of double-chirped mirrors", *IEEE J.Sel. Top. Quantum Electron* 4,197(1998).

13. I. D. Jung, F. X. Kartner, L. R. Brovelli, M. Kamp and U. Keller, " Experimental-verification of soliton mode-locking using only a slow saturable absorber", *Opt. Lett.*, 20(18), 1892-1894 (1995).

14. S. Tsuda,W. H. Knox, S. T. Cundiff,W.Y. Jan, J. E. Cunningham,"Mode-locking ultrafast solid-state lasers with saturable Bragg reflectors", *IEEE Journal of Selected Topics in Quantum Electronics*, 2(3), 454-464 (1996).

15. U. Keller, K. J. Weingarten, F. X. Kartner, D. Kopf, B. Braun, I. D. Jung, R. Fluck, C. Honninger, N.Matuschek and J.A. der Au," Semiconductor saturable absorber mirrors (SESAM's) for femto-second to nanosecond pulse generation in solid-state lasers", *IEEE Journal of Selected Topics in Quantum Electronics,* 2(3), 435-453 (1996).

16. B. Craig and A. Krueger, "Saturable Bragg reflectors simplify modelocking", *Laser Focus World* 36(8), 227-228 (2000).

17. S. N. Tandon, J. T. Gopinath, T. R. Schibli, G. S. Petrich, L. A. Kolodziejski, F. X. Kaertner, and E.P. Pippen, "Saturable Absorber with Large Area Broadband Bragg Reflectors for Femto-second Pulse Generation", CLEO 2003, Baltimore, MD (2003).

18. K. Weingarten, F. Kartner, D. Knopf, B. Braun, I. Jung, C. Honninger, N. Matuschek, J. Aus der Au, "Semiconductor saturable absorber mirrors (SESAMs) for femtosecond to nanosecond pulse generation pulse generation in solid- state lasers", *IEEE JSTQE* 2,435 (1996).

19. IUSL Triennial Progress Report (City College of New York, July 1, 2003 - June 30, 2006) pp. 43.

20. M. L. Dennis and I. N. Dulling III, "Experimental study of sideband generation in femtosecond fiber lasers", *IEEE J. Quantum Electron* 30(6), 1459-1477 (1994).

21. D. Anderson, M. Desaix, M. Lisak, and M. L. Quiroga-Teixeiro, "Wave breaking in nonlinear optical fibe", *J. Opt. Soc. Am. B,* 9, 1358 (1992).

CHAPTER 5

1. O. E. Martínez and R. L. Fork, "Theory of passively mode-locked lasers including self-phase modulation and group-velocity dispersion", *Opt. Lett.* 9 (5), 156 (1984).

2. A. J. DeMaria, D. A. Stetser, and H. Heynau, "Self mode-locking of lasers with saturable absorbers", *Appl. Phys. Lett.* 8, 174 (1966).

3. Knox, W.H., "Ultrafast technology in telecommunications",*IEEE Journal of Selected Topics in Quantum Electronics,* 2000. 6 (6): p. 1273-1278

4. Dennis, T., Curtis, E.A., Oates, C.W., Hollberg, Gilbert S.L., "Wavelength References for 1300-nm Wavelength-Division Multiplexing", *Journal of Lightwave Technology, 2002*. 20 (5): p. 776-782.

5. Svanberg, S., "Some applications of ultrashort laser pulses in biology and medicine", *Measurement Science & Technology, 2001*. 12 (11): p. 1777-1783.

6. Light-interactions “wwwShore Laser.com” website

7. Diamond I, Granelli S G, McDonagh A F, Nielsen S, Wilson C B and Jaenicke R “Photodynamic therapy of malignant-tumors “,*J.Opt.Soc.Am.* 64 534.

8. Fischer, P., A. McWilliam, C.T.A. Brown, K. Wood, M.MacDonald, W.Sibbett, and K. Dholakia, “Deep tissue penetration of radiation: modelling and experiments”, Paper CL-4-Wed, European Conference on Lasers and Electro-Optics (ECLEO), Munich, Germany, 2005.

9. Cheong, W.F., P.S.A., and A.J.Welch, “A review of optical properties of biological tissues”, *IEEE Journal of Quantum Electronics, 1990*. 26 (12): p. 2166-2185.

10. Konig K. Riemann I and Fritzsche W 2001 Nanodissection of human chromosomes with near-infrared femtosecond laser pulses *Opt. Lett*.26 819-21.

11. Laing H.Wright W H, Cheng S, He W and Bems M W 1993 Micromanipulation of chromosomes in Ptk2 cells using laser microsurgery (optical scalpel) in combination with laser- induced optical force (optical tweezers) *Exp. Cell Res.* 204 110-20**.**